

UCLA

UCLA Electronic Theses and Dissertations

Title

Flexible, Heterogeneously Integrated microLED Displays in Elastomeric Substrates using Fan-Out Wafer-Level Packaging

Permalink

<https://escholarship.org/uc/item/4kt2t2wn>

Author

Ezhilarasu, Goutham

Publication Date

2021

Peer reviewed|Thesis/dissertation

UNIVERSITY OF CALIFORNIA

Los Angeles

**Flexible, Heterogeneously Integrated microLED Displays in Elastomeric Substrates using
Fan-Out Wafer-Level Packaging**

A dissertation submitted in partial satisfaction

of the requirements for the degree

Doctor of Philosophy

in Electrical and Computer Engineering

by

Goutham Ezhilarasu

2021

© Copyright by
Goutham Ezhilarasu
2021

ABSTRACT OF THE DISSERTATION

Flexible, Heterogeneously Integrated μ LED Displays in Elastomeric Substrates using Fan-Out Wafer-Level Packaging (FOWLP)

by

Goutham Ezhilarasu

Doctor of Philosophy in Electrical and Computer Engineering

University of California, Los Angeles, 2021

Professor Subramanian Srikantes Iyer, Chair

In recent years there has been a growing demand to develop next-generation flexible displays that can achieve higher brightness, dynamic range, and contrast ratios compared to LCDs or OLEDs. This demand is driven by new application spaces such as wearable Augmented Reality (AR), conformable vehicular Head UP Displays (HUDs), and emerging medical fields such as Optogenetics, where implanted high brightness displays are used to stimulate biological cells such as neurons. The only display technology that can meet these requirements is flexible microLED displays. microLEDs are light-emitting devices made from compound semiconductor materials like GaN or InP that have demonstrated unparalleled brightness ($>10^6$ cd/m²), color quality, response times (in ns range), and lifetime ($>100,000$ hours). The task of fabricating flexible microLED displays has, however, proven to be complicated.

Inorganic microLEDs cannot be fabricated directly on flexible organic substrates due to the high processing temperatures and lattice matching considerations. Instead, they are fabricated on a growth substrate, released from it, and then assembled onto a target flexible substrate using a massively parallel transfer process, simply called mass transfer. However, flexible microLED display technology has not picked up due to (1) complex and expensive mass transfer processes that suffer from yield issues & (2) primitive flexible electronic integration approaches that use coarse interconnects and are not well suited to the heterogeneous integration of micron-sized LEDs. To overcome these challenges, we have developed a novel microLED mass transfer process based on thermoplastic adhesive (HD3007) bonding that is much simpler to implement, low cost, and can potentially attain many high yields (> 99%) and panel-level scalability. We also use a novel Fan-Out Wafer-Level Packaging (FOWLP) technology called FlexTrate™ to heterogeneously integrate 50 X 100μm² blue InGaN/GaN microLEDs with Si CMOS display driver ICs at < 40μm interconnect pitch to demonstrate a high density, functional, high resolution (> 150PPI) flexible microLED display. Detailed analytic and experimental studies of the various process steps, especially the Laser Lift-Off (LLO) process that is used to release GaN microLEDs from the growth substrate, is conducted in this thesis.

The dissertation of Goutham Ezhilarasu is approved.

Sam Emaminejad

Chee Wei Wong

Aydin Babakhani

Subramanian Srikantes Iyer, Committee Chair

University of California, Los Angeles

2021

DEDICATION

To my mother and late father...

TABLE OF CONTENTS

1. Introduction.....	01
1.1. Challenges of modern display technology.....	01
1.2. Need for flexible microLED displays.....	03
1.3. Challenges of making flexible microLED displays.....	04
1.3.1. Challenges of microLED fabrication and assembly.....	04
1.3.2. Challenges of conventional flexible electronic approaches.....	09
1.4. New approach to fabricating flexible microLED displays.....	11
1.4.1. Novel mass-transfer approach using adhesive bonding.....	11
1.4.2. Novel flexible electronic integration approach using FOWLP.....	12
1.5. Organization of this dissertation.....	15
REFERENCES.....	17
2. Process Flow for Flexible microLED Display.....	21
2.1. Mass Transfer Approach.....	23
2.2. Dielet Approach.....	30
REFERENCES.....	35
3. High Yield GaN Laser Lift-Off (LLO).....	36
3.1. Introduction to the GaN LLO process.....	36
3.2. GaN LLO using DPSS laser.....	38
3.3. Analytic Modeling of the GaN LLO process.....	41
3.4. Finite Element Modeling of the GaN LLO process.....	51
3.5. Experimental verification of stress buffer for high-yield LLO.....	61
3.5.1. Fabrication of samples for LLO yield testing.....	61

3.5.2. Evaluation of LLO quality and yield.....	62
3.5.3. Optical mapping of GaN islands on temp. glass carrier after LLO.....	62
3.5.4. AFM profile of GaN island surface after LLO.....	63
3.5.5. PL characterization of released GaN films.....	64
REFERENCES.....	66
4. Flexible microLED displays on FlexTrate™.....	67
4.1. Mass transfer approach for fabricating microLED display.....	68
4.1.1. Detailed process flow for performing mass transfer.....	68
4.1.2. Sample preparation and characterization pre-LLO.....	71
4.1.3. GaN LLO of the bonded samples using DPSS laser.....	73
4.1.4. Glass stamp fabrication and bonding.....	74
4.1.5. Transfer of microLEDs to glass stamp.....	75
4.1.6. Electrical characterization of microLEDs on glass stamp.....	78
4.1.7. Heterogeneous assembly on FlexTrate™.....	79
4.2. Dielet approach for fabricating microLED display.....	82
4.2.1. Design of microLED display on FlexTrate™.....	83
4.2.2. Fabricated FlexTrate™ microLED display.....	86
4.2.3. Testing of Fabricated FlexTrate™ microLED display.....	88
4.2.4. Calculation of WPE (%) of the fabricated display.....	90
4.2.5. Fabrication issues of current microLED display on FlexTrate™.....	96
REFERENCES.....	98
5. Future Work.....	99
5.1. FlexTrate™ microLED displays with custom microLEDs.....	99

5.2. Wireless power transfer for FlexTrate™ microLED display.....	101
5.3. Demonstration of full color microLED displays on FlexTrate™.....	106
REFERENCES.....	111
6. Summary of Contributions	113

LIST OF FIGURES

Figure 1.1. Comparison of performance metrics between microLEDs and other commercial display technologies.....	03
Figure 1.2. Schematic of the LLO process along with the band diagram of the GaN/sapphire interface.....	06
Figure 1.3. Summary of various stamp-based transfer-printing techniques in literature.....	07
Figure 1.4. Conventional flexible electronic integration approach for making microLED displays.....	10
Figure 1.5. Novel mass transfer approach used in this work using adhesive bonding and laser debonding.....	12
Figure 1.6. Fabrication process flow for FlexTrate™	14
Figure 1.7. FlexTrate™ integration approach for making microLED displays.....	15
Figure 2.1. Rough schematic of a typical mass transfer process.....	22
Figure 2.2. Mass Transfer approach to the fabrication of a flexible microLED display on FlexTrate™	30
Figure 2.3. Dielet approach to the fabrication of a flexible microLED display on FlexTrate™	34
Figure 3.1. Schematic of the LLO process along with the band diagram of the GaN/sapphire interface.....	37
Figure 3.2. Film failure and cracking during the process of GaN Laser LLO.....	38
Figure 3.3. Illustration of DPSS laser wafer-level LLO system used.....	40
Figure 3.4. Screen shots of in-process camera view of connecting DPSS LLO pulses at an interior pocket of a continuous GaN epi on sapphire wafer.....	41

Figure 3.5. Bucking of GaN thin films after LLO due to growth induced compressive stress.....	42
Figure 3.6. Strain excitation function Vs. time (left) and stress-strain relationship (right).....	43
Figure 3.7. Analytic model of normal stress wave generation in GaN thin film, assumed cylindrical, during LLO.....	44
Figure 3.8. Space-time (z-T) diagram depicting stress wave generation and propagation in GaN film.....	48
Figure 3.9. Simplified axisymmetric model of GaN LLO.....	52
Figure 3.10. Temperature transients at the GaN/sapphire interface during the LLO process simulated in ANSYS Explicit Dynamics.....	54
Figure 3.11. Temperature averaged within the β_{GaN}^{-1} region and plotted as a function of time.....	55
Figure 3.12. Illustration of the shear and normal components of thermomechanical shockwave (a) & normal component of N ₂ pressure shockwave.....	56
Figure 3.13. Simplified model for laser ablation at GaN/sapphire interface.....	57
Figure 3.14. Released N ₂ gas pressure as a function of time at the GaN/sapphire interface derived from the simplified model.....	58
Figure 3.15. ANSYS® Explicit Dynamics simulation of the normal stress in the LLO cross-section without Ni (a), and with a 10 μm Ni layer (b).....	59
Figure 3.16. ANSYS® Explicit Dynamics simulation of the normal deformation (X10) in the LLO cross-section without Ni (a), and with a 10 μm Ni layer (b).....	60
Figure 3.17. Peak compressive stress in GaN film as a function of time for 3 cases: No Ni, 5 μm Ni & 10 μm Ni.....	60

Figure 3.18. (a) GaN islands on sapphire after singulation. (b) Bonded sample for LLO.....	61
Figure 3.19. (a) nanotronics nSpec® PS microscope setup. Optical image of GaN islands, on the 4” temporary carrier, (b) with ~5μm support layer & (c) without support layer.....	62
Figure 3.20. Results of optical mapping of 4” temporary glass carrier with GaN islands after LLO.....	63
Figure 3.21. AFM surface profile of released and singulated GaN island (a) without a support layer and (b) with a 5μm Ni support layer.....	64
Figure 3.22. Results of photoluminescent (PL) measurements on the released GaN islands after LLO. A comparison with virgin devices on sapphire is established.....	65
Figure 4.1. Proposed process flow for GaN microLED assembly on FlexTrate™...	71
Figure 4.2. (a) Optical image of as-fabricated devices along with average I-V characteristic; (b) SEM image of singulated μLEDs with Ni layer.....	72
Figure 4.3. (a) Optical image depicting registration issues during glass stamp bonding while performing process at wafer scale; (b) Four backside polished sapphire dies (~10mm X 12mm) bonded to glass coupon ready for LLO.....	73
Figure 4.4. (a) Optical image of released GaN islands with & without Ni stress buffer post LLO; (b) SEM image of released microLEDs with ~ 5μm Ni layer.....	74
Figure 4.5. (a) SEM image of the two different glass stamp patterns with lithographically patterned HD3007 ready for bonding; (b) Optical images after adhesive bonding of stamp to released microLEDs on temporary carrier (looking through stamp). Inset shows a single coupon with four stamps bonded.....	75
Figure 4.6. (a) SEM image of as transferred microLEDs sitting on glass stamp (face up); (b) Optical image of microLEDs with exposed contacts after removal of Ni layer and seed; (c) Contact probing of microLEDs on stamp confirming successful operation.....	76

Figure 4.7. Contact delamination after the wet etching of Ni stress buffer. Regions where the contacts are delaminating is indicated by the red circles.....	78
Figure 4.8. microLED contacts looking through the polished sapphire side before device singulation (left), after singulation (right). The dark discolorations on the contacts are regions where the contact layer is slowly delaminating.....	78
Figure 4.9. Comparison of I-V measurements of the microLEDs on glass stamp vs. virgin devices on sapphire.....	79
Figure 4.10. Image of KGD glass stamp and Si dielets (1mm ²) tacked onto common TRT laminated on glass wafer. These samples are sent for laser debonding.....	80
Figure 4.11. After laser debonding of glass stamp, the microLED matrix array is completely transferred to the TRT on a 100mm glass wafer.....	81
Figure 4.12. SEM images of microLEDs and Si dielets embedded in PDMS ready for metallization. The globular topography of the PDMS is an artifact of the TRT.....	81
Figure 4.13. Photos of the released FlexTrate™ sample with microLEDs and Si dielets embedded in PDMS.....	82
Figure 4.14. Schematic of full FlexTrate™ microLED display design.....	84
Figure 4.15. Details of display driver ICs MIC5981 (left) & MAX6971(right).....	85
Figure 4.16. Functionality testing of bare die display driver ICs.....	85
Figure 4.17. Optical micrograph of fabricated FlexTrate™ microLED display (left), after full release of the fabricated display (right).....	86
Figure 4.18. Optical images of various heterogeneously integrated ICs on the fabricated display.....	87
Figure 4.19. Optical image of an individual sapphire dielet integrated on the FlexTrate™ display with a zoomed in view of the two metallizations levels.....	88
Figure 4.20. Row scan operation of fabricated passive matrix display.....	89

Figure 4.21. Electrical schematic of the fabricated 48 X 80 PM microLED display on FlexTrate™ using the dielet approach. The currents and voltages in different branches and nodes along the first scan line (ON) are also identified. All microLEDs on the first scan line are assumed to be lit.....	90
Figure 4.22. Schematic of MAX6971 current driver IC, MIC5891 voltage source IC, & top left-most sapphire dielets.....	91
Figure 4.23. Equivalent circuit diagram of a single scan line during selection while all microLEDs are ON.....	94
Figure 4.24. Nodular growth due to current crowding causing shorting of adjacent wires.....	97
Figure 5.1. Conventional LED process Vs. Mass transfer safe process.....	100
Figure 5.2. Mass transfer safe microLEDs fabricated at UCLA.....	100
Figure 5.3. Small form factor microLED displays used in AR (left) and Optogenetic cochlear implant (right).....	101
Figure 5.4. Circuit schematic of WPT system on FlexTrate™.....	103
Figure 5.5. Optical image of integrated system (left) & schematic of a system concept (right).....	103
Figure 5.6. Experimental setup for WPT link characterization.....	104
Figure 5.7. Characterization results of link PTE (%) for different conditions.....	105
Figure 5.8. Full wireless power transfer system characterization results.....	105
Figure 5.9. Operation of WPT system under different conditions of bending of the Implant coil.....	106
Figure 5.10. Process flow for the integration of colloidal QDs with an optical UV microLED ‘optical pump plane’ for the demonstration of a full color, flexible display on FlexTrate™.....	108

Figure 5.11. UV microLEDs exciting green and red QD color conversion layers respectively.....	109
Figure 5.12. Spectral data of color conversion from UV microLED backlight using green and red QD color conversion layers.....	110

LIST OF TABLES

Table 2.1. Comparison between the Mass Transfer and Dielet approaches to fabricating a flexible microLED display on FlexTrate™.....	34
Table 3.1. Commonly used laser systems for GaN LLO.....	38
Table 3.2. Comparison between Excimer lasers and DPSS lasers for GaN LLO.....	40
Table 4.1. Comparison between the demonstrated flexible microLED display and other such displays in literature.....	89

ACKNOWLEDGEMENTS

I take this opportunity to express my sincere gratitude to my advisor **Prof. Subramanian Iyer** for his invaluable guidance throughout my research work. His constructive feedback, encouragement, and patience have been the driving forces for the successful completion of my research and dissertation.

I thank **Prof. Sam Emaminejad**, **Prof. Chee Wei Wong**, and **Prof. Aydin Babakhani** for providing a critical review of this work and for serving as members of my dissertation committee.

I thank **Dr. Ajit Paranjpe** for guiding me through the microLED display project by providing valuable advice and insights, and for providing a critical review of this work.

I would like to express my sincere appreciation to **Frank Wei**, **Jay Lee**, and **Aris Bernales** of DISCO Corp. Japan for helping me with the sapphire polishing and GaN DPSS LLO process.

I would like to thank NMBC/AFRL, SRC, SEMI-FlexTech, the UC system, and the UCLA CHIPS consortium for supporting this work in parts.

I would like to thank **Prof. Takafumi Fukushima** for his help, advice, guidance, and for sharing his technical expertise throughout the development of FlexTrate™.

I thank **Dr. Amir Hanna** for being an excellent mentor and for helping me in the initial stages of my PhD.

I would also like to thank **Dr. Samatha Benedict**, **Dr. Adeel Bajwa**, **Dr. Boris Vaisband**, and **Dr. Umesh Mogera** for their guidance and support. I would like to thank all my colleagues: **Arsalan Alam**, **Randall Irwin**, **Guangqi Ouyang**, **Henry Sun**, **Dr. SivaChandra Jangam**,

Krutikesh Sahoo, Arpan Dasgupta, Saptadeep Pal, Kannan K. Thankappan, Yu-tao Yang, Niloofar Sharookzadeh, Pranav Ambhore, Eric Sorensen, Steven Moran, Premasagar Kittur, Dr. Zhe Wan, Jonathan Cox, and others for many successful collaborations and meaningful discussions. I am indebted to all my co-authors for their hard work. I would also like to thank the staff of UCLA Integrated Systems Nanofabrication Cleanroom, Nanolab Research Facility, and Center for High-Frequency Electronics for their help and support. I thank all our industry collaborators who provided hardware, technical support, equipment, and service required for my research. Parts of this dissertation were adapted from several publications during my doctoral studies.

I express my deep sense of gratitude to my family and friends for their never-ending love and moral support.

VITA

- 2011-2015 Bachelor of Engineering in Electrical & Electronics Engineering,
College of Engineering, Guindy, Anna University
- 2015-2017 Master of Science in Electrical Engineering,
University of California, Los Angeles

SELECTED PUBLICATIONS AND PATENTS

1. G. Ezhilarasu, A. Hanna, A. Paranjpe & S. S. Iyer, “High Yield Precision Transfer and Assembly of GaN μ LEDs using Laser Assisted Micro Transfer Printing,” 2019 IEEE 69th Electronic Components & Technology Conference (ECTC).
2. G. Ezhilarasu, A. Paranjpe, J. Lee, F. Wei & S. S. Iyer, “A Heterogeneously Integrated, High Resolution and Flexible Inorganic μ LED Display using Fan-Out Wafer-Level Packaging,” 2020 IEEE 70th Electronic Components & Technology Conference (ECTC).
3. G. Ezhilarasu, A. Hanna, R. Irwin, A. Alam & S. S. Iyer, “A Flexible, Heterogeneously Integrated Wireless Powered System for Bio-Implantable Applications using Fan-Out Wafer-Level Packaging,” 2018 IEEE International Electron Devices Meeting (IEDM).
4. S. S. Iyer and G. Ezhilarasu, “Flexible Inorganic microLED Display Device and Method of Manufacturing Thereof,” US Patent App. # 63/033,564.
5. S. S. Iyer, G. Ezhilarasu and H. Sun, “Post-Process Testing Station for Semiconductor Device Fabrication,” UCLA CASE NO. 2021-187-1.

1. Introduction

1.1. Challenges of modern display technology

The most traditional display technology developed in the modern age was a Cathode Ray Tube (CRT) display which was first commercialized in the 1950s [1]. The display essentially consisted of a vacuum tube and an electron gun which produced a high energy electron beam to be steered onto a phosphorescent screen to generate colors and display information [1]. The first color CRT TVs dominated the market for several decades until the early 2000s when two new display technologies were introduced: the Liquid Crystal Displays (LCDs) and the Plasma display panels. Both these technologies quickly replaced CRTs as they were less bulky and hence more portable, consumed less power, and cheaper in cost due to mass production [2]. Out of these two emergent technologies, the LCDs quickly came out on top. The main reasons for this are enormous investments made to improve both the performance & cost of these displays [2]. LCDs, although ubiquitous, are highly unpopular with consumers. They are not a self-emissive display technology and hence need a backlight leading to poor contrast ratios. They have slow response times, poor conversion efficiencies, low color saturation and limited viewing angles. They are a relatively low brightness display leading to issues while using them in ambient lighting conditions [3]. A new display technology was thus needed to overcome some of the challenges faced by LCDs. In the late 1990s, Organic Light Emitting Diode (OLED) displays were first introduced in the market [4]. This display unlike LCDs

was self-emissive, meaning that the user directly looks at the light emitters and hence no backlight technology is needed. The display can hence attain much wider viewing angles, higher contrasts, higher power savings and faster response times. This display technology, however, has not taken over the LCD market [4]. The organic nature of the materials used in OLEDs make them susceptible to high current degradation and make them less reliable in the long run [4]. Limitations in materials and mass production capabilities have also pushed up their costs thus limiting their use to luxury products. In 2000, a new era of display technologies was opened with the demonstration of the first microLEDs for display applications [5]. microLEDs are microscale (<100-microns), inorganic compound semiconductor-based light emitting diodes based on a Multiple Quantum Well (MQW) PIN diode structure. These devices were demonstrated to produce brightness exceeding 10^6 Cd/m², have nanosecond response times, high dynamic range, and contrast ratios [6]. A comparison between microLEDs and the other display technologies is summarized in **Figure 1.1**. We can clearly see the superiority of microLEDs compared to the other display technologies. There has hence been an enormous push in both industry and academia to demonstrate microLED displays [7]. The cost of these displays will always be higher as compared to LCDs and hence they are not expected to take over that market. However, this technology could easily compete with OLEDs for the luxury display market for TVs and mobile displays [8]. There are also some niche applications where microLEDs are the only viable technology owing to their unprecedented brightness & response times: wearable Augmented Reality (AR), automobile HUDs and emerging medical applications like Optogenetics [9].

	LCD-mini LED	Plasma	OLED	μLED
Contrast	3,000,000:1	2,000,000:1	>1,000,000:1	>3,000,000:1
Brightness (cd/m²)	300	1000	600	>10 ⁶
Viewing angle (Deg.)	170	170	>170	>170
Response time (ms)	10-25	<8	0.01	<0.0001
Power efficiency	low	medium	low	high
Lifetime	low	low	medium	high
Cost	medium	low	medium	high
Availability	high	medium	medium	low

Figure 1.1. Comparison of performance metrics between microLEDs and other commercial display technologies.

1.2. Need for flexible microLED displays:

There is also a specific need for flexible microLED displays, where the microLEDs are assembled on a flexible organic substrate, in the following application spaces:

(1) Defense Applications [10]:

- Conformable vehicular displays for efficient solid-state lighting
- Flexible & smart wearable displays for in-field combatants with clear visibility in ambient light.

(2) Medical Applications [11]:

- High spacial resolution Optogenetic excitation tools
- Visible light therapies (particularly blue μLEDs due to high brightness)

- Solid state lighting for smart scalpels

(3) Commercial Applications [12]:

- Wearable displays for Augmented Reality (AR)/Virtual Reality (VR)
- High brightness conformable displays for automobile HUDs
- Displays for flexible mobile devices in ambient light usage

Making microLED displays in general and flexible microLED displays in particular has been an extremely difficult task due to several reasons.

1.3. Challenges of making flexible microLED displays:

1.3.1. Challenges of microLED fabrication & assembly (parts from [35])

Unlike OLED materials that can directly be deposited on top of a flexible substrate like Polyimide (PI) [13], inorganic microLED stacks are based on a GaN or InP material system and are typically grown on rigid, lattice matched substrates at very high temperatures ($>900^{\circ}\text{C}$) [14]. To integrate such microLEDs on a flexible organic substrate, an indirect method of assembly is to be used.

As fabricated & singulated microLEDs on growth substrates are to be released and then transferred onto the final flexible organic substrate. Due to the small size and thickness of the individual device ($<100\mu\text{m}$ side, $<7\mu\text{m}$ thickness), sequential pick and place for assembly is not practical. Hence a mass transfer technique is used where in all the devices from the growth wafer are released and transferred to the target wafer using a high yield (typically $>99.9999\%$) massively parallel process [15]. Before releasing from the growth substrate, the fabricated microLEDs are attached to

a temporary carrier by bonding (metallic or adhesive) or stiction (Van der Waals forces or electromagnetic) for accurate registration [16]. If the devices are chemically released, they could also be left anchored to the growth substrate by using polymers or dielectrics, so that a stamp could be used to pick up selected arrays of the released microLEDs for final assembly [17]. The release process of the microLEDs from the growth substrate is done by either chemical or optical means. In the case of InAlGaP (red or yellow) microLEDs, the release is typically done by chemically wet etching an underlying sacrificial layer such as $\text{Al}_{0.97}\text{Ga}_{0.03}\text{As}:\text{Si}$ in hydrofluoric acid (HF) without affecting the overlying device layers [18]. This release process has shown to be high yield and can be done with relative ease. For high quality GaN microLEDs grown on c-plane sapphire, simple wet release techniques are not possible due to the chemical stability of GaN and sapphire [19]. Such devices are instead released by an optical process called Laser Lift-Off (LLO) [20]. In LLO of GaN, a high-power UV or Q-switched solid-state IR pulsed laser (pulse width $\sim 10\text{ns}$) is shone from the backside of the polished sapphire substrate (see **Figure 1.2**). The laser is not absorbed by sapphire due to the high bandgap and hence passes through with little attenuation until it reaches the interface where it is absorbed by the GaN layer within a few hundreds of nm, refer [20]. The high energy (dose $>600\text{mJ}/\text{cm}^2$) of the absorbed light induces a local hotspot with a temperature $>900^\circ\text{C}$ with causes spontaneous decomposition of GaN into liquid Ga and N_2 . The vapor pressure of released N_2 along with the high temperature gradients at the ablation interface, induces enormous stresses on the overlying GaN device and can cause pitting or crack formation on the surface which can either fully damage the device causing yield reduction or degrade

its performance by increasing leakage currents (see **Figure 1.2**) [21]. After the laser exposure, the sample can be heated to the melting point of Ga ($\sim 30^\circ\text{C}$) causing the release of the devices to the temporary carrier. Any metallic residue can then be cleaned using dilute acid treatment [22] and surface dry-etched to remove surface damage and incipient cracks.

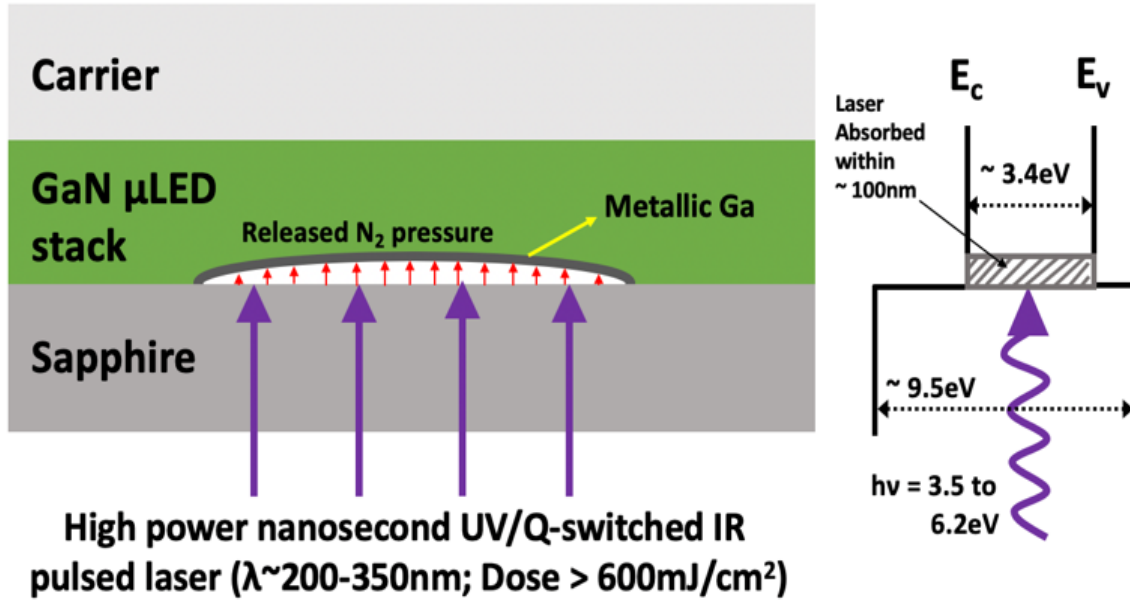


Figure 1.2. Schematic of the LLO process along with the band diagram of the GaN/sapphire interface [35].

The released microLEDs, held on the temporary carrier, are now selectively picked up using a stamp and then assembled onto the final target wafer using a process known as transfer printing or mass transfer [23]. Several conventional approaches for the stamp pick-up of microLEDs for mass transfer have been explored in literature and are summarized in **Figure 1.3**.

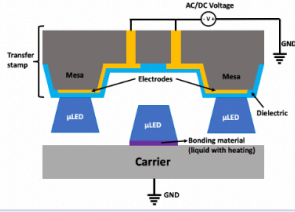
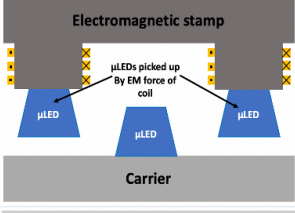
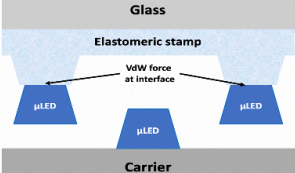
Transfer technique	Developer	Schematic of technique	Principle of operation	Operating challenges
Electrostatic stamp	LuxVue		<ul style="list-style-type: none"> • Uses electrostatic gripper action. • Applied voltage on transfer head capacitively attracts conductive surface of device. • Device and transfer head are separated by a thin dielectric. 	<ul style="list-style-type: none"> • Electrostatic attraction force is sensitive to applied voltage, thickness & dielectric constant of separating dielectric. • Yield affected by presence of air gaps or dust. • Not immune to wafer bow.
Magnetic Stamp	ITRI		<ul style="list-style-type: none"> • Based on Electromagnetic attraction. • Applied current to transfer head inductively couples and attracts the device. 	<ul style="list-style-type: none"> • Yield affected by presence of air gaps or dust. • Not immune to wafer bow. • Device modification needed for magnetic attraction.
Viscoelastic stamp	X-Celeprint		<ul style="list-style-type: none"> • Use Van der Waals (VdW) forces between viscoelastic stamp and device for transfer. • Stiction between stamp and device modulated using peel rate techniques or collapsible structures. 	<ul style="list-style-type: none"> • VdW forces are relatively weak and hence random device shifts or loss may occur during transfer. • Requires fine tuning of process parameters to attain high yields.

Figure 1.3. Summary of various stamp-based transfer-printing techniques in literature [35].

Although all the transfer approaches mentioned do work in principle, their commercial viability for high yield assembly onto a target substrate is doubtful. Transfer approaches based on electrostatic forces, developed by LuxVue [24], uses a transfer head with an applied high voltage AC or DC to electrostatically pick up microLEDs from the carrier for transfer. The technique is based on the electrostatic gripper action [25] wherein an applied voltage to an electrode on the transfer head capacitively induces charges on the conductive surface of a microLED, separated from the electrode by a thin dielectric (see **Figure 1.3**), to attract it. The electrostatic force attracting the microLED is sensitive to the applied voltage, thickness & dielectric constant of the separating dielectric and most importantly, the presence of

any air gaps or particles between the head and the microLED [26]. The complexity of operation and yield issues especially for warped wafers make this approach less attractive. Transfer printing using electromagnetic stamp techniques can only handle relatively large microLED pitches and require modification of the devices to make them magnetically attractive [27] in addition to similar problems mentioned for the electrostatic case. Mass transfer using viscoelastic stamps (PDMS) rely only on Van der Waals (VdW) forces between the stamp and microLED [28]. They are hence not very reliable in holding the devices in place during the mechanical transfer process from the temporary carrier to the target wafer. Some microLEDs could shift significantly or even be completely lost from their original positions, in random locations of the stamp, and this in turn could reduce transfer yields to <99.9% across the wafer unless tedious fine tuning of process conditions is done. Even if double printing of microLEDs [28] can be used to allow device redundancy to account for the yield loss, the high cost per microLED would significantly push up the total cost of the manufactured display. Also, the viscoelastic property of the elastomeric stamp, that causes it to exhibit peel-rate dependent interfacial adhesion, is often used for the transfer printing [29]. When the pulling speed of the stamp is increased, the adhesion of the stamp to the microLED increases and vice-versa. So, a higher pull rate is used during the device pick-up process from the temporary carrier and a lower pull rate is used for the final printing. As the dependence of the pull-off force (for delamination of stamp from a surface) versus the pulling speed, as discussed in [29], is highly non-linear, using such a property for the transfer printing process requires significant

tuning of process parameters. This could be difficult in a process setting where components of different sizes and materials are to be transfer printed at high yield.

1.3.2. Challenges of conventional flexible electronic approaches for microLEDs

Conventional approaches to the heterogeneous integration of microLEDs with other dies/components on a flexible substrate for making a fully functional display also suffers from several drawbacks:

(I) It involves printing of the microLEDs on the surface of the substrate followed by metallization. This technique however does not naturally support heterogeneity in die/component integration owing to thickness variation induced planarity issues (as illustrated in **Figure 1.4**) that can lead to packaging or processing difficulties down the line. Hence for practical purposes, all the dies integrated using this approach must be thinned down to a specific thickness. Thinning down of individual dies can be an expensive and low yield process [30].

(II) Dies must be flip-chip bonded onto metal terminations on the flexible substrate to form interconnection with the much thinner microLEDs ($\sim 2\text{-}7\text{ }\mu\text{m}$ thick) as shown in **Figure 1.4**. Flip chip thermo-compression bonding on a flexible substrate is difficult as the substrate cannot withstand the processing conditions involved [31]. Hence the use of an Anisotropic Conductive Paste (ACP) or reflow solder process is imperative which can significantly limit the achievable interconnect density to hundreds of microns [32].

(III) Conventional flexible electronic approaches use evaporated thin film metallization to interconnect various components/dies [33]. Such thin metallization

(< 1 μ m thickness) adds to significant series resistance to the components and can affect circuit performance. For example, it is a well-known fact that the series resistance of the interconnect can cause an increase in the effective turn-on voltage of a microLED affecting the drive circuitry and brightness of the display. A thin metallization (< 1 μ m) can also lead to thermal problems. As flexible substrates are made of organic materials with very poor thermal conductivities ($k < 1\text{W/mK}$), the metallization which has two orders of magnitude higher thermal conductivity ($k \sim 300\text{W/mK}$) plays a critical role in heat spreading. The heat dissipation capability of a thin metal however is significantly limited due to the higher thermal resistance which can impact the microLED operation (can lead to wavelength shifts & efficiency droop, see [34]).

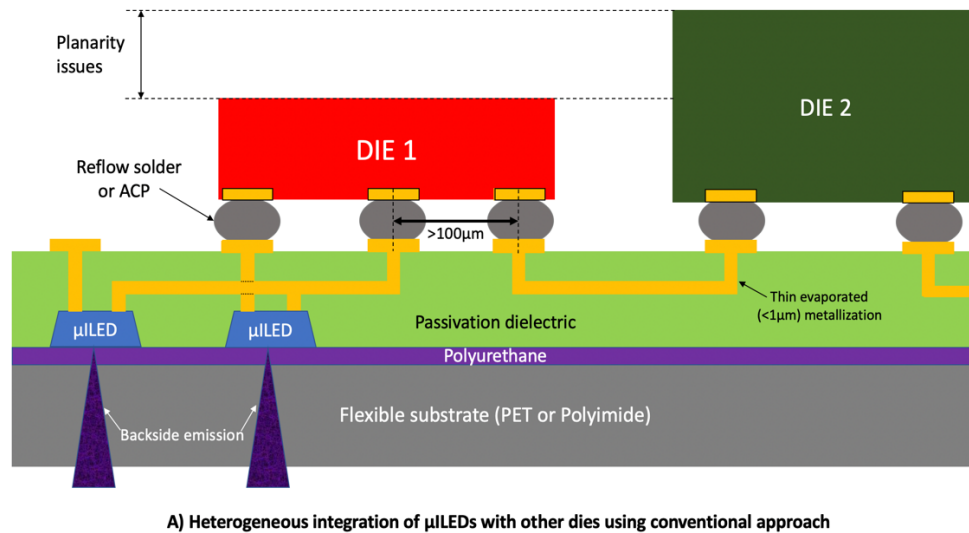


Figure 1.4. Conventional flexible electronic integration approach for making *microLED* displays.

To overcome these limitations of conventional mass transfer and flexible electronic integration approaches in fabricating flexible microLED displays, we have come up

with two innovations: a new mass transfer process based on adhesive bonding & a new flexible electronic integration approach called FlexTrate™.

1.4. New approach to fabricating flexible microLED displays:

1.4.1. Novel mass-transfer approach using adhesive bonding

In this work [34], we develop and demonstrate a new wafer-level microLED mass transfer and assembly process using adhesive bonding and laser debonding [35] that can potentially attain > 99% transfer yields, see **Figure 1.5**. A thermoplastic, laser-debondable Polyimide based adhesive (HD3007) is used to attach the microLEDs to a temporary glass carrier before the LLO process [35]. The same adhesive, deposited on a lithographically patterned glass ‘stamp’, is used to transfer print selected arrays of programmably debonded microLEDs from the temporary carrier to a target flexible substrate. As strong adhesive bonding, instead of weaker electrostatic/electromagnetic or VdW forces, is used for the transfer printing, registration errors for the assembled devices can be kept to a minimum. The stamp used in this process is also very simple and no new equipment is needed to perform the mass transfer while using this approach. It is also less sensitive to sample planarity as the thickness of the adhesive used can be changed to account for non-planarity. Before the release process, the microLEDs are also supported using a 5-10µm thick electroplated Ni layer [35]. This electroplated support layer serves to protect the device from the high stresses involved during the LLO process thus preventing device cracking or surface pitting, see **Chapter 3**. We have demonstrated nearly a 100% LLO yield using this Ni stress buffer layer.

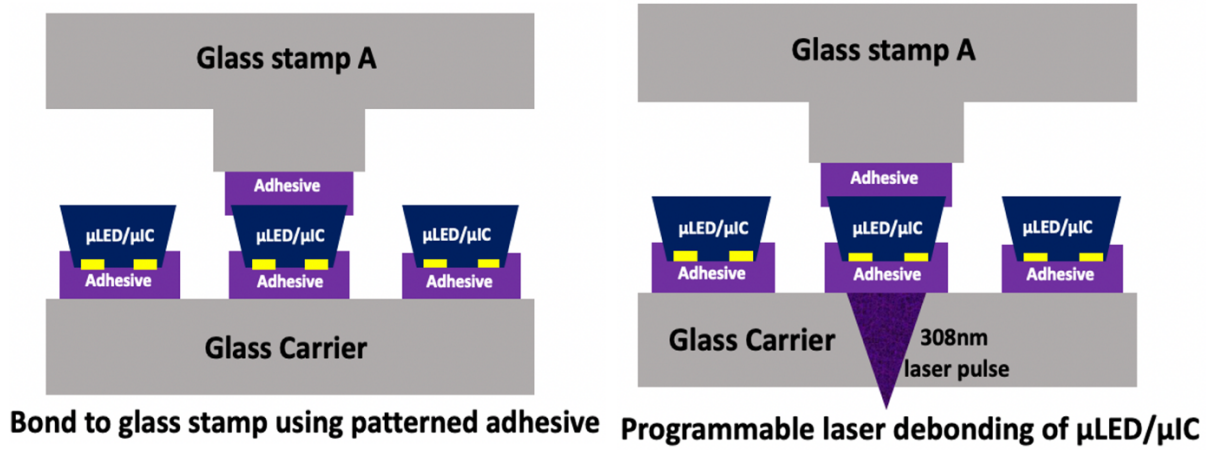


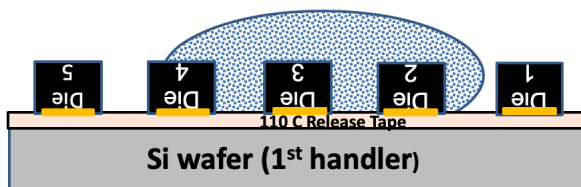
Figure 1.5. Novel mass transfer approach used in this work using adhesive bonding and laser debonding.

1.4.2. Novel flexible electronic integration approach using FOWLP

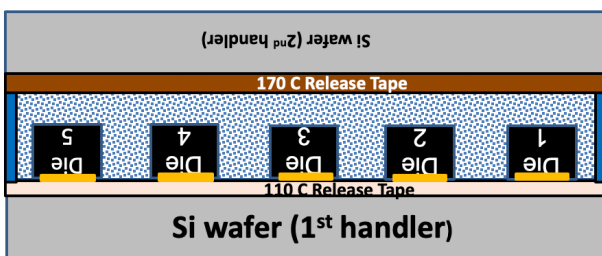
FlexTrate™ is a die first Fan-Out Wafer-Level Packaging (FOWLP) platform where dies are first assembled, using pick & place with $\sim 1\mu\text{m}$ placement accuracy, on a thermally releasable adhesive [36]. The wafer is then reconstituted by compression molding with a soft, biocompatible elastomeric compound (PDMS, Silastic MDX4-4210) that is cured at room temperature for 24 hours. The use of a low young's modulus molding compound ($E \sim 0.5\text{MPa}$) and room temperature curing allows us to attain less than $6\mu\text{m}$ die-shift across a 100mm diameter wafer. After the molding process, standard Si Back End of Line (BEOL) processes are used to interconnect the dies with electroplated Cu metallization at very fine interconnect pitch down to $20\mu\text{m}$. The process flow for FlexTrate™ is shown in **Figure 1.6**.



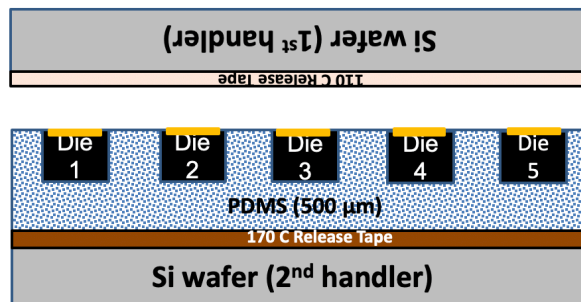
1. Placement of dies



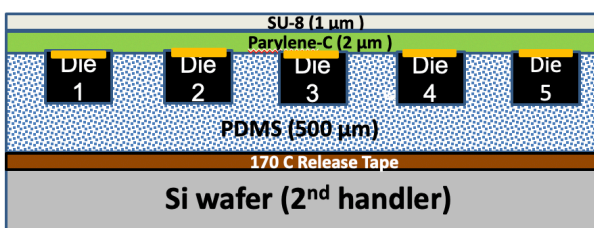
2. Dispense PDMS for molding



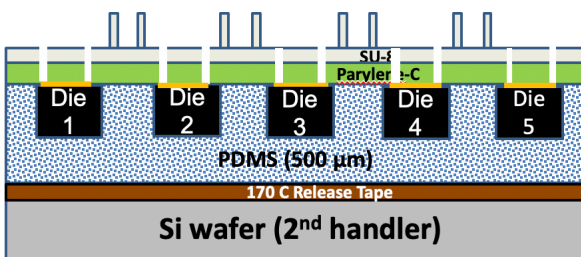
3. PDMS compression molding



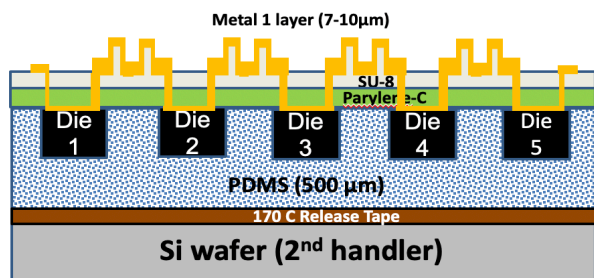
4. Thermal release of 1st handler



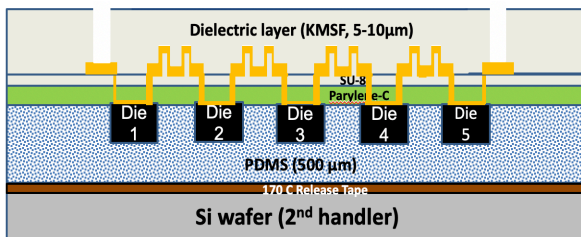
5. Deposition of stress buffer layers



6. SU-8 Corrugation and contact holes to dies



7. Plating of metal layer 1 (7 μm, semi-additive)



8. Spin coating and patterning of dielectric layer (SU-8 or KMSF)

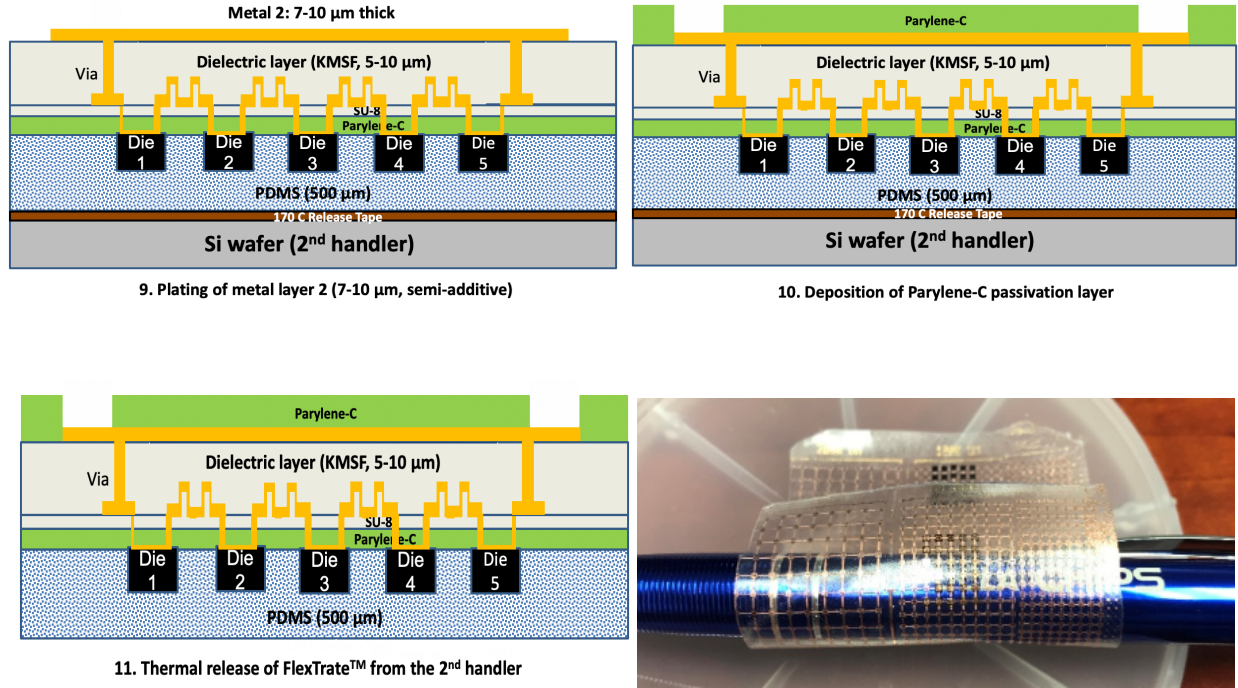


Figure 1.6. Fabrication process flow for FlexTrate™ [36].

In this work, FlexTrate™ process is used (along with the novel adhesive bonding based mass transfer approach) to demonstrate flexible microLED displays with unparalleled integration densities, heterogeneity, and overall performance. It overcomes several issues that were faced with the conventional flexible electronic integration approaches when applied to microLED display fabrication, see **Figure 1.7**:

(I) If we use a wafer reconstitution approach with embedded dies/components as in FlexTrate™, we can attain very planar surfaces irrespective of the die/component thickness variation.

(II) The FlexTrate™ process naturally supports heterogeneous integration by integrating the dies and the microLEDs in a seem-less fashion using die-first FOWLP,

hence avoiding flip-chip bonding, and can theoretically attain $< 20\mu\text{m}$ interconnect pitch.

(III) FlexTrate™ uses standard Back-End-Of-Line (BEOL) processing techniques for fabricating the RDL interconnects. Thick electroplated Cu metallization ($\sim 7\text{-}10\mu\text{m}$) is used and hence the issues described in section 1.3.2 with the thin film metallization of conventional flexible electronic integration approaches can be avoided.

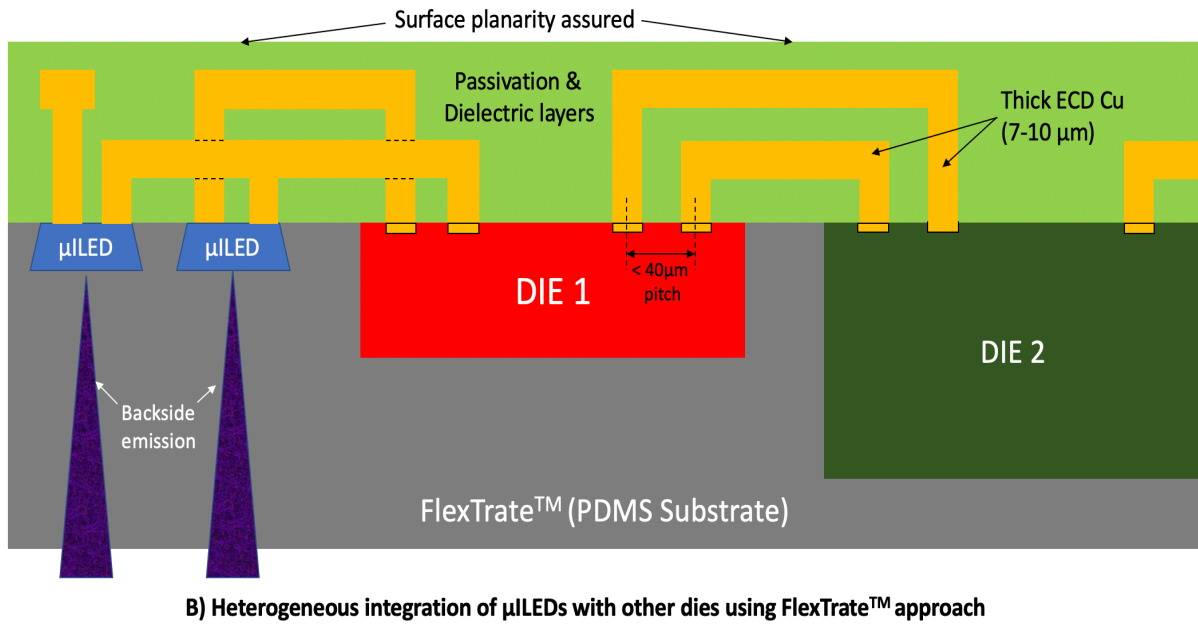


Figure 1.7. FlexTrate™ integration approach for making microLED displays.

1.5. Organization of this dissertation:

The remainder of this dissertation is organized as follows:

Chapter 2 illustrates the various process flows that are used for the fabrication of the flexible microLED displays on elastomeric (PDMS) substrates using the adhesive bonding-based mass transfer and FlexTrate™ process.

Chapter 3 talks about the work that has been done in developing an ultra-high yield GaN Laser Lift-Off (LLO) process using Ni stress buffer layers and a DPSS LLO process. Both experimental and theoretical work towards this development is discussed.

Chapter 4 goes into the experimental details of fabricating a flexible microLED display on FlexTrate™ using the processes developed and optimized in **Chapters 2 & 3**. Both the experimental results of a mass transfer approach and a dielet approach towards fabricating an InGaN/GaN blue microLED flexible display are discussed in detail.

Chapter 5 presents a summary of future work and potential research directions. It talks about preliminary work done in fabricating mass transfer safe microLEDs, demonstration of a wireless power transfer system on FlexTrate™ for powering of a microLED display for Optogenetics & potential demonstration of full color microLED displays on FlexTrate™ using colloidal Quantum Dots (QDs).

Chapter 6 presents a summary of contributions made in this dissertation.

REFERENCES

1. Robert, L.; Barbin, A.S.P. Cathode-ray tube displays. In *Wiley Encyclopedia of Electrical and Electronics Engineering*; Wiley Online Library: Hoboken, NJ, USA, 1999.
2. Tingzhu Wu et al., “Mini-LED and Micro-LED: Promising Candidates for the Next Generation Display Technology,” *Appl. Sci.* 2018, 8, 1557; doi:10.3390/app8091557.
3. L. E. Tannas, E. Glenn, J. W. Dorne (Eds.), *Flat-panel Display Technologies*, Noyes Publications, Parkridge, NJ (1995).
4. Gloria Hong et al., “A Brief History of OLEDs-Emitter Development and Industry Milestones,” *Adv. Mater.* 2021, 33, 2005630.
5. Jiang H. X., Jin S. X., Li J., Shakya J., Lin J. Y., 2001 III-nitride blue microdisplays, *Appl. Phys. Lett.* 78 1303-5.
6. Han E. L. et al., “Micro Light-Emitting Diodes for Display and Flexible Biomedical Applications,” *Adv. Funct. Mater* 2019, 29, 1808075.
7. Vincent W. Lee, Nancy Twu and Ioannis Kymissis, “Micro-LED Technologies and Applications,” *Information Displays* 06/2016.
8. Ajit Paranjpe et al., “Micro-LED Displays: Key Manufacturing Challenges and Solutions,” *SID 2018 Digest*, 597.
9. Zhen Chen et al., “MicroLED technologies and applications: characteristics, fabrication, progress, and challenges,” *J. Phys. D: Appl. Phys.* 54(2021) 123001 (34pp).
10. S. Aukstakalnis, “Practical Augmented Reality: A guide to the technologies, applications, and human factors for AR and VR,” *Pearson Education*, ISBN: 9780134094359.
11. J. Y. Lin, H. X. Jiang, “Development of microLED,” *Appl. Phys. Lett.* 116, 100502 (2020).

12. Francois Templier, "GaN-based emissive microdisplays: A very promising technology for compact, ultra-high brightness display systems," *Journal of the SID*, 24/11, 2016.
13. Linlin Chen et al., "Highly Transparent and Colorless Nanocellulose/Polyimide Substrates with Enhanced Thermal and Mechanical Properties for Flexible OLED Displays," *Adv. Mater. Interfaces* 2020, 7, 2000928.
14. R. F. C. Farrow et al., "Thin Film Growth Techniques for Low-Dimensional Structures," *Springer-Verlag US* 1987, ISBN: 978-1-4684-9147-0.
15. Khaled Ahmed, "Yield Statistics for Fault Tolerant Micro LED Displays," *Book I: Session 37: MicroLEDs: Manufacturing and Characterization*.
16. Kai Ding et al., "Micro-LEDs, a Manufacturability Perspective," *Appl. Sci.* 2019, 9, 1206; doi:10.3390/app9061206.
17. C. A. Bower et al., "Emissive displays with transfer-printed assemblies of $8\mu\text{m} \times 15\mu\text{m}$ inorganic light-emitting diodes," 2327-9125/17/020A23-07 *Journal 2017 Chinese Laser Press*.
18. Sang-il Park et al., "Printed Assemblies of Inorganic Light-Emitting Diodes for Deformable and Semitransparent Displays," *Science* Vol. 325, 21 August 2009.
19. C. H. Ko et al., "Photo-enhanced chemical wet etching of GaN," *Material Science and Engineering B96* (2002), 43-47.
20. T. Ueda et al., "Separation of Thin GaN from Sapphire by Laser Lift-Off Technique," 2011 *Jpn. J. Appl Phys.* 50041001.
21. Y. Sun et al., "Properties of GaN-based light-emitting diode thin film chips fabricated by laser lift-off and transferred to Cu," *Semicond. Sci. Technol.* 23(2008) 125022(4pp).

22. L. Li et al., "Heterogeneous Integration of Microscale GaN Light-Emitting Diodes and Their Electrical, Optical, and Thermal Characteristics on Flexible Substrates," *Adv. Mater. Technol.* 2018, 3, 1700239.
23. A. Carlson et al., "Transfer Printing Techniques for Materials Assembly and Micro/Nanodevice Fabrication," *Adv. Mater.* 2012, 24, 5284-5318.
24. A. Bibl et al., "Method of Transferring a Micro Device," LuxVue Technology Corporation, *US Patent No. 8333860 B1*, Dec 18, 2012.
25. K. Asano, F. Hatakeyama, and K. Yatsuzuka, "Fundamental Study of an Electrostatic Chuck for Silicon Wafer Handling," *IEEE Transactions On Industry Applications*, Vol. 38, No. 3, May/June 2002.
26. Andreas B., Higginson J. A., Law H-F S and Hu H-H 2013, "Micro device array for transfer to a receiving substrate," US8558243B2.
27. Peter J. Parbrook et al., "Micro-Light Emitting Diode: From Chips to Applications," *Laser Photonics Rev.* 2021, 15, 2000133.
28. David Gomez et al., "Manufacturing Capability of Micro-Transfer Printing," *Smart Systems Integration; 13th International Conference and Exhibition on Integration Issues of Miniaturized Systems*, April 2019.
29. H. Cheng et al., "A Viscoelastic Model for the Rate Effect in Transfer Printing," *Journal of Applied Mechanics*, Vol. 80 / 041019-1, July 2013.
30. P. Ramm, J. Lu, M. Taklo, "Handbook of Wafer Bonding," 2012 Wiley-VCH Verlag GmbH & Co. KGaA, ISBN: 978-3-5273-2646-4.
31. P. Garrou et al., "Handbook of 3D Integration, Vol. 3: 3D Process Technology," Wiley-VCH, July 2014, ISBN: 978-3-527-33466-7.

32. S. S. Iyer, "Heterogeneous Integration for Performance and Scaling," *IEEE transactions on components, packaging, and manufacturing technology*, Vol. 6, No. 7, July 2016.
33. Tae-il Kim et al., "Microscale Inorganic Light-Emitting Diodes on Flexible and Stretchable Substrates," *IEEE Photonics Journal*, Vol. 4, No. 2, April 2012.
34. Gong Z. et al, "Size-dependent light output, spectral shift, and self-heating of 400nm InGaN light-emitting diodes," *J. Appl. Phys.* 107 013103.
35. G. Ezhilarasu et al., "High Yield Precision Transfer and Assembly of GaN microLEDs using Laser Assisted Micro Transfer Printing," © 2019 IEEE 69th ECTC.
36. T. Fukushima et al., "FlexTrateTM – Scaled Heterogeneous Integration on Flexible Biocompatible Substrates using FOWLTP," © 2017 IEEE 67th ECTC, Orlando, FL, USA.

2. Process Flow for Flexible microLED Display

There are two approaches to making a flexible microLED display that were explored in this work:

(1) The mass transfer approach

(2) The dielet approach.

The mass transfer approach involves four major steps [1]:

- a. Release of prefabricated microLEDs from the growth substrate to a temporary carrier wafer.
- b. Selective adhesive bonding of a glass stamp to the released microLEDs on the temporary carrier.
- c. Selective transfer of bonded microLEDs from the temporary carrier to the stamp.
- d. Final transfer of microLEDs from the stamp to a target substrate using programmable laser de bonding
- e. Perform the FlexTrateTM flexible FOWLP process [2] for heterogeneous integration of microLEDs with display driver ICs for full display fabrication.

A schematic overview of the mass transfer process is given in **Figure 2.1**.

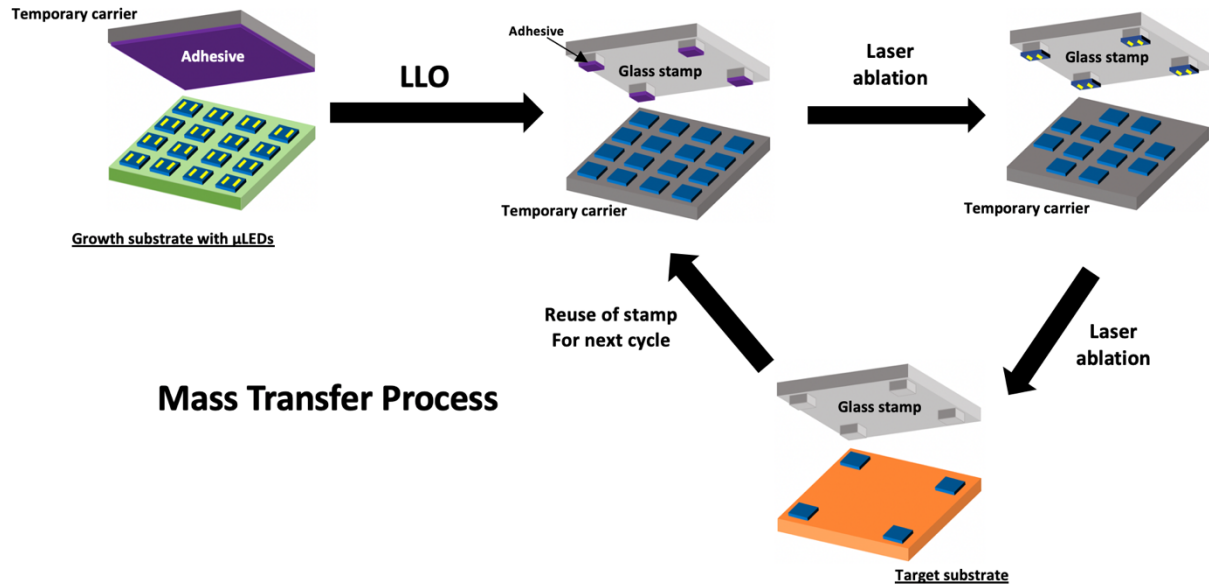


Figure 2.1. Rough schematic of a typical mass transfer process.

The dielet approach to making the flexible microLED display is much simpler and involves the following steps:

- a. Thinning of the growth substrate (sapphire) with the microLEDs to less than 200 μ m. The sapphire is also polished after the thinning to < 10nm RMS roughness to allow scattering-free light emission.
- b. Dicing of the substrate after thinning to < 1mm² dielets for assembly
- c. Pick & place of the 1mm² dielets with the microLEDs directly onto a target substrate using a standard die to wafer border.
- d. Perform the FlexTrateTM flexible FOWLP process for heterogeneous integration of microLEDs with display driver ICs for full display fabrication.

Now let us look at both these processes in more detail.

2.1. Mass Transfer Approach:

Figure 2.2 shows the detailed process flow of the mass transfer approach, refer [3] & [4]. Firstly, microLEDs prefabricated on c-plane sapphire substrates were purchased from a commercial manufacturer. The microLEDs are not yet completely singulated and have a 1 μ m thick uGaN layer between the fabricated device mesas as shown in **Figure 2.2(1)**.

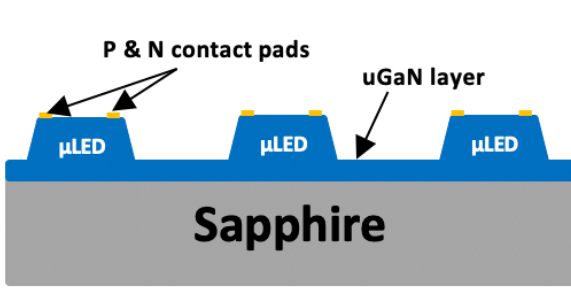
Next, a 5–10 μ m thick layer of Ni is electroplated on top of the microLED mesas using semi-additive electroplating. The Nickel layer is meant to serve as a stress buffer layer during the high stress laser ablation process used to detach the microLEDs from the sapphire called Laser Lift-Off (LLO) [5], discussed in **Chapter 3**. The same Ni layer is also used as a hard mask to dry etch the uGaN between the microLED mesas in a Cl₂/BCl₃/Ar plasma [6] to completely singulate the microLEDs, see **Figure 2.2(2)**. The singulated microLEDs with the protective Ni on top is now bonded to a temporary glass carrier using adhesive bonding as show in **Figure 2.2(3)**. The adhesive used is a thermoplastic, laser de-bondable polyimide from HD Microsystems called HD3007 [7]. The adhesive is spin coated on the temporary glass carrier to around 1- 2 μ m and then cured at 250°C. It is bonded to the devices at a temperature of around 265°C at a pressure of around 0.4 MPa. The next step is to detach the microLEDs from the sapphire and transfer them completely to the temporary glass carrier. This is done using a process called GaN Laser Lift-Off (LLO) where a high-power pulsed UV laser is excited from the sapphire side and used to ablate the GaN/Sapphire interface causing the microLED release [5], see **Figure 2.2(4)**.

The released microLEDs now sitting face down on the temporary glass carrier are first cleaned using a 5% (v/v) HCl solution to remove any metallic Ga residue [8] produced by the LLO process followed by ashing in an O₂ plasma (300W RF Power, 100 SCCM flow rate) to dry etch the adhesive between the devices; see **Figure 2.2(5)**. Now the sample is ready for the transfer printing process. A glass stamp with the same spin coated adhesive, HD 3007 is now aligned and bonded to the microLEDs sitting face down on the temporary glass carrier to selectively pick up the pattern of microLEDs to be assembled as shown in **Figure 2.2(6)**. The glass stamp is fabricated by dry etching 3µm tall mesas on a Borofloat-33 glass substrate in a C₄F₈/Ar plasma. The HD 3007 adhesive is then spin coated on the stamp and cured as before (about 1-2µm). The cured adhesive is then dry etched in an O₂ plasma to pattern it within the stamp mesas to control the amount of adhesive reflow. Alignment marks on the stamp are used to align to complimentary marks on the temporary carrier for accurate registration (less than 2µm accuracy). The bonded microLEDs are now to be selectively released to the glass stamp. This is done by laser de bonding using a 308 nm XeCl laser system (Excimer) as shown in **Figure 2.2(7)**. The laser debonding can be done in a selective or programmable manner: A shadow mask can be used in the system to pattern the incident focused light pulse to illuminate and hence debond only those microLEDs that are bonded to the stamp mesas, see **Figure 2.2(7)**. The microLEDs that are left on the temporary carrier can be used in the next cycle of mass transfer. The released microLEDs sitting exclusively (face up) on the glass stamp are now cleaned using O₂ plasma ashing followed by wet etching of the Ni stress buffer using Ferric Chloride to expose the contacts. The contacts can be probed at this stage

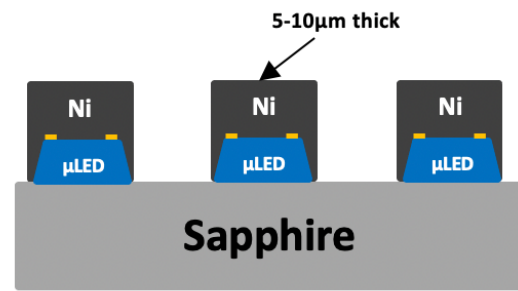
and device performance evaluations can hence be done before the final assembly on the target substrate, see **Figure 2.2(8)**. Now that we have the microLEDs sitting face up on the glass stamp, we can perform the FlexTrate™ process [2] to fabricate the full microLED display.

A 100mm Si or glass handler wafer laminated on one side with a Thermally Releasable adhesive Tape (TRT) is used as the FlexTrate™ carrier 1. The TRT has a release temperature of 110°C. The glass stamp with the tested microLEDs is now flip-chip placed on the TRT with alignment, see **Figure 2.2(9)**. Laser debonding using the 308 nm XeCl (Excimer) laser is now used to fully transfer the face down microLEDs to the TRT, see **Figure 2.2(10)**. This concludes the mass transfer process. Other components such as Si-CMOS display driver ICs, microcontrollers, power management chips etc., all in bare die form, can now be flip-chip placed on the same TRT with alignment (1-2µm accuracy) as shown in **Figure 2.2(11)**. After all the components have been assembled, PDMS is dispensed and then compression molded on top using a FlexTrate™ carrier 2, see **Figure 2.2(12) & 2.2(13)**. The Flextrate carrier 2 is also laminated with a TRT but having a higher release temperature of 170°C. The PDMS is cured at room temperature for 24 hours to minimize the die shift issue, see [2]. After fully curing the PDMS, the sample is heated to the release temperature of the carrier 1 to detach it, exposing a planar surface with the embedded microLEDs & ICs ready for metallization, see **Figure 2.2(14)**. The metallization process used is a standard Back End Of Line (BEOL) Redistribution layer (RDL) process, refer [9]. In this process, a seed layer of Ti/Cu is sputtered, followed by semi-additive electroplating of the Cu metal interconnects through a photoresist

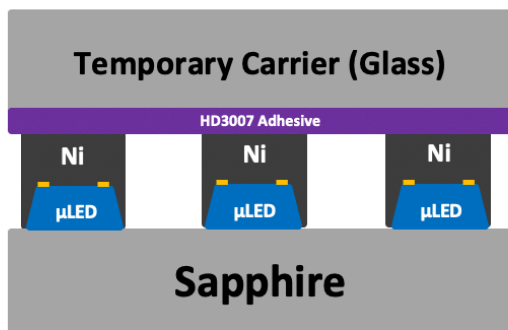
mask. The process is repeated to fabricate multiple levels of metallization. Up to two levels of Cu metal interconnects are needed for the display application. There are some subtleties to making flexible RDL interconnects on PDMS such as the need to vertically corrugate the interconnects to avoid buckling and the use of stress buffer layers on top of the PDMS to avoid metal delamination. These are discussed in more detail in reference [2]. After the fabrication of the two metallization layers, the sample is finally released by heating to the release temperature of carrier 2. The released sample thus heterogeneously integrates the GaN microLEDs and other IC components in a seamless fashion in the reconstituted PDMS substrate, see **Figure 2.2(15)**. This concludes the mass transfer approach of fabricating the flexible microLED display on FlexTrate™.



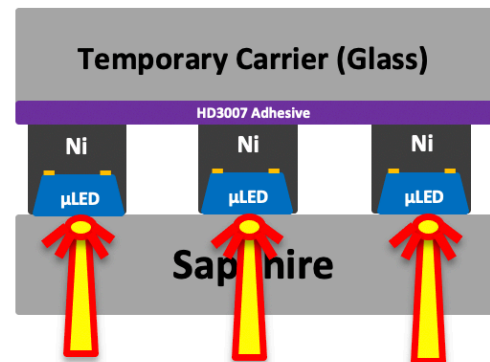
1. Fabricated μ LED on growth substrate



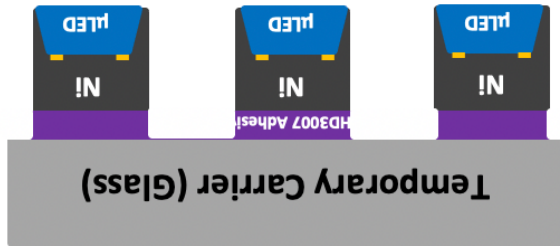
2. Deposition of a stress buffer & singulation



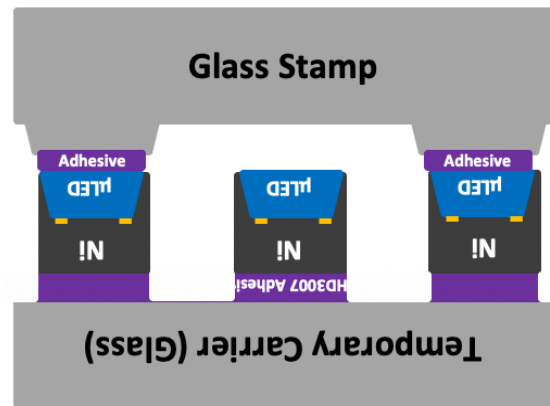
3. Adhesive bonding to temporary glass carrier



4. Release of μ LED using Laser Lift-Off (LLO)



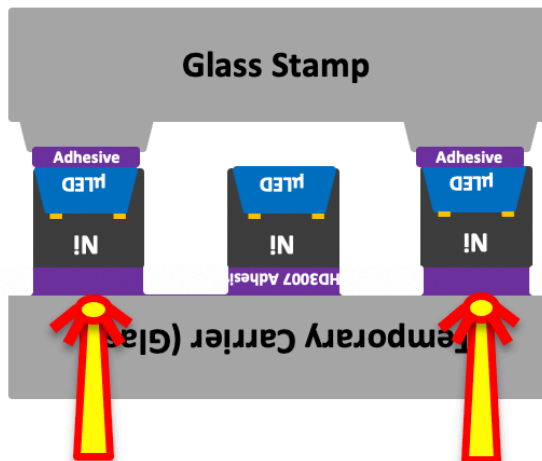
5. Dry etching of adhesive between devices



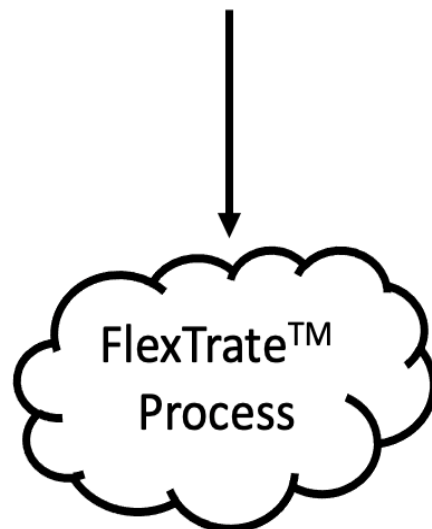
6. Adhesive bond to glass stamp

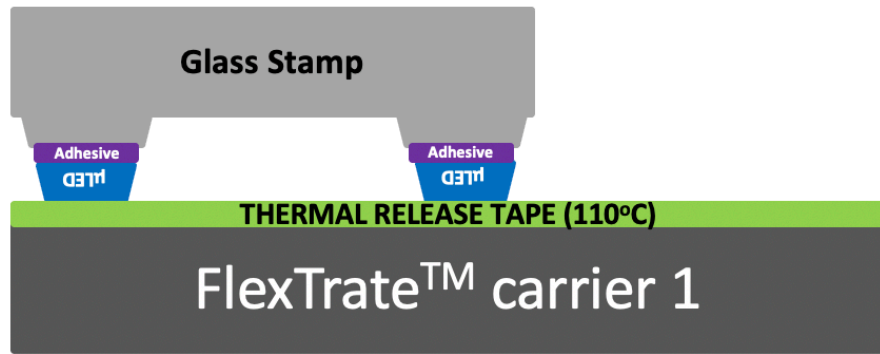


8. Removal of stress buffer with wet etch

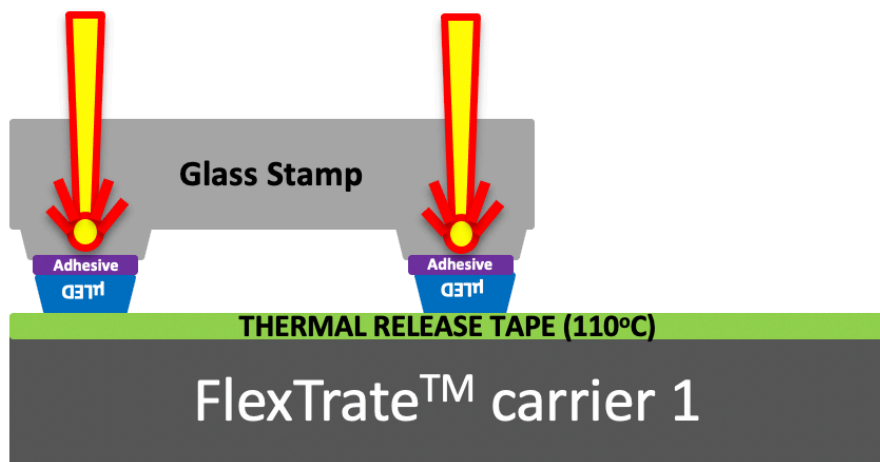


7. Programmable laser debonding with Excimer laser

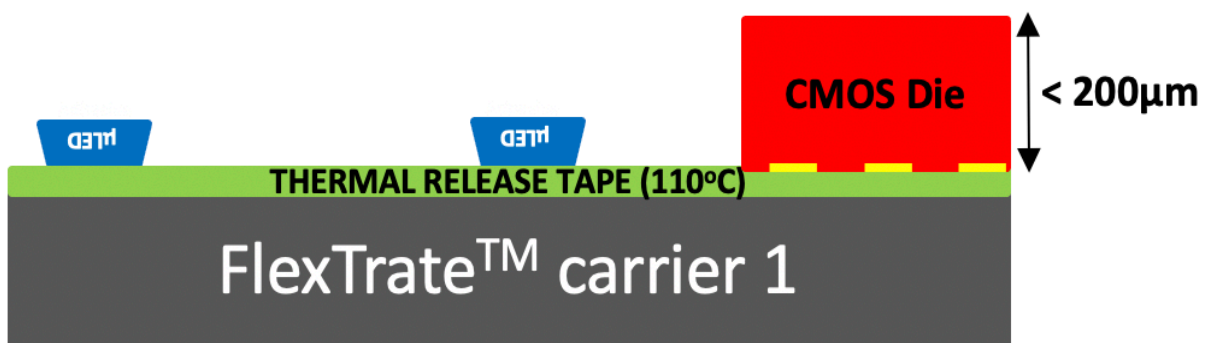




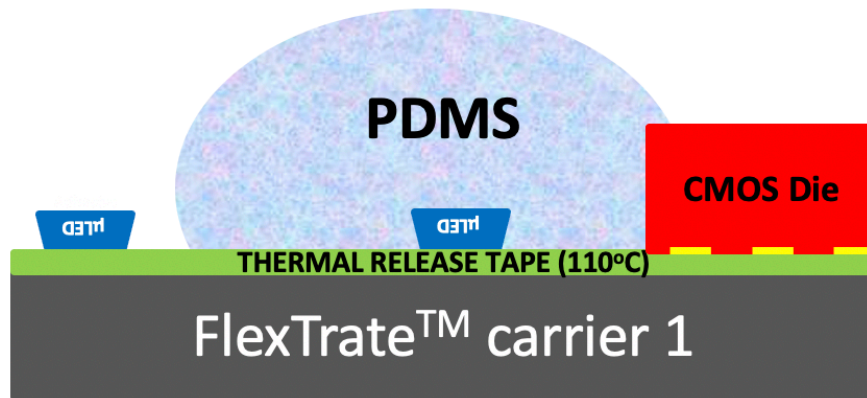
9. Assembly of Stamp on FlexTrate™ carrier 1



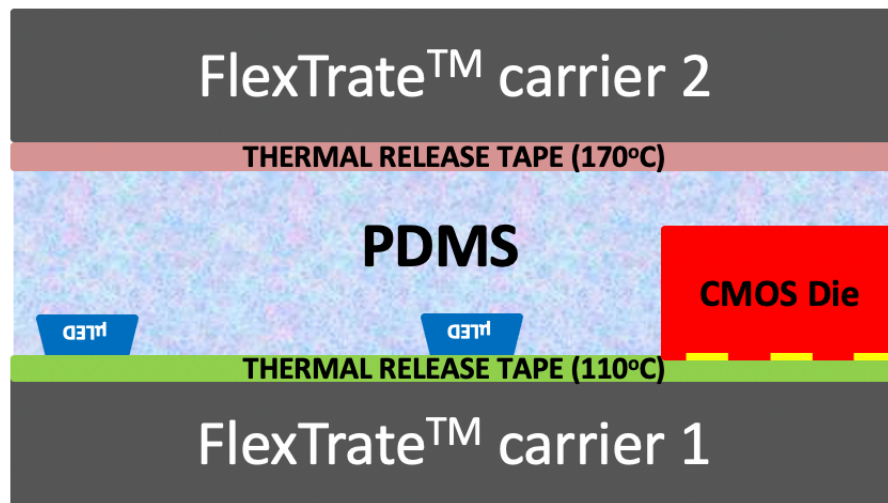
10. Laser debonding of Glass Stamp with Excimer laser



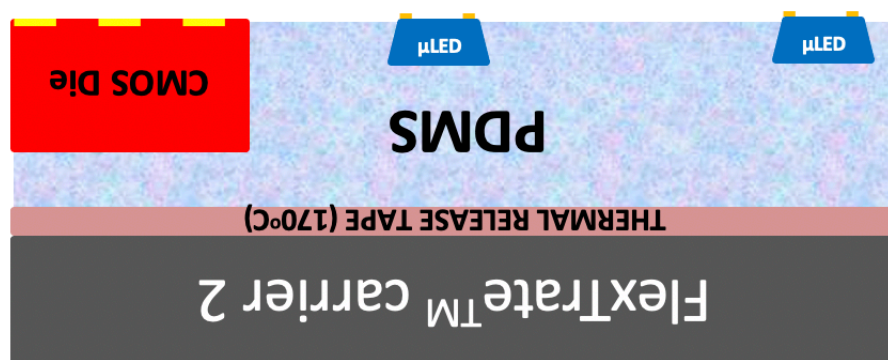
11. Flip chip bonding of other IC dielets



12. Dispensing of PDMS on assembled components



13. Compression molding of PDMS with FlexTrate™ carrier 2



14. Thermal debonding of FlexTrate™ carrier 1

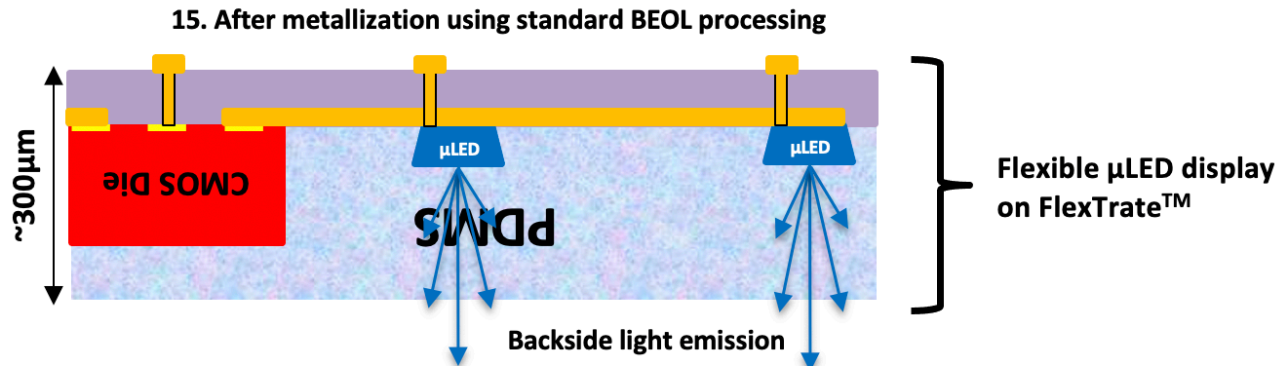


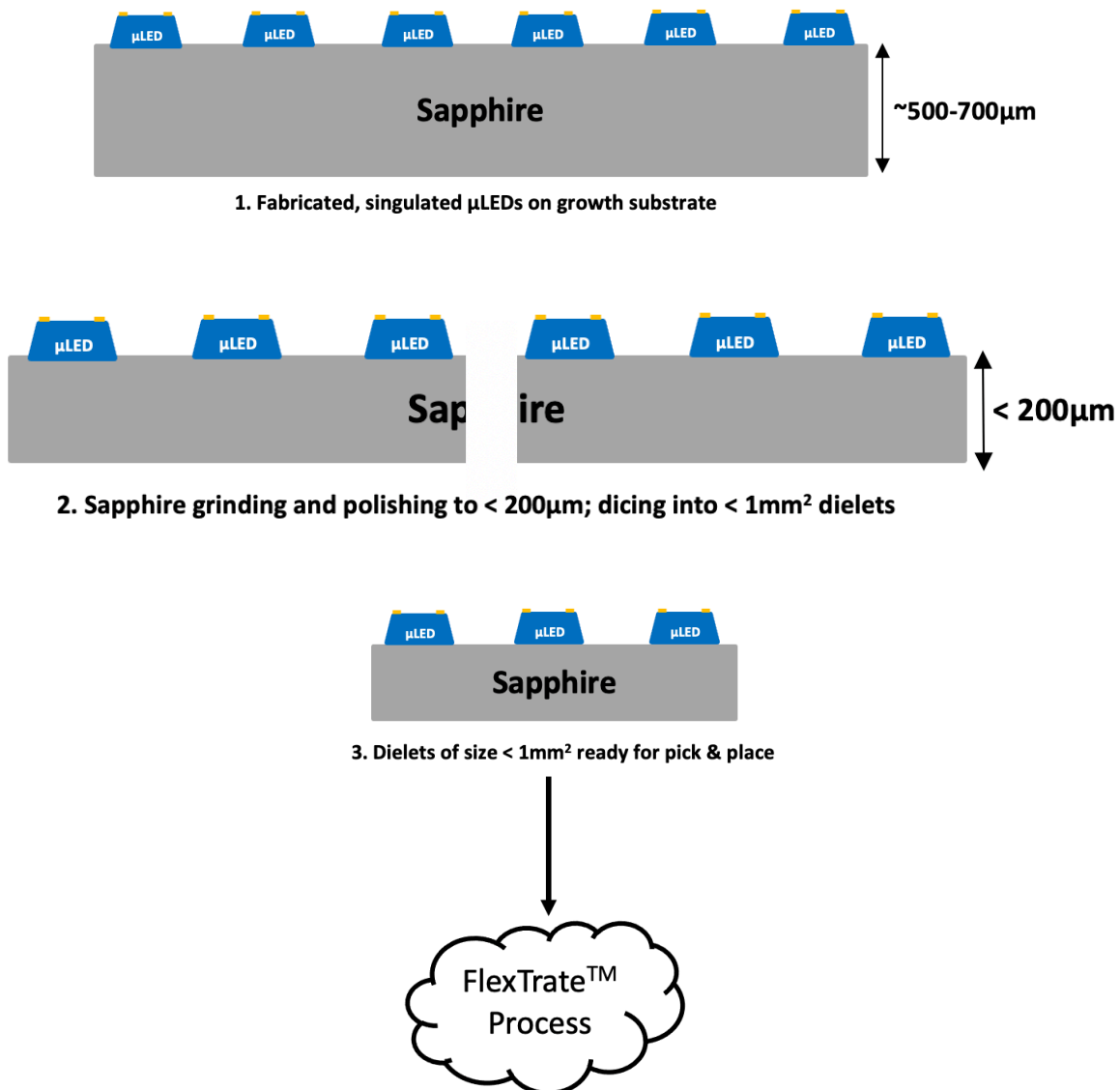
Figure 2.2. Mass Transfer approach to the fabrication of a flexible microLED display on FlexTrate™.

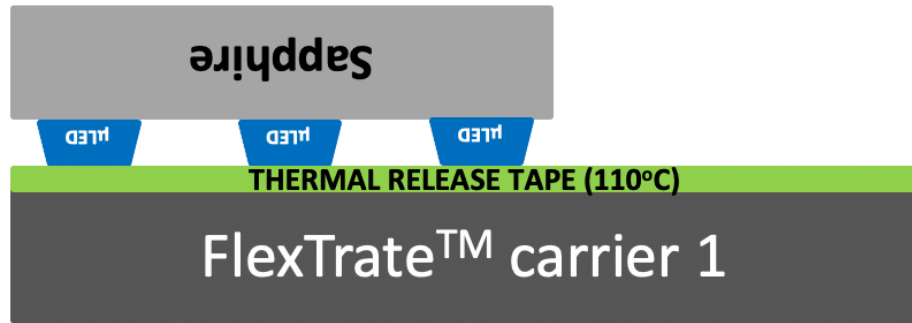
2.2. Dielet Approach:

Figure 2.3 shows a detailed schematic of the dielet approach to fabricating the flexible microLED display on FlexTrate™. Firstly, a sapphire substrate with singulated GaN microLEDs is obtained from a manufacturer as shown in **Figure 2.3(1)**. The typical sapphire substrate has a thickness of around 500-700μm. The substrate is then lapped and ground down to a thickness of around 200μm. The thinning process is followed by a polish step to an RMS roughness of less than 10 nm. The thinned, polished sapphire substrate with the singulated microLEDs is then diced into less than 1mm² dielets, see **Figure 2.3(2)** for details. The sapphire dielets with the microLEDs is now ready for pick & place assembly on the target flexible substrate using the FlexTrate™ process, see **Figure 2.3(3)**.

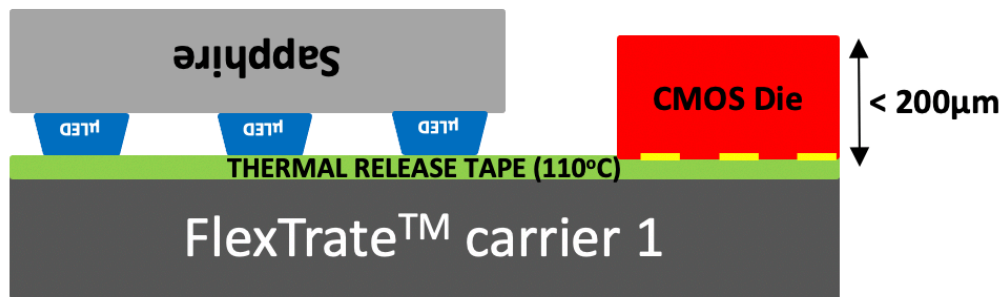
The Flextrate process is now done as before: the sapphire dielets with the microLEDs is picked & placed onto the TRT of the FlexTrate™ carrier 1 using a die to wafer bonder, see **Figure 2.3(4)**. Other components are now also flip chip placed onto the

TRT followed by the typical FlexTrate™ process: **Figures 2.3(5)-(9)**. The main difference in this approach is that the microLEDs are still attached to their growth substrate which is embedded in the PDMS. The light emission here happens first through the sapphire, then PDMS, before coming out as shown in the Figure. The flexibility of the fabricated display in this approach comes from the bicycle chain concept: rigid segments (sapphire dielets) separated by the flexible links (PDMS in inter-dielet space) makes the overall chain (FlexTrate™) flexible.

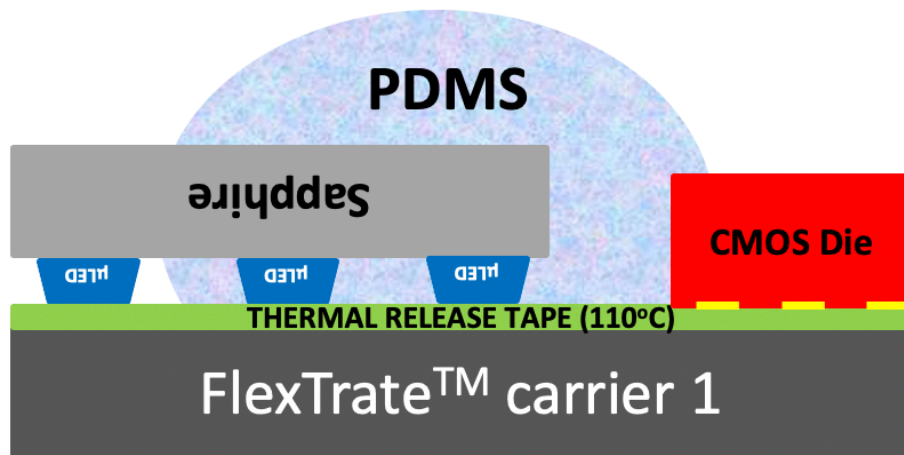




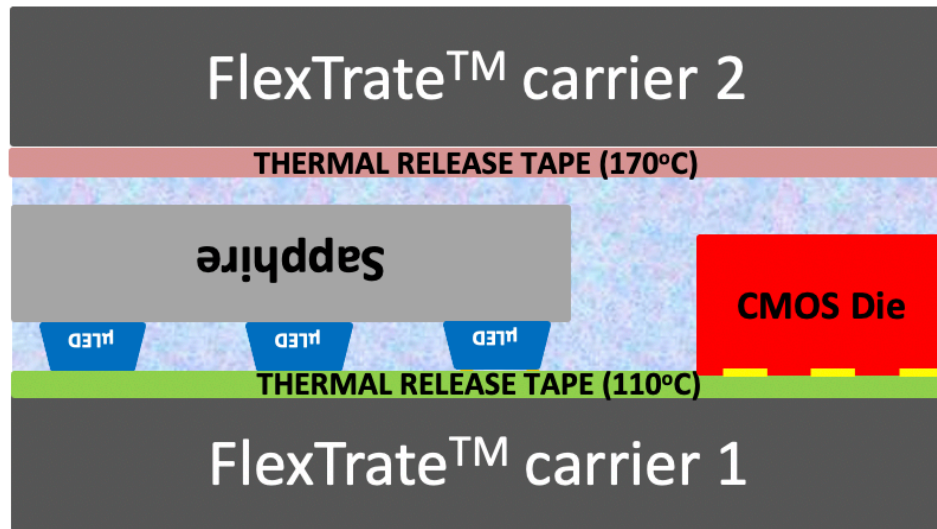
4. Flip chip placement of μ LED Sapphire dielet



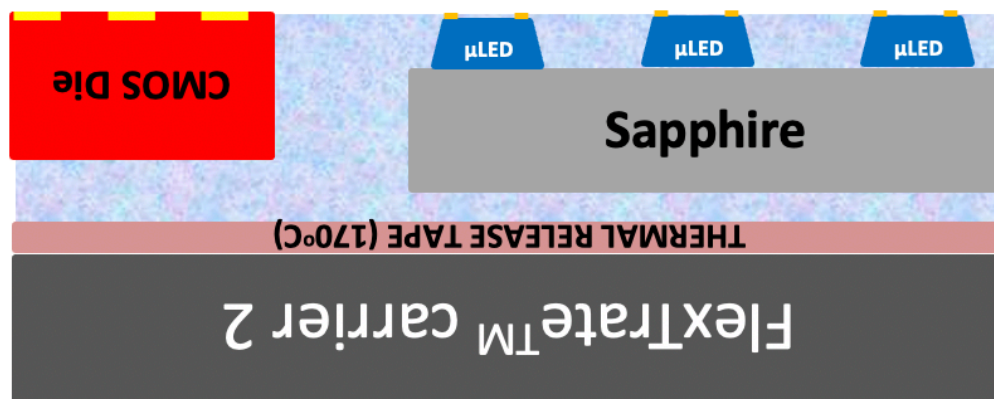
5. Flip chip placement of other IC components



6. Dispensing of PDMS on assembled components



7. Compression molding of PDMS with FlexTrate™ carrier 2



8. Thermal debonding of FlexTrate™ carrier 1

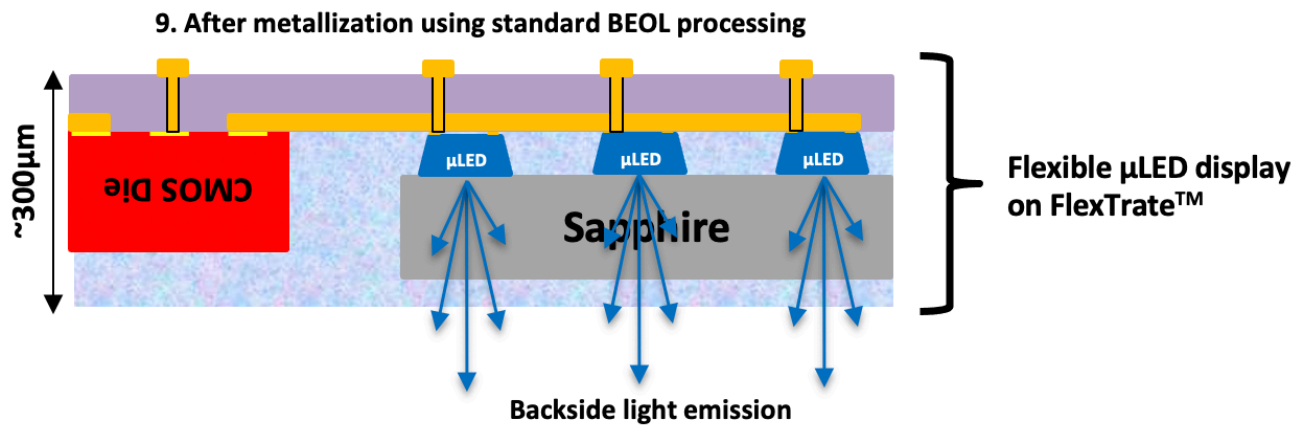


Figure 2.3. Dielet approach to the fabrication of a flexible microLED display on *FlexTrate™*.

A comparison between the two approaches to fabricating the flexible microLED display on FlexTrate™ is established in **Table 2.1**.

For most small-scale display prototyping applications, the dielet approach would be preferred due to its simplicity. For large scale manufacturing of microLED displays, the mass transfer approach would be preferable.

Attribute	Mass Transfer Approach	Dielet Approach
Process complexity	2 adhesive bonding and 3 laser debond steps needed for assembly onto target (COMPLEX)	Wafer thinning, dicing and dielet pick & place are the only steps needed for assembly onto target (SIMPLE)
Process Throughput	High throughput as large stamps can be used	Low throughput as dielet size needs to be small for flexibility
μLED structure dependence	Does not work with conventional LED structure; stress buffer layers needed to make contacts robust	Independent of μLED structure
Pixel Per Inch (PPI)	PPI limited by adhesive reflow and thermal expansions during stamping; PPI > 500 difficult	PPI limited by spacing between dielets on FlexTrate; PPI > 300 difficult
Flexibility	Limited by flexibility of the metallization on FlexTrate™, 1mm bending possible (A. Hanna et al., ECTC.2018.00229)	Comes from bicycle chain concept hence limited by die spacing. For a 1mm ² die with 0.3mm spacing, ~5mm bending possible

Table 2.1. Comparison between the Mass Transfer and Dielet approaches to fabricating a flexible microLED display on *FlexTrate™*.

REFERENCES

1. H. E. Lee et al., "Micro Light-Emitting Diodes for Display and Flexible Biomedical Applications," *Adv. Funct. Mater.* 2019, 29, 1808075.
2. A. Hanna et al., "Extremely Flexible (1mm bending radius) Biocompatible Heterogeneous Fan-Out Wafer-Level Platform with the Lowest Reported Die-Shift ($<6\mu\text{m}$) and Reliable Flexible Cu-based Interconnects," *2018 IEEE 68th ECTC*.
3. G. Ezhilarasu et al., "High Yield Precision Transfer and Assembly of GaN microLEDs using Laser Assisted Micro Transfer Printing," *2019 IEEE 69th ECTC, Las Vegas, NV*.
4. G. Ezhilarasu et al., "A Heterogeneously Integrated, High Resolution and Flexible Inorganic microLED Display using Fan-Out Wafer-Level Packaging," *2020 IEEE 70th ECTC*.
5. T. Ueda et al., "Separation of Thin GaN from Sapphire by Laser Lift-Off Technique," *Japanese Journal of Applied Physics* 50(2011) 041001.
6. S. J. Pearton, R. J. Shul and Fan Ran, "A Review of Dry Etching of GaN and Related Materials," *MRS J. Nitride Semicond. Res.* 5, 11 (2000).
7. K. Zoschke et al., "Polyimide Based Temporary Wafer Bonding Technology For High Temperature Compliant TSV Backside Processing and Thin Device Handling," *SUSS MicroTec report* 02/2012.
8. Tae-il Kim et al., "High-Efficiency, Microscale GaN Light-Emitting Diodes and Their Thermal Properties on Unusual Substrates," *small* 2012, 8, No. 11, 1643-1649.

3. High Yield GaN Laser Lift-Off (LLO)

In this chapter, we will dwell further into the GaN Laser Lift-Off (LLO) process that is used to separate the fabricated microLEDs from their growth substrate, sapphire. We will discuss how the GaN LLO process is performed, what its challenges are and how the yield of the process can be significantly improved by adopting the appropriate laser system and using stress buffers.

3.1. Introduction to the GaN LLO Process

Figure 3.1 shows a cross section of the GaN LLO process. A high-power UV (200-350 nm) pulsed laser is illuminated through the polished sapphire side. Sapphire has a large bandgap of 9.5eV and hence the light passes through without much attenuation. However, when the light hits the interface, it is absorbed within a few hundred nanometers of the GaN. Due to the pulsed nature of the incident laser light source, it can deliver a very high power to the GaN film within a very short time of 10-20ns. The absorbed light power is immediately converted to heat and the temperatures at the interface can soar to 1000s of degrees Celsius. This intense temperature would cause spontaneous dissociation of the GaN (s) to Ga(s) and N₂ (g).



This process is commonly referred to as laser ablation. The released Nitrogen gas absorbs the heat and expands rapidly providing the force necessary for the GaN film to release, refer to [1]. There are however significant yield issues with this process,

see [2]. The main reason for the yield issues is the cracking or damage to the released GaN thin films due to the high stresses produced during the ablation process: (1) The large transient temperature gradients near the interface produces a thermomechanical stress shockwave that travels up into the GaN film. This wave has both a shear and normal component. (2) The rapid thermal expansion of the released Nitrogen gas produces a pressure shockwave that acts normally on the released GaN film and travels up in the film at the speed of sound. A combination of both these mechanical stresses can cause significant damage to the released GaN films such as pitting, or even cracking, see **Figure 3.2**. In this work, the use of a Diode Pumped Solid State (DPSS) laser to perform the LLO in combination with an engineered protective stress buffer layer on top of the microLEDs prior to liftoff, helps to significantly improve yield to nearly a 100% [3] & [4].

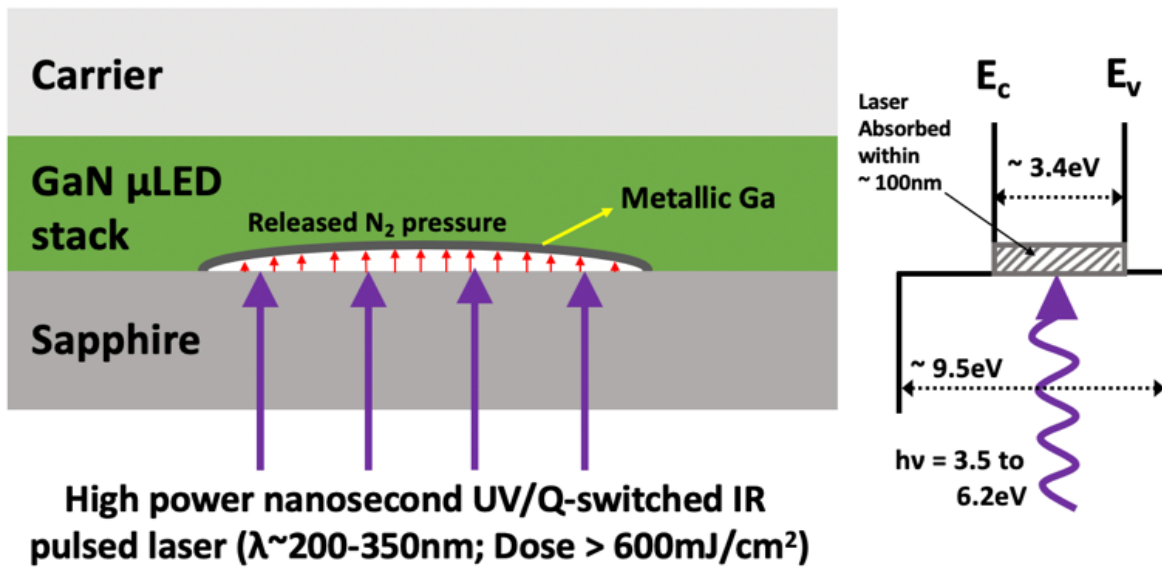


Figure 3.1. Schematic of the LLO process along with the band diagram of the GaN/sapphire interface [3].

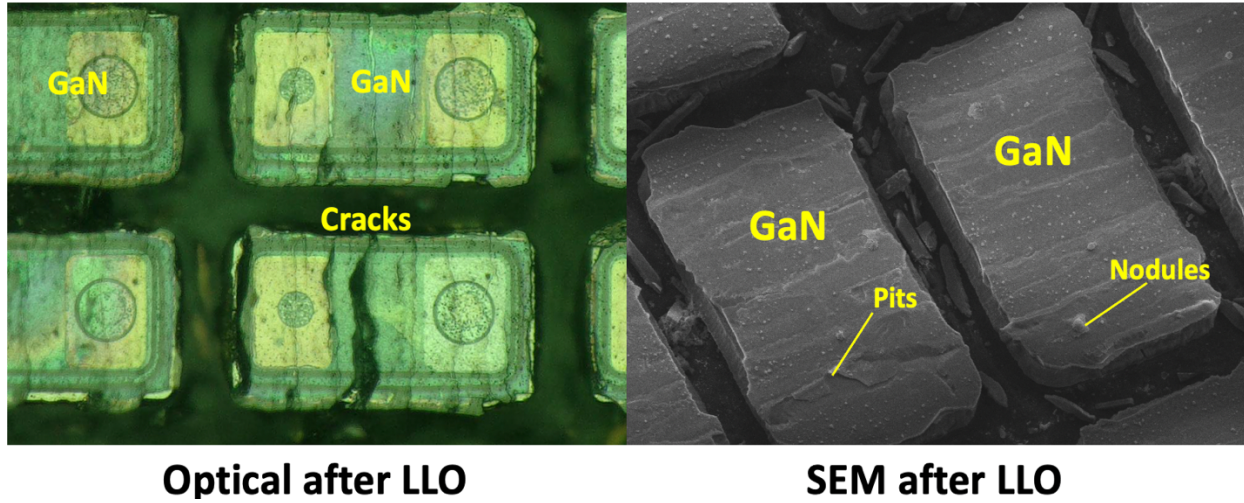


Figure 3.2. Film failure and cracking during the process of GaN Laser Lift-Off (LLO).

3.2. GaN LLO using DPSS laser

Any pulsed laser with a high enough pulse power can be used to perform the liftoff. The commonly used laser systems for performing the liftoff process are summarized in **Table 3.1**.

Attribute	Excimer Laser		Q-switched 3 rd harmonic solid state (Nd:YAG)
	KrF	XeCl	
Energy(mJ)/pulse	~600	~400	~200
Pulse width (ns)	~40	~30	~10
Rep. rate (Hz)	~50-100	~50-100	<10
Wavelength (nm)	248	308	355

Table 3.1. Commonly used laser systems for GaN LLO.

An Excimer laser uses a gas such as XeCl or KrF as the lasing medium. The output laser intensity profile is relatively rough even after homogenization [4]. This roughness in the light intensity profile could cause non-uniform local heating after being absorbed inducing damages. Excimer lasers also have an extremely high fluence per pulse $\gg 1\text{J}/\text{cm}^2$ with a large spot size spanning millimeters. They are hence not suitable for microLED fabrication or wafer-level sapphire liftoff, where epi features are extremely close to each other and/or epi layer is continuous along the sapphire interface. Any overlapping of the beam spots would result in epi-burning or damages, yet any small gaps in between the pulses will result in skipping LLO for fine features of microLED devices. A DPSS laser system on the other hand would be more suitable for the liftoff of microLEDs [4]. The fluence per pulse is smaller, $< 1\text{J}/\text{cm}^2$ while the repetition rate of the laser is extremely fast (10s to 100s of Hz). Furthermore, DPSS laser beam intensity profiles are close to a well-defined Gaussian shape due to solid state laser beams always achieving low transverse modes upon leaving the resonant cavities. The highest intensity spot within a DPSS laser pulse is always known to be at the beam center. Consequently, during LLO, any epi location at the GaN/sapphire interface can be lifted-off by 10s to 100s of overlapping 'gentle' Gaussian pulses with small beam spot sizes. Also, the precise overlapping of the gaussian pulses can help avoid any gaps during the liftoff.

A comparison between the two LLO systems is summarized in **Table 3.2**. Due to the advantages of the DPSS LLO process, it was selected for this work. The process was done at DISCO Corp., Japan using the commercially available DFL7560L laser System. A schematic of the laser control system used for overlapping and rastering

of the Gaussian pulses is given in **Figure 3.3**. The in-process camera view of connecting DPSS LLO Gaussian pulses at an interior pocket of a continuous GaN epi-layer on a sapphire wafer is given in **Figure 3.4**.


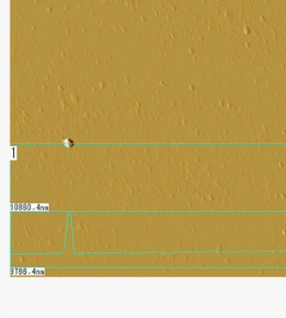
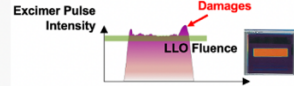

Laser type	Excimer	DPSS
AFM / OM Inspection		
Damage	Epi Peeling & Burning	No damages to epi
Pulse intensity profile		

Table 3.2. Comparison between Excimer lasers and DPSS lasers for GaN LLO [4].

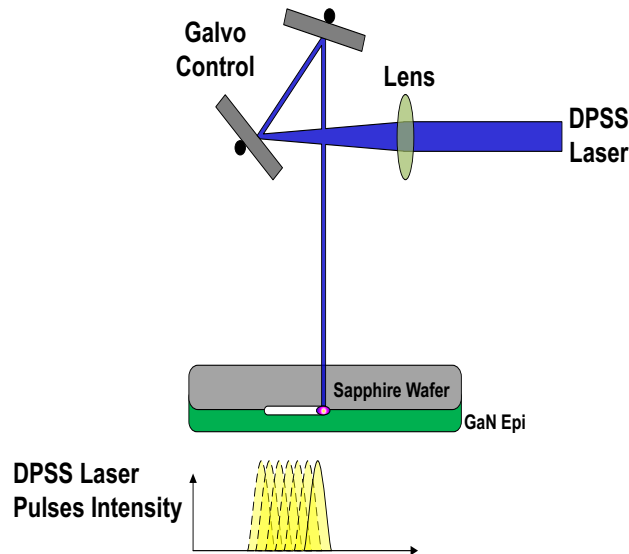


Figure 3.3. Illustration of DPSS laser wafer-level LLO system used at DISCO Corp. [4].

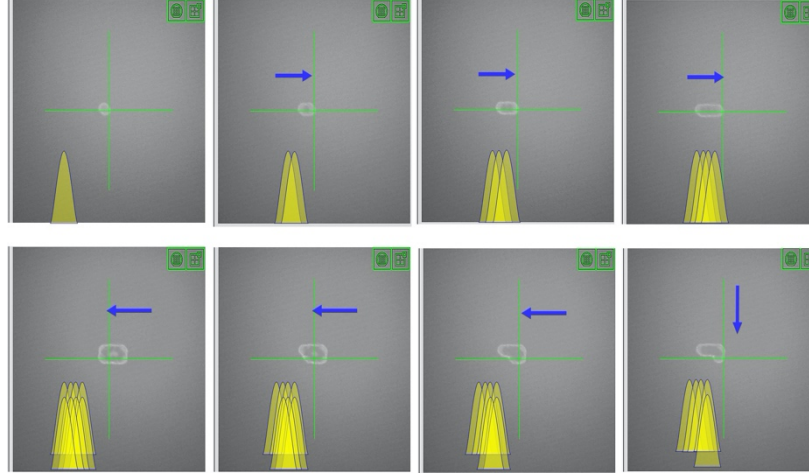


Figure 3.4. Screen shots of in-process camera view of connecting DPSS LLO pulses at an interior pocket of a continuous GaN epi on sapphire wafer [4].

3.3. Analytic Modeling of the GaN LLO process

For a general GaN thin film on sapphire as shown in **Figure 3.5**, due to the high growth temperature of the film ($\sim 900^\circ\text{C}$) and the CTE mismatch between GaN ($\sim 3\text{--}5\text{ppm}/^\circ\text{C}$) & sapphire ($\sim 8\text{ppm}/^\circ\text{C}$), at room temperature the film is under extreme compressive stresses of around 1GPa [5]. During the LLO of GaN, when the film is delaminated from the underlying sapphire substrate, this compressive stress is released causing the bucking of the GaN thin film upwards as shown in **Figure 3.5**. This bucking up of the film could induce significant cracking if the buckling height ‘h’ is too high [5]. For patterned GaN thin films (singulated microLEDs of $<100\mu\text{m}$ size) as used in this work, the compressive stress within the film which varies inversely with the film aspect ratio (height/width), decreases significantly. Also, by using larger beam spot sizes larger than the width of the GaN thin film, this bucking up of the film after LLO can be completely prevented. Contribution of these intrinsic

compressive stress effects and film buckling during LLO for our case can hence be neglected. The main contribution to the LLO induced cracking is hence solely due to the thermomechanical shockwave and pressure shockwave of the released N_2 gas as discussed in section 3.1 and will be studied in detail in section 3.4.

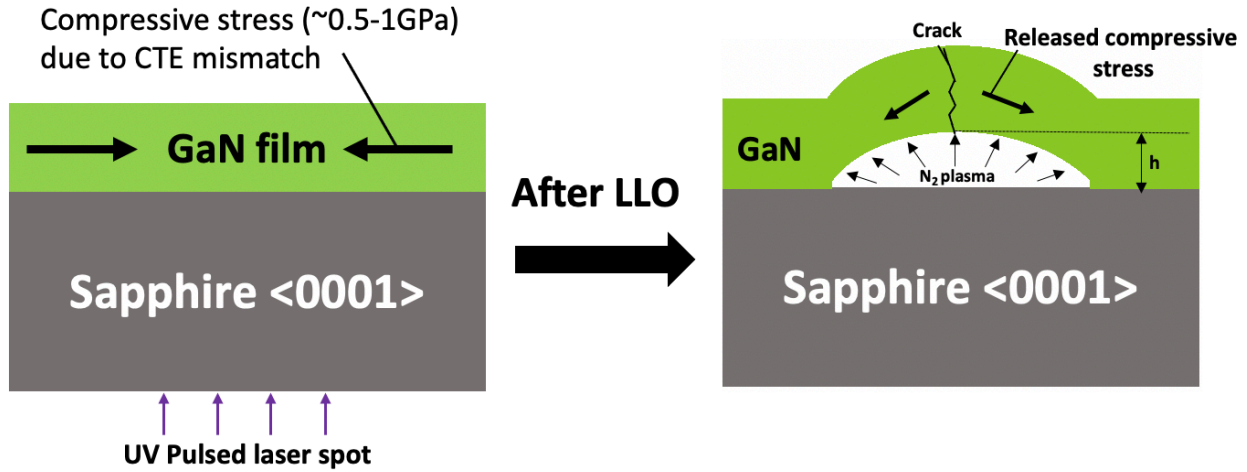


Figure 3.5. Bucking of GaN thin films after LLO due to growth induced compressive stress.

To get a first order understanding of stress wave generation and propagation in the GaN thin films during the LLO process, a simple analytic model was derived (following [6]) by considering only the normal component of the stress due to the expanding N_2 plasma at the ablation interface. Let us model the GaN thin film as a cylindrical volume of area A with the end released from the sapphire ($z=0$) being subjected to the following time-varying strain excitation function $\epsilon(0,t)$ that closely emulates the effect of the expanding and then rapidly cooling hot N_2 plasma:

$$\epsilon(z=0,t) = \frac{\epsilon_0}{t_0} t \quad \text{for } 0 \leq t \leq t_0 ; \text{Linearly increasing strain due to gas expansion}$$

$\epsilon(z=0, t) = \epsilon_0$ for $t_0 \leq t \leq t'$; Breif duration of constant strain

$\epsilon(z=0, t) = 0$ for $t \geq t'$; Gas cools off rapidly hence strain $\rightarrow 0$

At any location within the GaN film, stress (σ) and strain (ϵ) are related and given by the following analytic expression (see [6]):

$\sigma(\epsilon) = E\epsilon$, $\epsilon < \epsilon_y$; Elastic regime where ϵ_y is the yield strain

$\sigma(\epsilon) = E\epsilon_y + \frac{a(\epsilon - \epsilon_y)}{b - (\epsilon - \epsilon_y)}$, $\epsilon \geq \epsilon_y$; Plastic regime where $a = 6.41e^5 \frac{Kg}{m^2}$ & $b = 0.9$

The values of a and b given are for <0001> oriented GaN thin films grown on c-plane sapphire substrates. A plot of the strain excitation function ($\epsilon(0, t)$ vs t) and the stress-strain relationship of GaN is given in **Figure 3.6**.

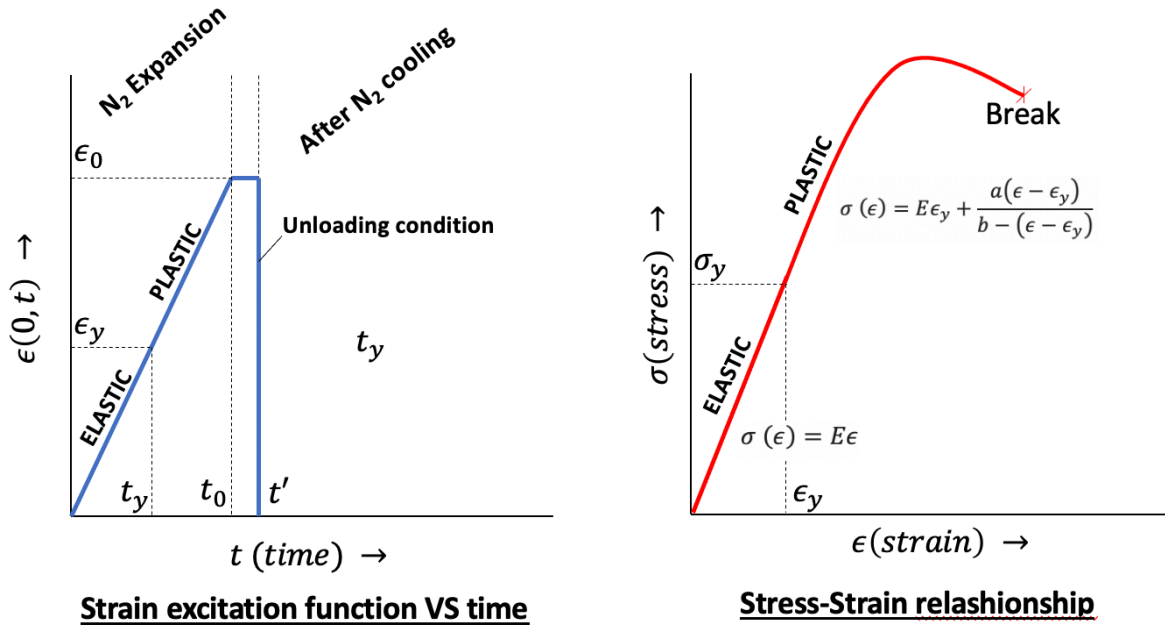


Figure 3.6. Strain excitation function Vs. time (left) and stress-strain relationship (right).

Now to understand the stress wave generation within the film due to this strain excitation at the GaN film ablation interface at $z=0$, refer to **Figure 3.7** to derive the equation of motion.

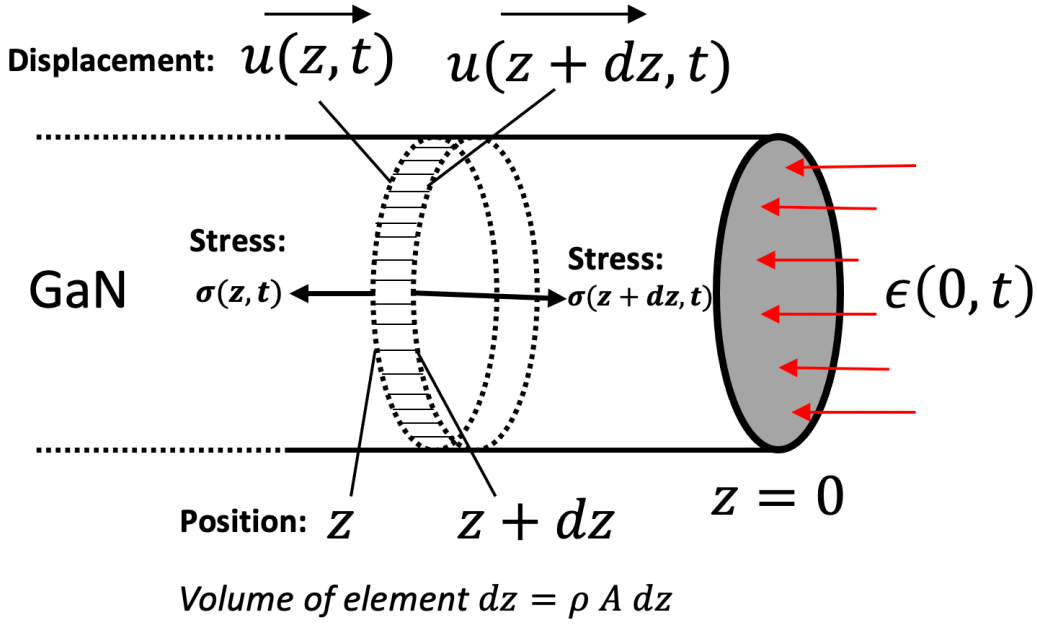


Figure 3.7. Analytic model of normal stress wave generation in GaN thin film, assumed cylindrical, during LLO.

According to Newton's second law of motion, the force acting on any element dz along the length of the GaN thin film is given by:

$$F = ma = (\rho A dz) \frac{\partial^2 u(z, t)}{\partial t^2} \quad (3, 1)$$

Where $\rho = 6.15 \text{ g/cm}^3$, and $u(z, t)$ is the local displacement of the GaN thin film at a location z . The strain on an element dz , which is nothing but the ratio of the change in the length of the element to the original length of the element ($\epsilon = \Delta l/l$) is given by:

$$\epsilon(z, t) = \frac{[(z + u(z, t)) - (z + dz + u(z + dz, t))] - [z - (z + dz)]}{z - (z + dz)} \quad (3, 2)$$

$$\epsilon(z, t) = \frac{u(z + dz, t) - u(z, t)}{dz} = \frac{\partial u(z, t)}{\partial z} \quad (3, 3)$$

Now to find an expression for force on an element dz in the cylinder, referring again to **Figure 3.7**, we find that:

$$\text{Force on an element } dz = [\sigma(z + dz, t) - \sigma(z, t)]A \quad (3, 4)$$

Plugging the expression for force **(3,4)** into the equation of motion **(3,1)** we get:

$$\begin{aligned} [\sigma(z + dz, t) - \sigma(z, t)]A &= (\rho Adz) \frac{\partial^2 u(z, t)}{\partial t^2} \\ \Rightarrow \frac{\sigma(z + dz, t) - \sigma(z, t)}{dz} &= \rho \frac{\partial^2 u(z, t)}{\partial t^2} \\ \Rightarrow \frac{\partial \sigma(z, t)}{\partial z} &= \rho \frac{\partial^2 u(z, t)}{\partial t^2} \quad (3, 5) \end{aligned}$$

We know that the stress, $\sigma(z, t)$ is an exclusive function of the strain (ϵ) at any location z , $\sigma = \sigma(\epsilon(z, t))$; we can thus use the chain rule of differentiation to re-write equation **(3,5)**:

$$\begin{aligned} \frac{\partial \sigma(\epsilon)}{\partial z} &= \left[\frac{d\sigma(\epsilon)}{d\epsilon} \frac{\partial \epsilon(z, t)}{\partial z} \right] = \rho \frac{\partial^2 u(z, t)}{\partial t^2} \\ \Rightarrow \left[\frac{d\sigma(\epsilon)}{d\epsilon} \frac{\partial}{\partial z} \left(\frac{\partial u(z, t)}{\partial z} \right) \right] &= \rho \frac{\partial^2 u(z, t)}{\partial t^2}, \text{ using equation (3,3)} \quad (3, 6) \end{aligned}$$

Rearranging the terms in equation **(3,6)**, we get the normal stress wave equation as:

$$\Rightarrow \frac{\partial^2 u(z, t)}{\partial z^2} - \frac{1}{\left(\sqrt{\frac{1}{\rho} \frac{d\sigma(\epsilon)}{d\epsilon}} \right)^2} \frac{\partial^2 u(z, t)}{\partial t^2} = 0 \quad (3, 7)$$

where $c = \sqrt{\frac{1}{\rho} \frac{d\sigma(\epsilon)}{d\epsilon}}$ is the speed of the normal stress wave in the GaN thin film

The stress waves are generated at the ablation interface due to the strain excitation function (Page **61-62**) and propagate in the GaN thin film with different speeds depending on whether the strain is in the elastic or plastic region of the stress-strain curve. In the elastic region ($\epsilon < \epsilon_y$), all generated stress waves travel with the same speed $c_E = \sqrt{E/\rho}$, where E (~ 180 GPa) is the Young's modulus of the GaN thin film. As all the stress waves generated in the elastic region of the excitation travel with the same speed c_E , they never meet at any location in the film and hence no shockwave is formed. In the plastic region ($\epsilon \geq \epsilon_y$), the generated stress waves travel with a strain dependent speed $c_p(\epsilon)$ given by:

$$c_p(\epsilon) = \sqrt{\frac{1}{\rho} \frac{d}{d\epsilon} \left[E\epsilon_y + \frac{a(\epsilon - \epsilon_y)}{b - (\epsilon - \epsilon_y)} \right]} = \sqrt{\frac{ab}{\rho} \frac{1}{(b - (\epsilon - \epsilon_y))^2}} \quad (3, 8)$$

We thus find that as the strain excitation in the plastic region increases ($\epsilon \uparrow$), the speed of the generated stress wave (from the ablation interface) c_p also increases. Thus, in this region, latter generated stress waves travel faster than the former ones and can hence potentially meet at some point within the GaN film and constructively add forming a shockwave. The formation and propagation of such a shockwave in the GaN thin film can cause significant cracking or film damage due to the large stress.

To find an expression for the location z^* within the GaN film where and the time T^* when the shockwave forms, consider the space-time (z - T) diagram depicting stress wave generation and propagation in response to the strain excitation function (page 61-62) as shown in **Figure 3.8**.

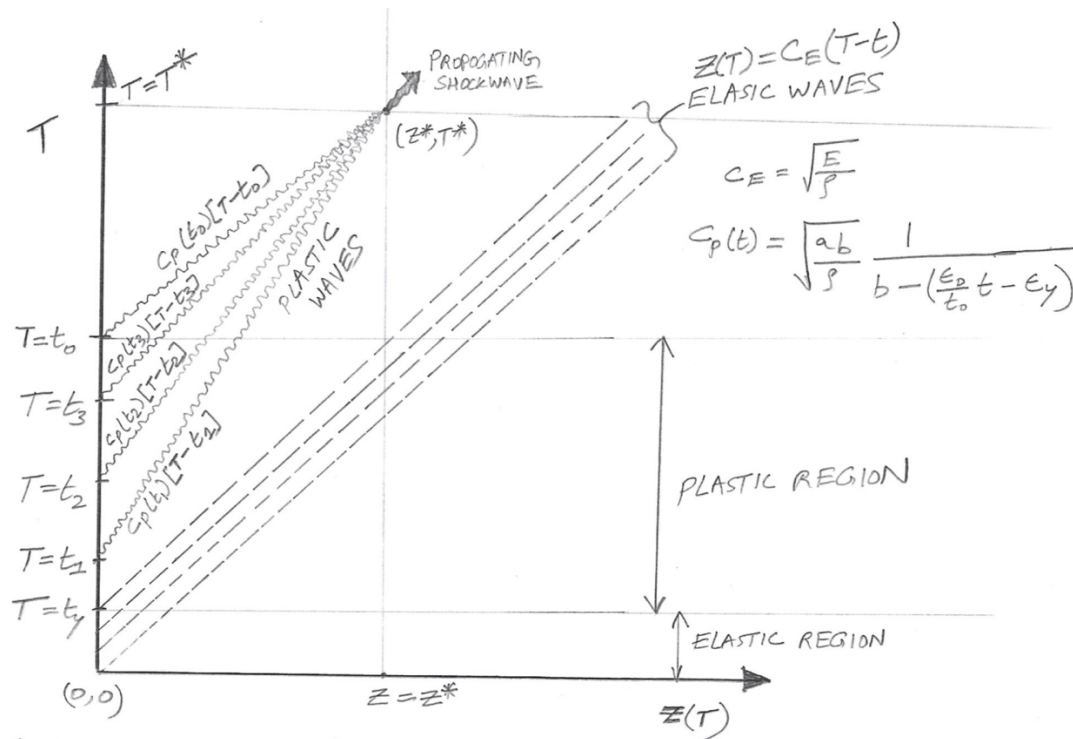
$$a = 6.41 \times 10^5 \frac{\text{kg}}{\text{m}^2}, \quad b = 0.9, \quad \rho = 6.15 \text{ g/cm}^3, \quad E = 180 \text{ GPa}$$

$$t_0 = 10 \text{ ns}, \quad \epsilon_0 = 0.6, \quad \epsilon_y = 0.083, \quad \sigma_y = 15 \text{ GPa}$$

$$t_y = \left(\frac{\epsilon_y}{\epsilon_0} \right) t_0 = \left(\frac{0.083}{0.6} \right) 10 \text{ ns} = 1.38 \text{ ns}; \quad C_E = \sqrt{\frac{E}{\rho}} = 5400 \text{ m/s}$$

$$z^* = \sqrt{\frac{ab}{\rho}} \left(\frac{t_0}{\epsilon_0} \right) = 161 \text{ nm}; \quad T^* = \frac{t_0}{\epsilon_0} (b + \epsilon_y) = 16.38 \text{ ns}$$

Thus crack could form 161 nm above ablation interface and propagate through the crystal



Assume units where $C_E = \sqrt{\frac{E}{\rho}} = 1$

Figure 3.8. Space-time (z - T) diagram depicting stress wave generation and propagation in GaN film.

Each travelling wave in the z - T diagram can be described by a straight line given by the expression:

$$z(T) = c_E[T - t] \text{ for } 0 \leq t \leq t_y ; \text{ Elastic region}$$

$$z(T) = c_p(t)[T - t] \text{ for } t_y \leq t \leq t_0 ; \text{ Plastic region} \quad (3,9)$$

Within the plastic region, using the expression for $c_p(\epsilon)$ from (3,8) and the strain excitation function $\epsilon(0,t)$ in equation (3,9), we get:

$$z(T) = \sqrt{\frac{ab}{\rho}} \frac{1}{b - \left(\frac{\epsilon_0}{t_0}t - \epsilon_y\right)} [T - t] \quad (3,10)$$

Solving for at least two travelling waves within the plastic region ($t_y \leq t \leq t_0$), we find that all the generated stress waves in the plastic region meet at a common location z^* at a common time T^* given by:

$$z^* = \sqrt{\frac{ab}{\rho}} \left(\frac{t_0}{\epsilon_0}\right) \quad (3,11)$$

$$T^* = \frac{t_0}{\epsilon_0} (b + \epsilon_y) \quad (3,12)$$

A shockwave is thus formed at location z^* ($\sim 161\text{nm}$ from ablation interface) at time T^* ($\sim 16.38\text{ns}$) that now propagates in the GaN film. This shockwave causes a significant increase in the local stress around that region potentially causing film cracking. If the film in that region cracks, the crack could also potentially propagate

deep within the GaN thin film. In the time $t_0 \leq t \leq t'$, no new stress waves are generated as the strain excitation function is a constant ($\epsilon(0,t) = \epsilon_0$). At time $t \geq t'$, the value of the strain excitation function is 0. This is known as the unloading condition and generates another ‘unloading’ stress wave (at instant $t = t'$) that travels with the elastic speed $c_E = \sqrt{\frac{E}{\rho}}$ in the GaN thin film. As c_E is larger than the speed of the shockwave [6], it eventually catches up with the shockwave causing stress relaxation and potentially more cracks in that region. The unloading wave is also reflected from the shockwave front and can undergo multiple reflections and stress relaxations at the ablation interface and shockwave front respectively till the shockwave is completely dissipated in the crystal.

When stresses are generated at any region within the GaN thin film, the potential ability of the film to crack depends on its fracture toughness K_F . The fracture toughness of the GaN thin film can be obtained from the Vicker’s Indentation method [7] and is given by the expression:

$$K_F = k \sqrt{\frac{E}{H_V} \frac{P}{c^{1.5}}} \quad (3, 13)$$

The constant k is for calibration and has a value ~ 0.016 . E is the Young’s modulus of the material ($E \sim 180 \text{ GPa}$ for GaN) and H_V is the material hardness (Vicker’s hardness). Hence one clue as to how to make the GaN thin film (of thickness $t_{\text{GaN}} = 5 \mu\text{m}$) more resilient to cracking is to simply increase the ratio (E/H_V) .

Now the Young's modulus of GaN, $E_{\text{GaN}} = 180 \text{ GPa}$ with a Vicker's hardness $H_{\text{GaN}} = 10.2 \text{ GPa}$. if we now put another material say a ductile metal like nickel on top of the GaN film of appropriate thickness ($t_{\text{Ni}} = 10 \mu\text{m}$ say), with Young's modulus $E_{\text{Ni}} = 190 \text{ GPa}$ with a Vicker's hardness $H_{\text{Ni}} = 0.64 \text{ GPa}$, the effective Young's modulus (E_{eff}) of the composite would remain approximately the same while the effective Vicker's hardness (H_{eff}) of the composite would reduce significantly if we take the thickness weighted average of the Young's modulus and hardness:

$$E_{\text{eff}} = \frac{t_{\text{GaN}} E_{\text{GaN}} + t_{\text{Ni}} E_{\text{Ni}}}{t_{\text{GaN}} + t_{\text{Ni}}} = 187 \text{ GPa} \quad (3, 14)$$

$$H_{\text{eff}} = \frac{t_{\text{GaN}} H_{\text{GaN}} + t_{\text{Ni}} H_{\text{Ni}}}{t_{\text{GaN}} + t_{\text{Ni}}} = 3.82 \text{ GPa} \quad (3, 15)$$

Thus, from this heuristic argument, it is conceivable that by using a protective layer of a ductile material like Cu or Ni ($\sim 10 \mu\text{m}$) on top of the GaN film, the fracture toughness K_F of the composite ($\propto \sqrt{\frac{E_{\text{eff}}}{H_{\text{eff}}}}$) can be increased by a factor of at least 1.8X, significantly reducing both the stress in the GaN film as well as the incidence of cracks during LLO. The validity of this heuristic argument for the use of a protective stress layer needs to be confirmed by a more detailed analysis, see section 3.4.

As we see, this phenomenon of stress wave and shockwave generation and propagation in the GaN thin films during LLO can get very complicated and hence full analytic modeling to capture all the underlying physics may not be practical. In this chapter we hence use FEM modeling using ANSYS[®] Explicit Dynamics to simulate the GaN LLO physics.

3.4. Finite Element Modeling of the GaN LLO process

To accurately simulate all the stress components involved during the GaN LLO process, a semi-analytic model of the process was developed. Based on this model and following analysis, a 5-10 μm thick metallic stress buffer layer was determined to be used to protect the microLEDs before the liftoff to obtain nearly 100% LLO yield. To model the GaN LLO process, several approximations to the real situation was made.

We assume an axisymmetric geometry for the LLO cross-section as shown in **Figure 3.9**. The diameter of the GaN thin film is $d=25\mu\text{m}$. The Ni layer, which we will prove later helps to relieve the LLO stresses, is present between the GaN and the temporary glass carrier (Borofloat-33). It is assumed that the thickness of the GaN film being lifted-off is $7\mu\text{m}$. We also assume that the incident laser pulse has a uniform lateral beam intensity profile as a first order approximation to simplify the analysis. The temporal intensity variation of the incident light pulse is assumed to be gaussian with a pulse width (2τ) = 10ns. The peak of the gaussian pulse is also set to occur at a time $t_0=25\text{ns}$ from the start of the analysis at time $t_0=0\text{ns}$. The wavelength of the incident light pulse is $\lambda=355\text{nm}$. At this wavelength, the characteristic absorption depth of the light pulse (β_{GaN}^{-1}) in GaN is approximately 100 nm. β_{GaN} is the extinction or absorption coefficient of the light in GaN. The dose of the incident light is $D = 600 \text{ mJ/cm}^2$ which is the critical dose of incident light that is needed to cause ablation of the GaN at the interface.

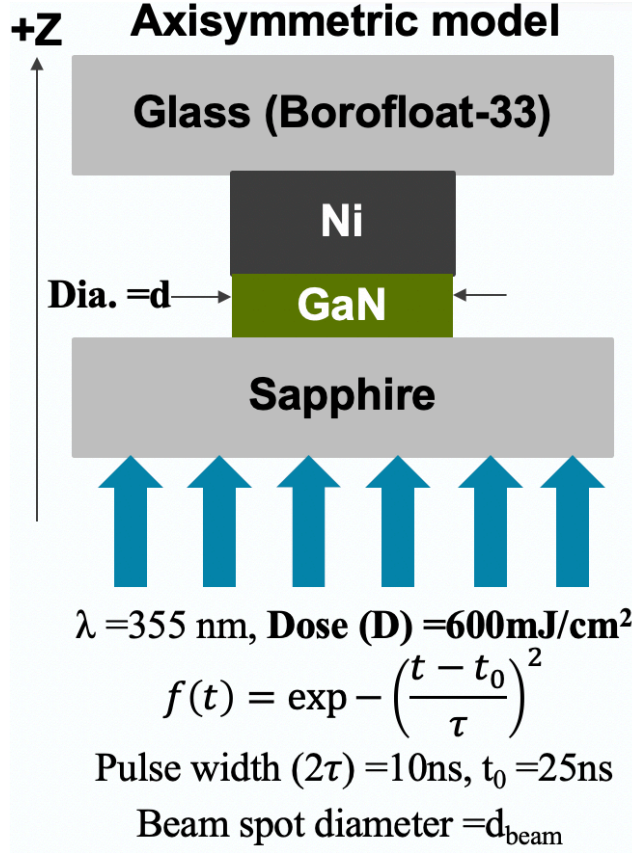


Figure 3.9. Simplified axisymmetric model of GaN LLO.

Based on these assumptions, we can now write the following equation for the intensity variation of the incident light pulse within the GaN thin film near the interface:

$$I_{\text{GaN}}(z, t) = \frac{D}{\sqrt{\pi\tau}} [1 - R_s][1 - R_{\text{GaN}}] e^{-\beta_{\text{GaN}} z} f(t) \quad (3, 16)$$

$$\text{where, } f(t) = \exp - \left(\frac{t - t_0}{\tau} \right)^2$$

From this intensity variation of the light within the GaN, we can obtain the heat generation rate $G(z, t)$ by assuming that all the light absorbed is converted to heat. The heat generation rate $G(z, t)$ within the GaN thin film near the sapphire interface is simply given by the gradient of the light intensity:

$$G(z,t) = -\frac{\partial I_{GaN}}{\partial z} \quad (3,17)$$

Once we have obtained the heat generation rate within the GaN, it can simply be substituted into the heat continuity equation to solve for the temperature variation within the GaN thin film as given in the equation below (cylindrical coordinates):

$$\frac{1}{\rho} \frac{\partial}{\partial \rho} \left(\rho \frac{\partial T}{\partial \rho} \right) + \frac{\partial^2 T}{\partial z^2} + \frac{G(z,t)}{k_{GaN}} = \frac{1}{\alpha} \frac{\partial T}{\partial t} \quad (3,18)$$

The model can be further simplified by observing that the thermal conductivity of the GaN thin film is much larger than the sapphire substrate by 10X and the surrounding air; hence, within the timescales of interest which lie within 10s of ns, the radial (ρ) flow of heat is negligible compared to the flow of heat up the GaN thin film along the + Z direction. Hence the differential equation to be solved reduces to a 1D form:

$$\frac{\partial^2 T}{\partial z^2} + \frac{G(z,t)}{k_{GaN}} = \frac{1}{\alpha} \frac{\partial T}{\partial t} \quad (3,19)$$

This system can be modelled with relative ease using ANSYS® Explicit dynamics to obtain the temperature transients at the GaN/Sapphire interface during the ablation process. The results of the ANSYS® simulations are shown in **Figure 3.10**.

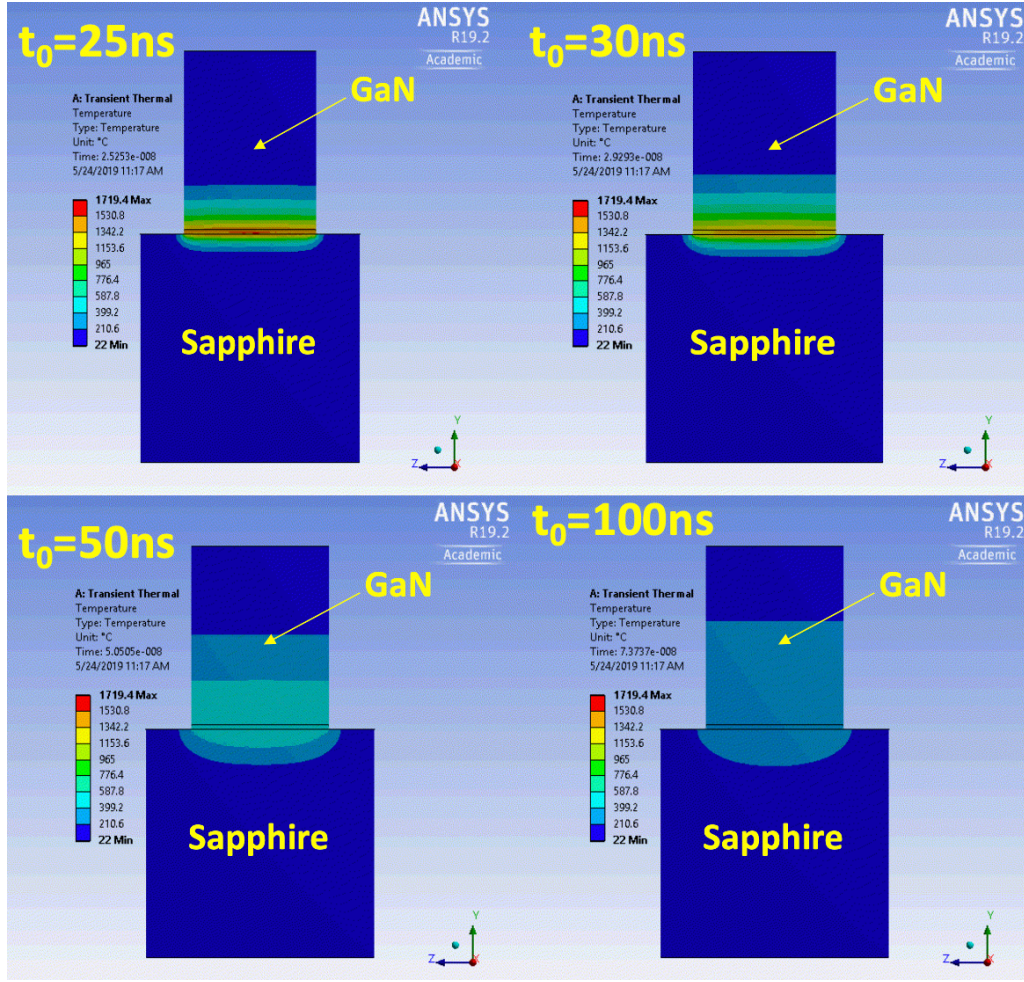


Figure 3.10. Temperature transients at the GaN/sapphire interface during the LLO process simulated in ANSYS® Explicit Dynamics.

We find that as the incident light pulse hits the GaN/sapphire interface and is absorbed within a β_{GaN}^{-1} region, the temperature quickly rises to nearly 1800°C and then starts falling rapidly as the heat is quickly conducted away from the interface. We can also notice how most of the heat is conducted in the + Z direction and how the temperature distribution within the GaN region has a very weak radial dependence. This justifies the ID model.

The temperature was averaged in the β_{GaN}^{-1} region and is plotted as a function of time in **Figure 3.11**. Notice how the temperature rises sharply as the incident light pulse hits and then falls exponentially as the heat is conducted away.

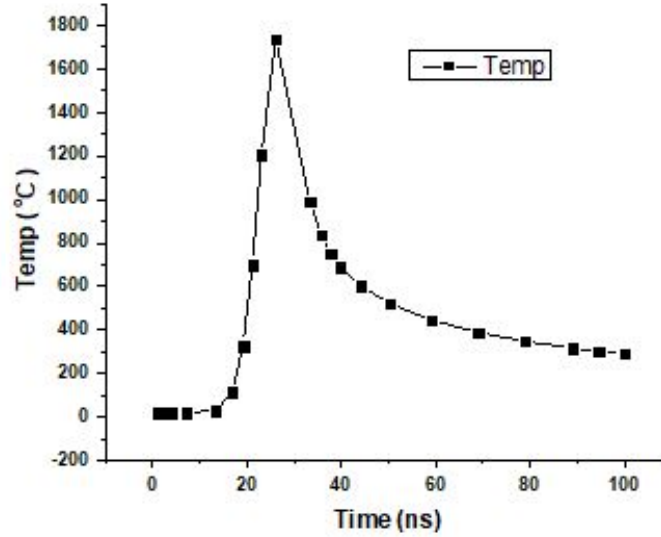


Figure 3.11. Temperature averaged within the β_{GaN}^{-1} region and plotted as a function of time.

The sharp temperature rises at the interface within 10s of nanoseconds cause two major mechanical effects:

- A thermomechanical shockwave due to the large transient temperature gradients at the interface. This shockwave is generated at the interface and travels upwards through the GaN at the speed of sound. It has a shear component as well as a normal component as shown in **Figure 3.12(a)**.
- Pressure shockwave due to the rapid expansion of the released N_2 gas that absorbs the heat. This only has a normal stress component as shown in **Figure 3.12(b)**.

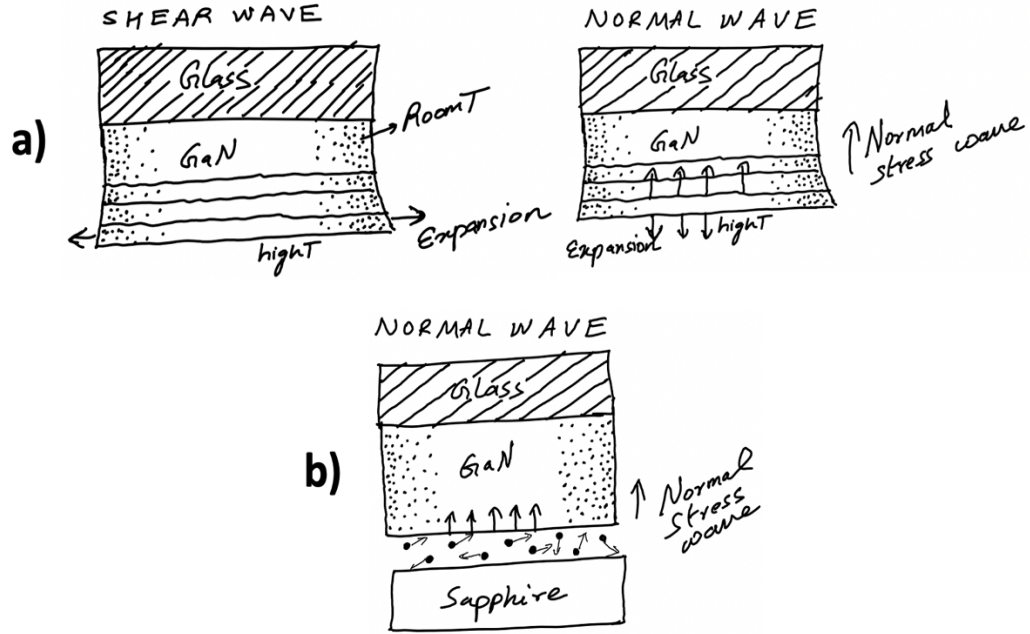


Figure 3.12. Illustrations of shear and normal components of thermomechanical shockwave (a) & normal component of pressure shockwave (b).

The thermomechanical shockwave can be readily simulated in Ansys using the interfacial temperature information that was derived earlier. For extracting the interfacial N_2 gas pressure information, however, further simplification using physical insights is necessary.

A simplified model of the ablation cross-section is shown in **Figure 3.13**. We assume that all the GaN within the β_{GaN}^{-1} region at the interface is ablated producing the nitrogen gas. Observe that the diameter of the GaN thin film $d \gg \beta_{GaN}^{-1}$ and within the time scales of interest, the diffusion length of the released N_2 at the interface is very small compared to d . Under these conditions, it is a good approximation to treat the nitrogen gas as trapped within the β_{GaN}^{-1} region.

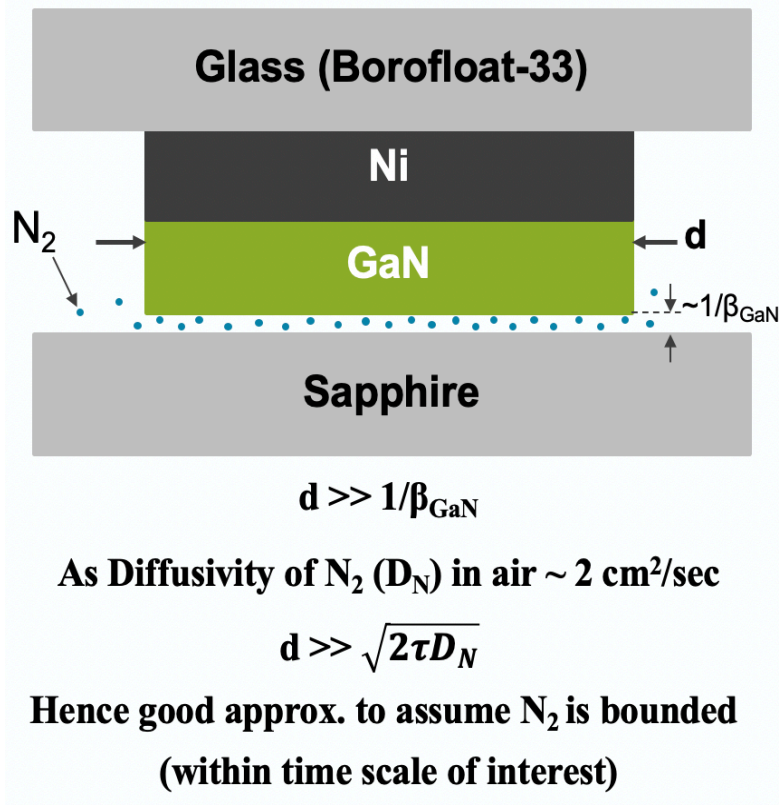


Figure 3.13. Simplified model for laser ablation at GaN/sapphire interface.

For a trapped gas at a certain temperature, the pressure exerted by the gas can be derived from its equation of state. If we assume an ideal gas equation of state to describe it, the N_2 pressure can be obtained as:

$$P_{\text{N}_2}(t) = \frac{nRT(t)}{V} \quad (3,20)$$

The pressure of N_2 is plotted vs. time in nanoseconds in **Figure 3.14**. The pressure rapidly rises to around 400MPa at the peak temperature and then falls rapidly as the system cools. This complex pressure transient at the interface is approximated by a gaussian pressure pulse that is used in the simulation.

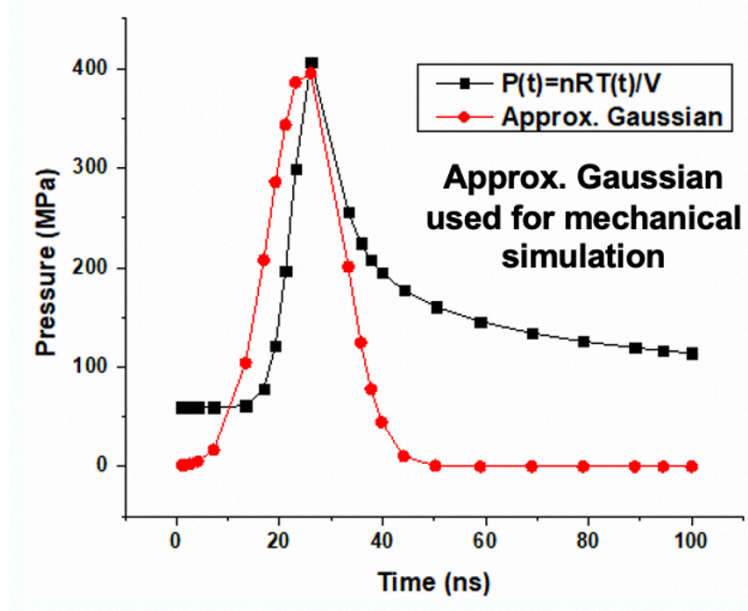


Figure 3.14. Released N_2 gas pressure as a function of time at the GaN/sapphire interface derived from the simplified model.

The results of the ANSYS® Explicit Dynamics simulations of the transient mechanical stresses in the GaN film during the LLO process is given in **Figures 3.15-3.17**. The simulation models both the thermo mechanical stress waves due to the transient temperature gradients as well as the derived pressure shockwave due to expansion of the nitrogen gas at the GaN/sapphire interface. **Figure 3.15(a)** plots the normal stresses in the GaN film without the Ni layer at different simulation times. **Figure 3.15(b)** plots the normal stress in the GaN film when a $10\mu\text{m}$ Ni stress buffer layer is used at different simulation times. We observe that the peak normal stress in the GaN film with no Ni layer reaches around 1GPa while the one with the $10\mu\text{m}$ Ni layer is reduced by an order of 5X to around 0.2-0.3MPa. This significant reduction in the peak normal stresses occurs because when the stress waves are generated in the GaN films protected by the Ni, the metal acts as a shock cushion by plastically deforming

in response to the incident stress wave. This plastic deformation of the Ni absorbs the stress thus reducing it in the GaN film. This can clearly be seen in **Figure 3.16(b)** where the normal deformation in the cross section with the Ni stress buffer is plotted as a function of time. **Figure 3.17** plots the peak compressive stress in the GaN thin film as a function of time for three different cases: No Ni, 5 μm Ni and 10 μm Ni. Again, we see how the use of the Ni stress buffer significantly reduces the peak compressive stresses in the GaN film. The delay in the occurrence of the peak compressive stress in GaN for the cases with the Ni by around 10ns is due to the time it takes for the Ni "Spring" to compress.

Thus, to conclude, the analytic and FEM modeling confirms that the use of a 5 - 10 μm Ni stress buffer layer on top of the GaN microLEDs before LLO prevents cracking and reduces film damage.

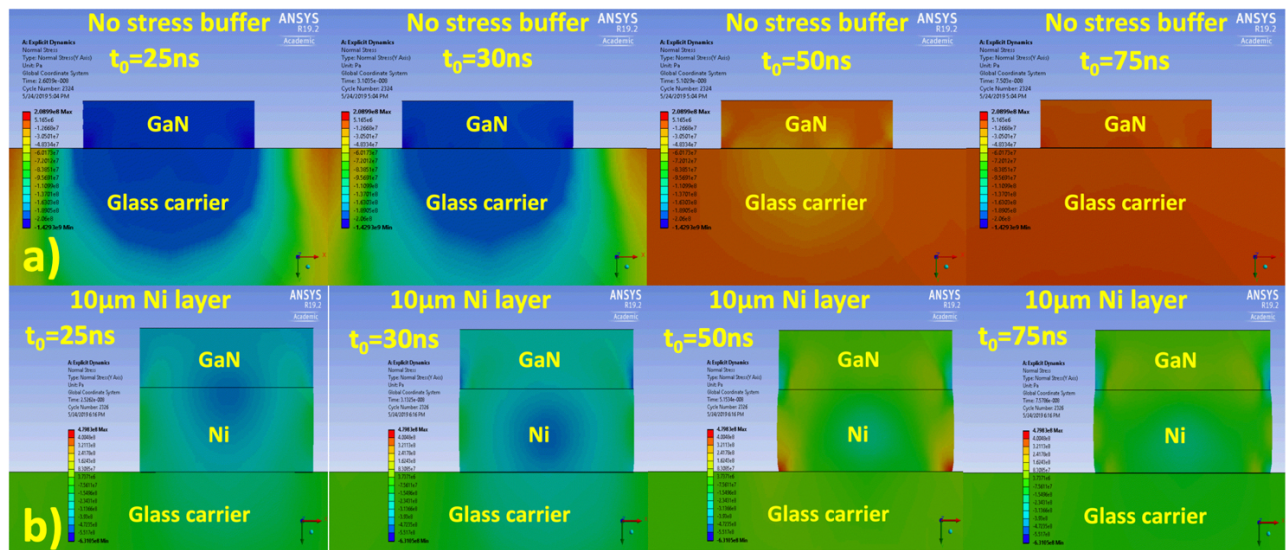


Figure 3.15. ANSYS® Explicit Dynamics simulation of the normal stress in the LLO cross-section without Ni (a), and with a 10 μm Ni layer (b).

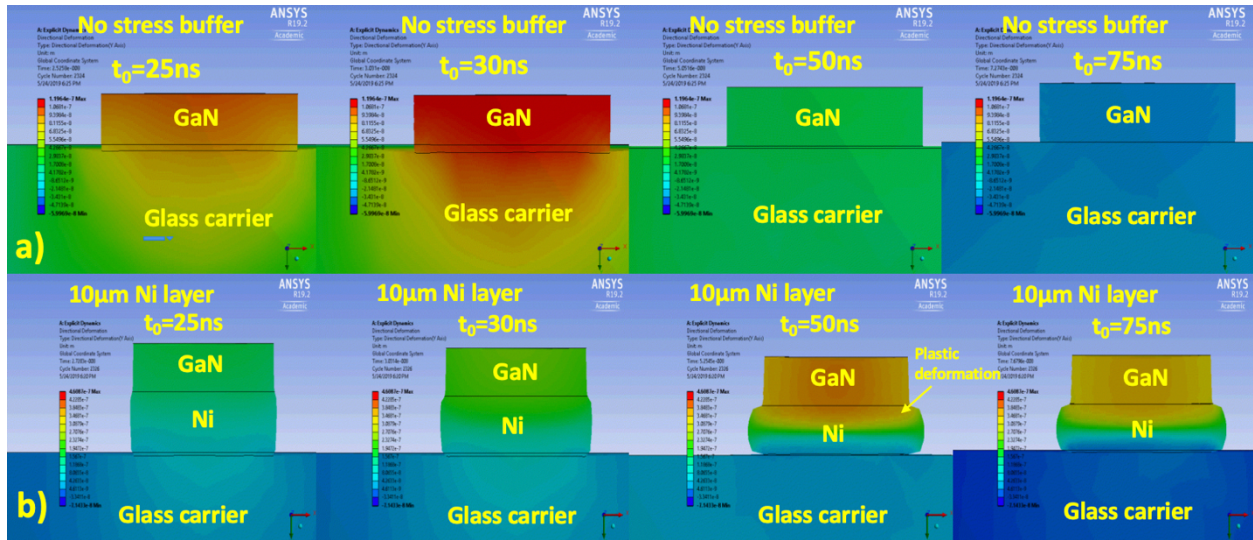


Figure 3.16. ANSYS® Explicit Dynamics simulation of the normal deformation ($X10$) in the LLO cross-section without Ni (a), and with a $10\mu\text{m}$ Ni layer (b).

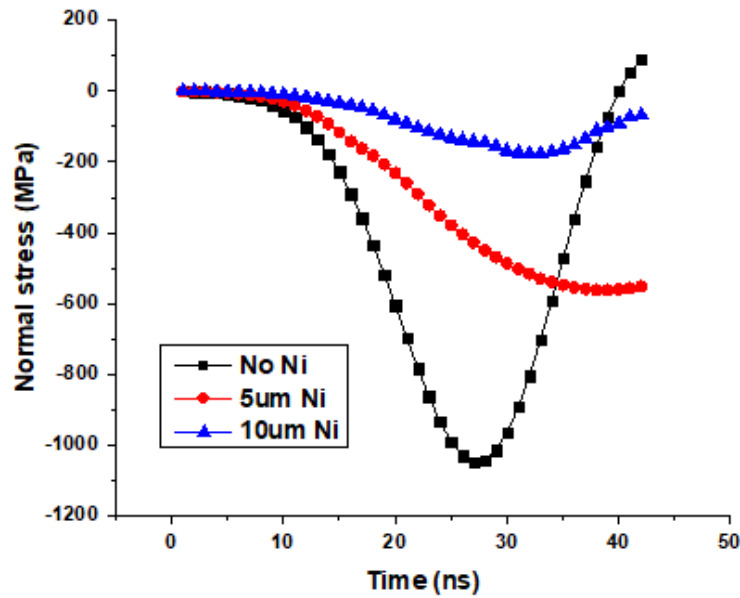


Figure 3.17. Peak compressive stress in GaN film as a function of time for 3 cases: No Ni, $5\mu\text{m}$ Ni & $10\mu\text{m}$ Ni.

3.5. Experimental Verification of Stress Buffer for high-yield LLO

3.5.1. Fabrication of samples for LLO yield testing:

For the initial testing of LLO yield and quality, blanket 4" GaN wafers (no functional devices) were used [3]. A layer of Ti(20nm)/Au(200nm) was used as seed layer. Patterned AZ4620 ($\sim 10\mu\text{m}$) was then used to perform semi-additive plating to form the Ni support layer. Two different thicknesses of this layer were formed: $5\mu\text{m}$ and $10\mu\text{m}$. The Ni layer is then used to dry etch about $7\mu\text{m}$ of the exposed GaN using a $\text{BCl}_3/\text{Cl}_2/\text{Ar}$ ICP to singulate GaN islands, see **Figure 3.18(a)**. The Ni support layer on some samples is removed to perform a comparison. The samples are then bonded to a 4" glass wafer using the adhesive HD3007 and sent for DPSS LLO process to DISCO Corp., Japan, see **Figure 3.18(b)**.

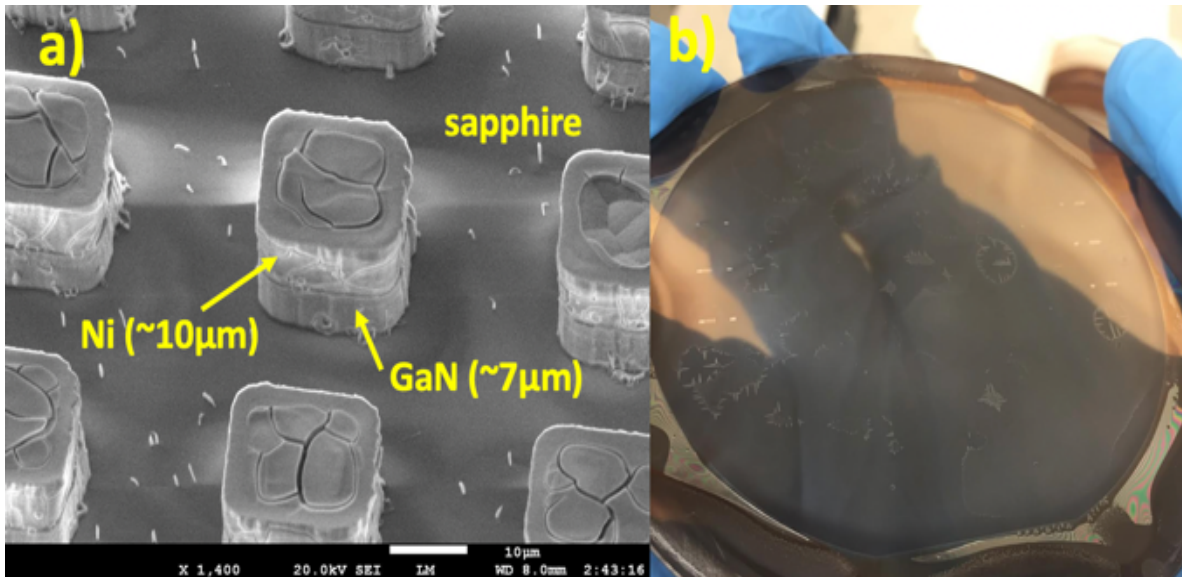


Figure 3.18. (a) GaN islands on sapphire after singulation. (b) Bonded sample for LLO [3].

3.5.2. Evaluation of LLO quality and yield:

After performing LLO, the glass carrier with the released GaN islands is cleaned with dilute HCl to remove any residual Ga. Any adhesive between the islands is also etched using O₂ plasma. The samples are then optically mapped (imaged) throughout the 4" area using a Nanotronics nSpec[®] PS microscope to detect for the presence of any visual cracks on the GaN islands [3], see **Figure 3.19**.

For further evaluation of the LLO quality, an AFM map of the GaN surface is also taken for the samples with and without the support layer.

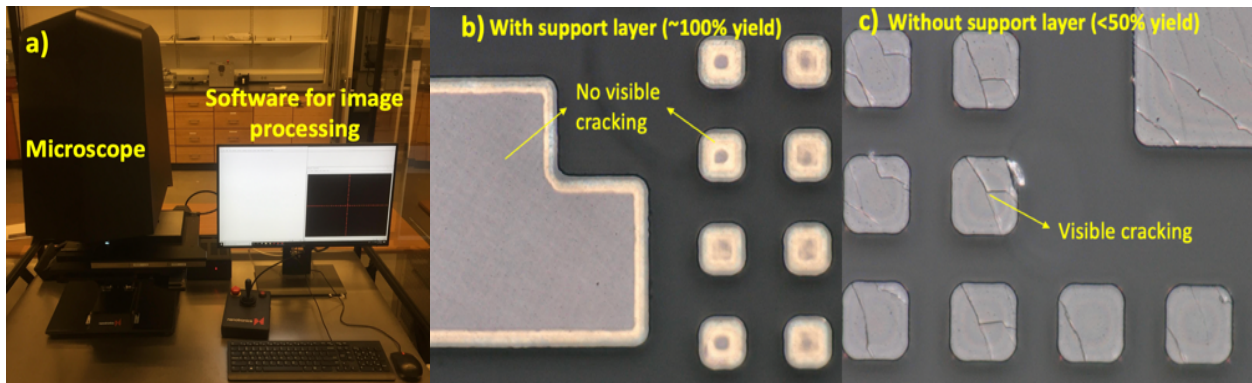


Figure 3.19. (a) nanotronics nSpec[®] PS microscope setup. Optical image of GaN islands, on the 4" temporary carrier, (b) with $\sim 5\mu\text{m}$ support layer & (c) without support layer [3].

3.5.3. Optical mapping of GaN islands on temporary glass carrier after LLO:

The results of the optical mapping of the 4" temporary glass carrier with GaN islands [3] is given in **Figure 3.20** for 3 cases: samples with no support layer, 5 μm and 10 μm support layers. We find that for samples with the 5 μm and 10 μm support layers, we get nearly 100% yield of crack free GaN islands throughout the area of the 4" wafer.

For the unsupported samples however, > 50% of the GaN islands have developed surface cracks. These results thus demonstrate the effectiveness of the Ni support layer in preventing the stress induced GaN cracking due to LLO process.

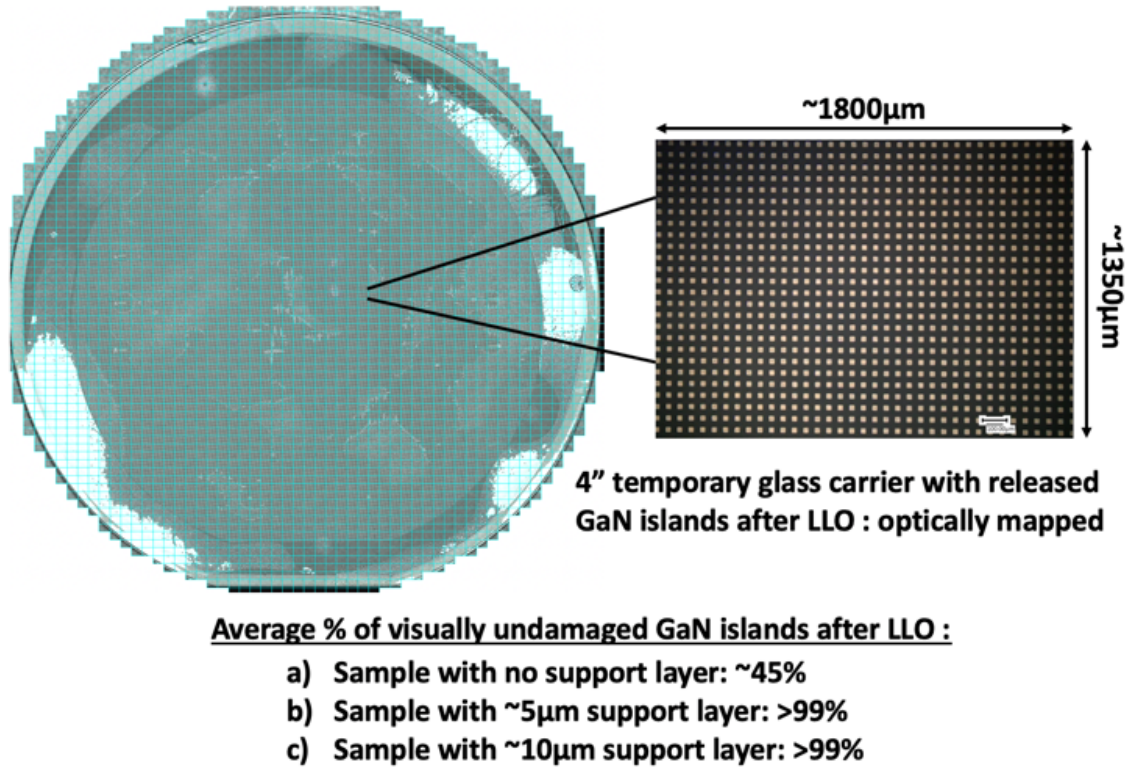


Figure 3.20. Results of optical mapping of 4" temporary glass carrier with GaN islands after LLO [3].

3.5.4. AFM profile of GaN island surface after LLO:

The results of the AFM profile of the GaN island surface after LLO with a 5 μ m support layer and without one [3] is given in **Figure 3.21**. For the sample with the 5 μ m Ni support layer, we find that the RMS roughness of the surface is ~ 6.5nm. The surface is thus relatively smooth with the presence of some shallow (<3nm) surface

pits and no surface cracks. The sample with no support layer however shows considerable surface cracking as can clearly be seen from the AFM profile.

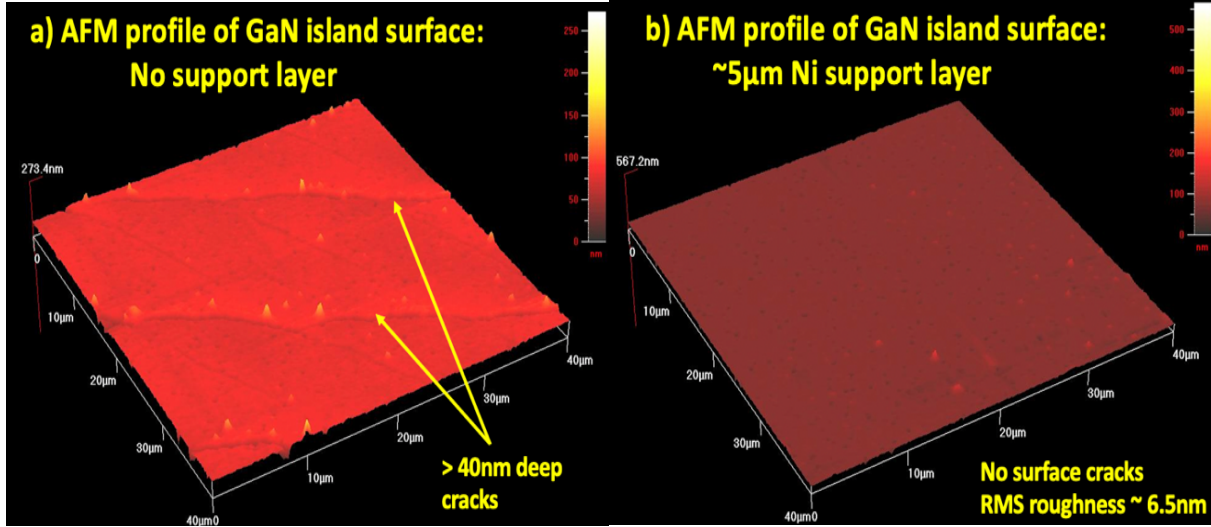


Figure 3.21. AFM surface profile of released and singulated GaN island (a) without a support layer and (b) with a 5 μm Ni support layer [3].

3.5.5. Photoluminescent characterization of the released GaN films:

The results of photoluminescent (PL) measurements on the released GaN devices after LLO [4] is given in **Figure 3.22**. For this experiment, dummy GaN singulated islands (~ 25 μm squares) with and without a Ni stress buffer layer were released from sapphire to the temporary glass carrier 1. PL measurements were then made on the released devices and compared with those of virgin devices on sapphire. For the GaN islands released without a Ni layer, nearly a 2.5X reduction in PL intensity (a.u.) at peak emission wavelength (λ_{peak}), compared to the device on sapphire, was observed. The islands released with the 10 μm Ni layer however had negligible degradation in the PL intensity at λ_{peak} indicating minimized damage.

- Resolution of 1 mm used for PL
- Three 4" samples measured: **(1)** Released GaN islands on carrier 1 **without Ni**
(2) Released GaN islands on carrier 1 with **10 μm Ni**
(3) GaN on Sapphire for comparison

Sample	λ_{peak} (nm)	StdDev (nm)	FWHM (nm)	PL intensity (a.u.)
(1) Released, No Ni	460.6	1.266	17.3	2.724
(2) Released, 10 μm Ni	461.1	0.676	17.3	6.059
(3) GaN on Sapphire	461.9	1.251	16.9	6.284

* Reported λ_{peak} , FWHM & PL intensity are average values

Figure 3.22. Results of photoluminescent (PL) measurements on the released GaN islands after LLO. A comparison with virgin devices on sapphire is established [4].

REFERENCES

1. T. Ueda et al., "Separation of Thin GaN from Sapphire by Laser Lift-Off Technique," *Japanese Journal of Applied Physics* 50(2011) 041001.
2. X. J. Su et al., "Shock-induced brittle cracking in HVPE-GaN processed by laser lift-off techniques," *J. Phys. D: Appl. Phys.* 46(2013) 205103(6pp).
3. G. Ezhilarasu et al., "High Yield Precision Transfer and Assembly of GaN microLEDs using Laser Assisted Micro Transfer Printing," © 2019 IEEE 69th ECTC, Las Vegas, NV.
4. G. Ezhilarasu et al., "A Heterogeneously Integrated, High Resolution and Flexible Inorganic microLED Display using Fan-Out Wafer-Level Packaging," © 2020 IEEE 70th ECTC.
5. Liuxi Tan, Jia Li, Sheng Liu, "Modeling and Simulation of Laser Lift-Off Process for LED's Substrates," 1-4244-1392-3/2007 IEEE.
6. W. H. Chen et al., "Study of the structural damage in the (0001) GaN epilayer processed by laser lift-off techniques," *Appl. Phys. Lett.* 91, 121114(2007).
7. Chen J. and Bull J. 2007, "Indentation fracture and toughness assessment for thin optical coatings on glass," *J. Phys. D: Appl. Phys.* 40 5401.

4. Flexible microLED displays on FlexTrate™

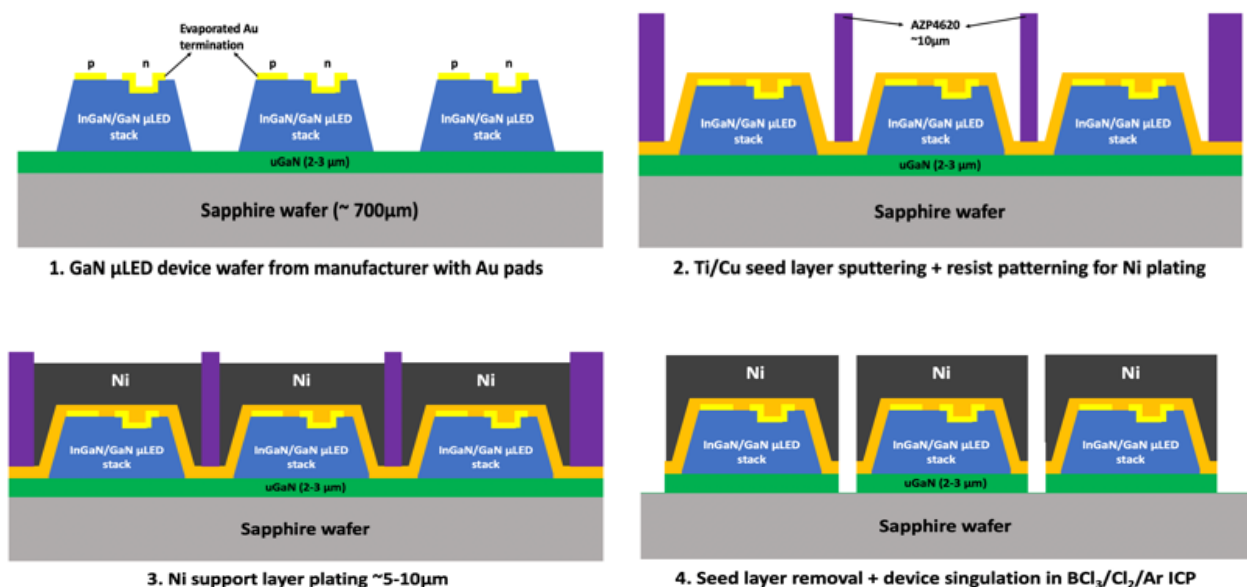
In this chapter, we shall see how the two different approaches to flexible microLED display fabrication, namely the mass transfer approach and dielet approach are experimentally realized. The mass transfer approach allows us to make the ultimate flexible microLED display where a thin layer of $<10\mu\text{m}$ InGaN/GaN microLEDs are embedded on the surface of PDMS [1]. This display would be highly flexible down to a bending of 1mm radius. This approach was tried first but went through a major challenge. The microLEDs that were used for the mass transfer were based on a conventional LED process that is not specifically designed to undergo mass transfer. The contacts of the devices were found to delaminate while performing the process hence preventing us from demonstrating a functional prototype display [1]. The mass transfer was however successfully demonstrated to assemble $100\times 50\mu\text{m}^2$ LEDs on PDMS substrates without any film cracking. To demonstrate a functional flexible microLED display, the dielet approach was used instead to assemble 1 mm^2 sapphire dielets with microLEDs on FlexTrate™ in a 10×10 array to fabricate an 80×48 display in passive matrix configuration at 150PPI resolution. The microLED display was heterogeneously integrated with CMOS display driver ICs (MAX6971 current drivers & MIC5891 voltage drivers) to demonstrate full functionality. Let us now look at the details of these processes in the coming sections.

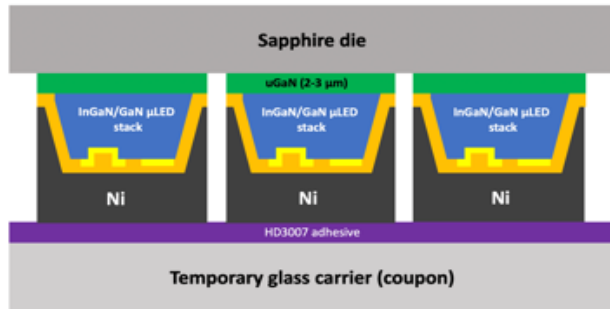
4.1. Mass transfer approach for fabricating microLED display

4.1.1. Detailed process flow for performing the GaN microLED mass transfer

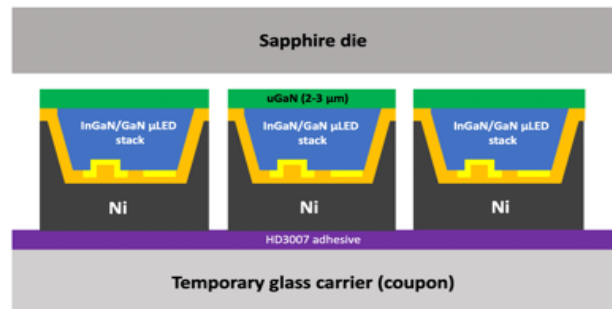
The process flow for the mass transfer and assembly of prefabricated GaN microLEDs (100mm device wafers from manufacturer) from c-plane sapphire wafer onto the target flexible PDMS substrate is given in **Figure 4.1**. The microLEDs are not completely singulated to start with, i.e., there is a thin layer of undoped GaN (uGaN) between them. The P and N contacts of the microLEDs are terminated with gold to allow easy metallization with the FlexTrate™ process, see [2]. A seed layer of Ti (30nm)/Cu (250nm) is then sputtered on the wafer followed by patterning of a thick layer ($\sim 10\mu\text{m}$) of AZP4620 resist. Semi-additive electroplating is then used to deposit the Ni stress buffer layer. After resist removal & seed etching, the same Ni layer is used as a hard mask to dry etch the exposed u-GaN between the microLEDs in a $\text{BCl}_3/\text{Cl}_2/\text{Ar}$ ICP to singulate the devices. The sapphire wafer is now backside polished to an RMS roughness of $\sim 1\text{nm}$ by employing a Chemical Mechanical Polishing (CMP) process (performed at DISCO Japan) and then diced into 10mm by 12mm dies. The dies are bonded to a temporary glass carrier (20mm by 24mm coupon, 4 sapphire dies per coupon) coated with a $2\mu\text{m}$ thick layer of HD3007 using a K&S die to wafer bonder. The need for a die scale process rather than wafer scale will be explained in 4.1.2. The bonded samples can then be sent for GaN LLO. Post LLO, the temporary glass carrier with the released devices is cleaned in a 10% (v/v) HCl solution followed by O_2 plasma etching of the residual adhesive between the microLEDs. Lithographically patterned glass ‘stamp’ dies (10mm by 12mm) coated with a 2-4 μm layer of HD3007 are now bonded to the released devices on the

temporary glass carrier. An alignment accuracy of $\sim 2\mu\text{m}$ was demonstrated for this bonding. Programmable laser debonding is now performed on the samples to transfer the microLEDs from the temporary carrier to the glass stamps. After O_2 plasma ashing to clean residual adhesive on the stamp, the electroplated Ni layer and protective Ti (30nm) seed are wet etched to expose the contact pads of the microLEDs. Individual glass stamps are now tested for electrical functionality by contact probing. Known Good Die (KGD) stamps along with other components such as Si dielets are now tacked to a common Thermal Release Tape (TRT, from Nitto Denko) laminated on a silicon/glass wafer (handler 1). The final laser debonding step is performed to remove the stamp thus completely transferring the microLEDs to the tape. The FlexTrate™ process is now performed: compression molding of PDMS (Silastic MDX4-4210) with silicon handler 2, thermal release of handler 1, BEOL metallization, passivation, and finally thermal release of handler 2. The freestanding PDMS package now has all the microLEDs and other heterogeneous components integrated in a seamless fashion as shown schematically in **Figure 4.1**.

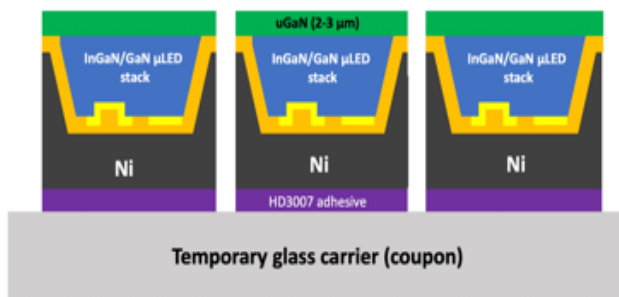




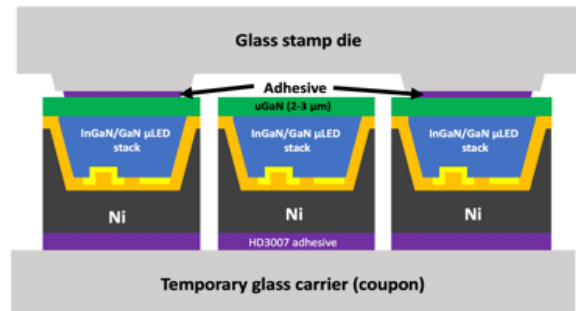
5. Bonding to temporary glass carrier using laser-debondable adhesive



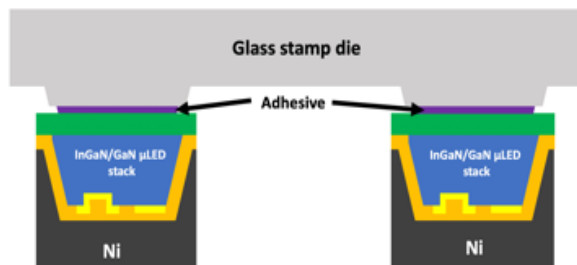
6. Laser Lift-Off of GaN using high power pulsed, Q-switched IR laser



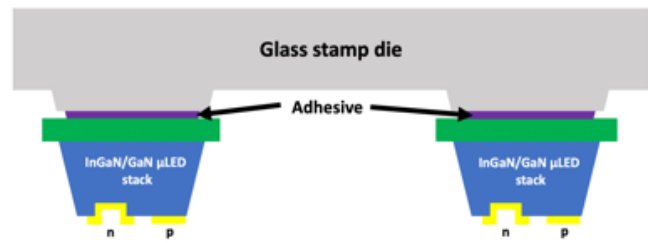
7. Cleaning of released sample using dil. HCl + adhesive etching



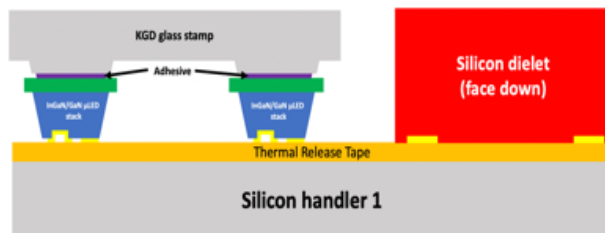
8. Bonding to glass 'stamp' die



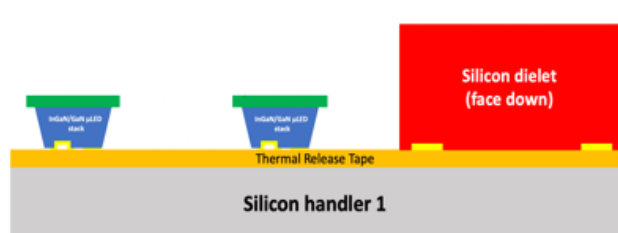
9. Programmable laser debonding + transfer to stamp



10. O₂ plasma clean + wet etch of Ni and seed layers



11. Tacking of KGD stamp with μLEDs & other dielets on TRT



12. Laser debonding of stamp for final transfer of μLEDs

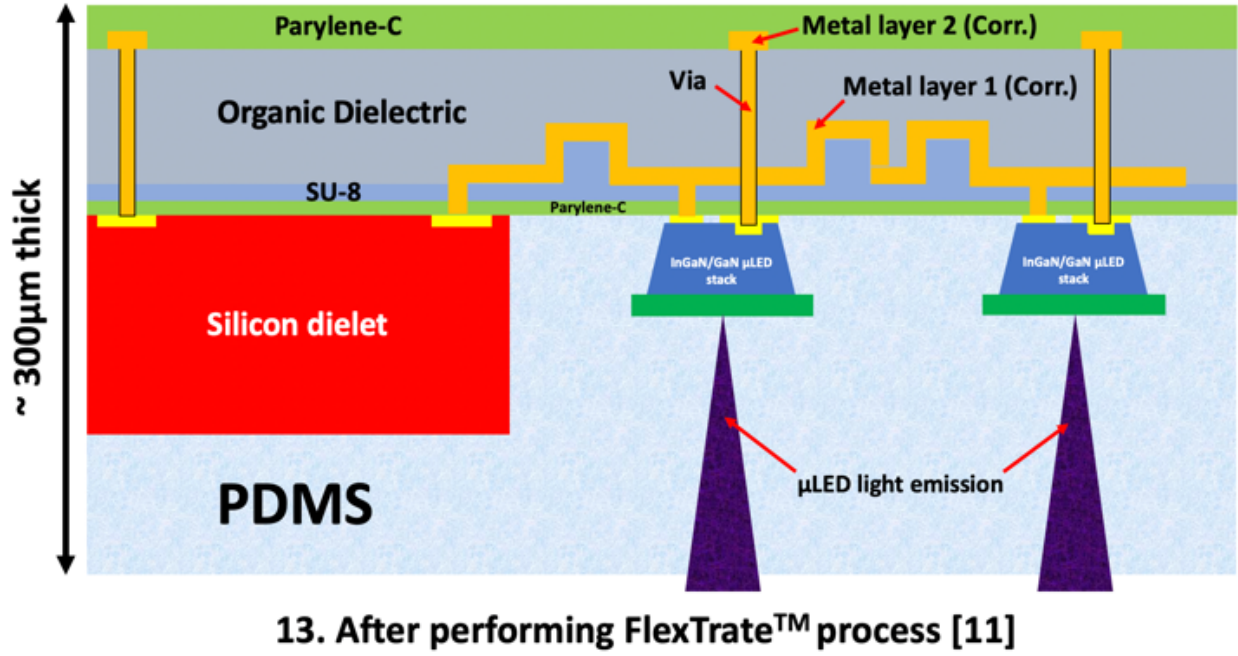


Figure 4.1. Proposed process flow for GaN microLED assembly on FlexTrate™ using mass transfer [3].

4.1.2. Sample preparation & characterization pre-LLO

The GaN on sapphire device wafers were commercially bought with the microLEDs (50μm by 100μm) having same side contacts [1]. An optical micrograph of the as fabricated devices along with the average I-V characteristics is given in **Figure 4.2(a)**. An SEM image of the sample after electroplating the Ni layer & singulating the microLEDs is also given in **Figure 4.2(b)**.

Due to the high stress of GaN epilayer growth on sapphire, the 100mm device wafers have a significant warpage of about 60-80μm from center to edge. This warpage leads to significant bond failures and registration errors down the line when performing the process at wafer scale, see **Figure 4.3(a)**. To overcome this fundamental issue, we

have chosen to go with a die approach. The polished sapphire wafer is hence diced into 10mm by 12mm pieces and then individually bonded to the temporary glass carrier (20mm by 24mm coupons) using the HD3007 adhesive ready for the LLO process, see **Figure 4.3(b)**. The warpage within each die is negligible hence avoiding the issues mentioned earlier. The die approach gives us a bonus of KGD classification pre-assembly which significantly boosts yields.

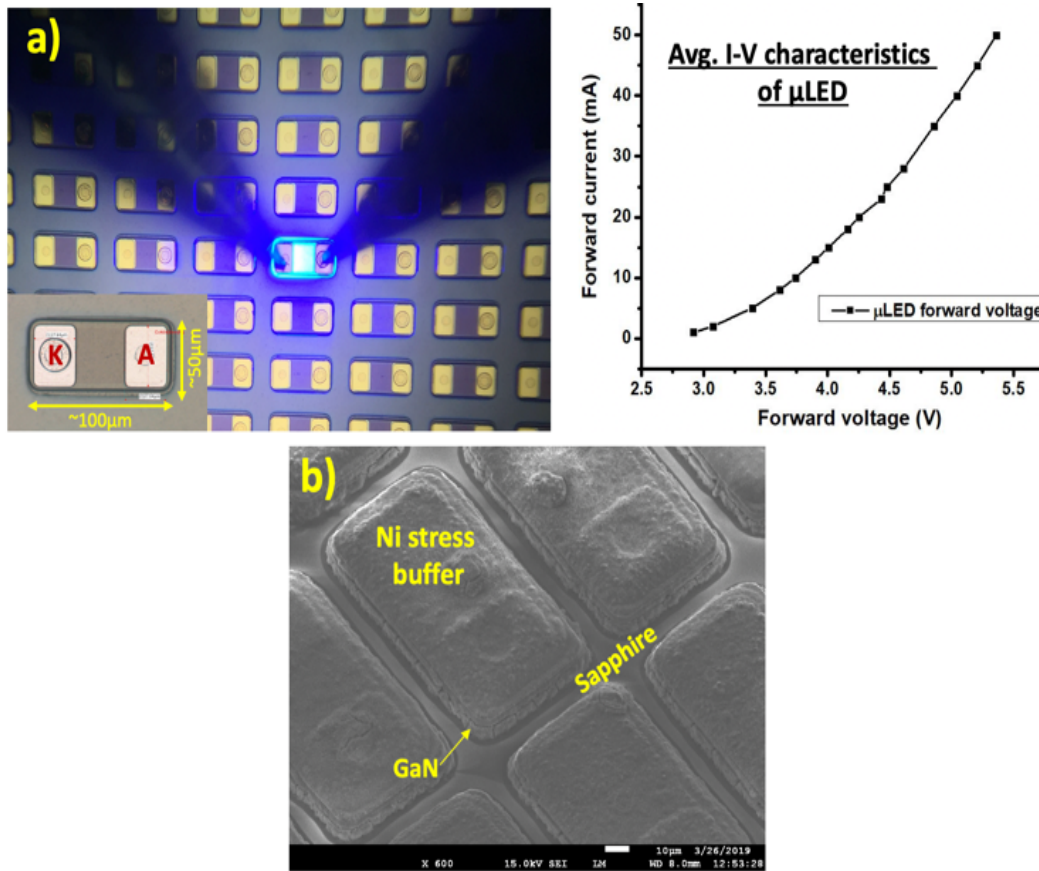


Figure 4.2. (a) Optical image of as-fabricated devices along with average I-V characteristic; (b) SEM image of singulated microLEDs with Ni layer [1].

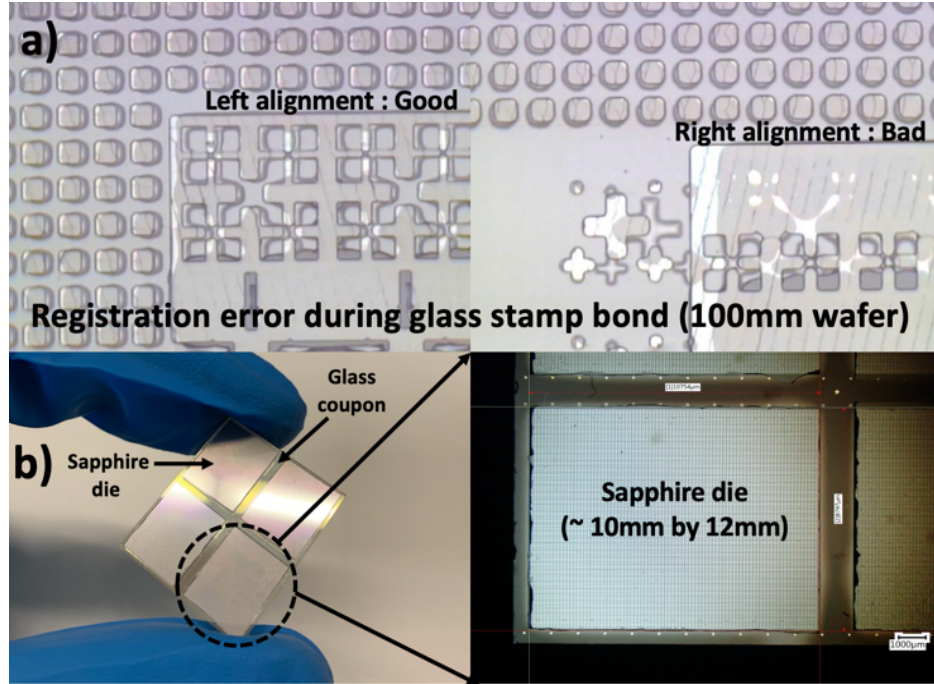


Figure 4.3. (a) Optical image depicting registration issues during glass stamp bonding while performing process at wafer scale; (b) Four backside polished sapphire dies (~10mm X 12mm) bonded to glass coupon ready for LLO [1].

4.1.3. GaN LLO of the bonded samples using DPSS laser

In the last chapter, reproduced in **Figure 4.4(a)**, we had reported experimental data on the use of a 5-10µm thick Ni stress buffer (support) layer to prevent cracking or damage to dummy GaN islands (25µm squares) during the DPSS LLO process. We had found that by using the stress buffer layer, we could boost the LLO yield from < 50% to nearly 100% across a 100mm wafer for the same process conditions. Keeping with the above trend, the current devices with ~ 5µm Ni layer were also released at nearly 100% LLO yield without any device cracking or damage, see SEM image in **Figure 4.4(b)**.

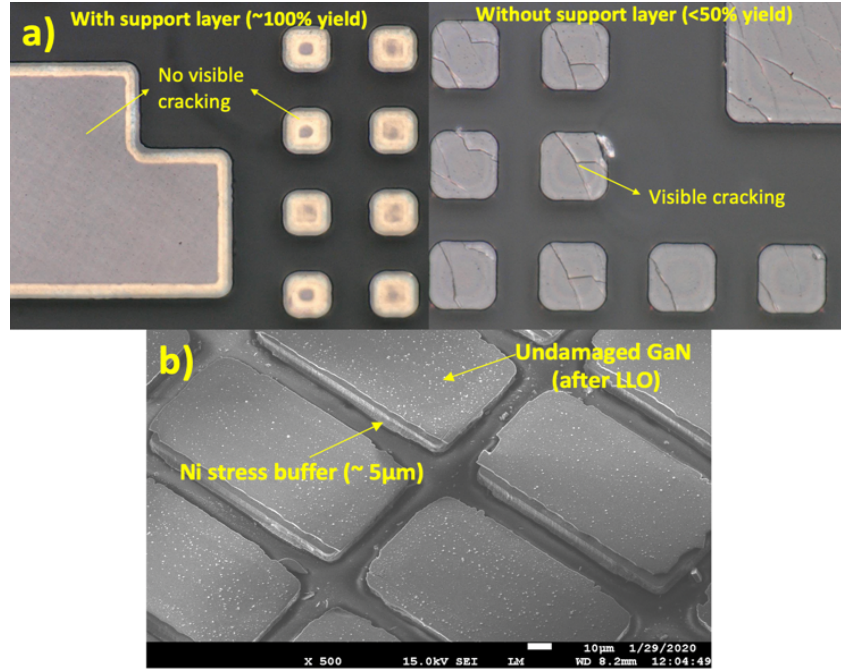


Figure 4.4. (a) Optical image of released GaN islands ($25\mu\text{m} \times 25\mu\text{m}$) with & without Ni stress buffer post LLO; (b) SEM image of released microLEDs with $\sim 5\mu\text{m}$ Ni layer.

4.1.4. Glass stamp fabrication & bonding

A reusable glass ‘stamp’ is used for transfer printing selected patterns of microLEDs from the temporary carrier to the final target substrate [1]. The glass stamp is fabricated by dry etching a Borofloat-33 glass wafer in a $\text{C}_4\text{F}_8/\text{Ar}$ plasma to form $3\mu\text{m}$ tall mesas followed by coating a lithographically patterned layer of HD3007 on top of them. The wafer is then diced into corresponding 10mm by 12mm pieces for adhesive bonding to the released microLEDs on the temporary carrier. Two different patterns of microLED transfer printing were explored: a normal pattern where all the microLEDs/die are transferred (~ 260 PPI) and a checkerboard pattern where half of the microLEDs/die are transferred (~ 180 PPI). An SEM image of the two different

glass stamp patterns ready for bonding is given in **Figure 4.5(a)**. Optical images after adhesive bonding of the stamp to the released microLEDs on the temporary glass carrier is also shown in **Figure 4.5(b)**. The HD3007 adhesive was patterned on top of the mesas to avoid reflow induced failures.

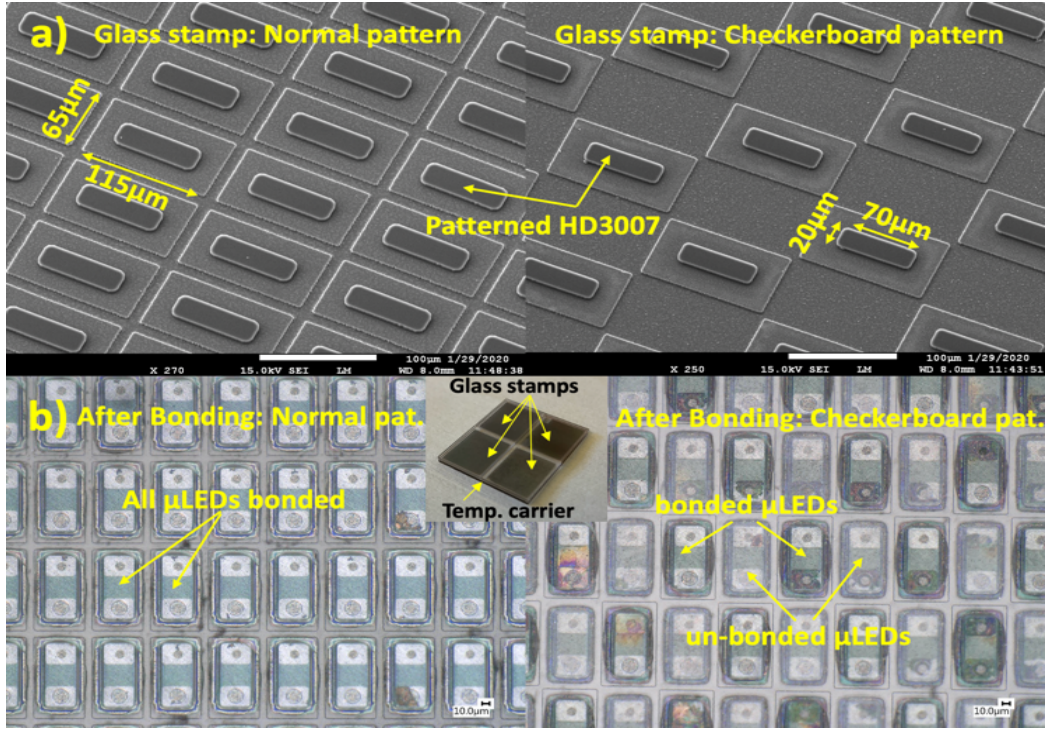


Figure 4.5. (a) SEM image of the two different glass stamp patterns with lithographically patterned HD3007 ready for bonding; (b) Optical images after adhesive bonding of stamp to released microLEDs on temporary carrier (looking through stamp). Inset shows a single coupon with four stamps bonded [1].

4.1.5. Transfer of microLEDs to glass stamp

Laser debonding of the samples for the transfer of microLEDs from the temporary carrier to the glass stamp was performed using a standard 308nm (XeCl) excimer laser [1]. An SEM image of the as transferred microLEDs sitting on the glass stamp, face

up is given in **Figure 4.6(a)**. Residual adhesive is dry etched in an O₂ plasma followed by wet chemical etching of the Ni stress buffer and Ti seed layers exposing the P & N contacts of the microLEDs, see optical image in **Figure 4.6(b)**. The microLEDs can now be electrically tested through contact probing (Figure 4.6(c)) allowing us to perform KGD classifications.



Figure 4.6. (a) SEM image of as transferred microLEDs sitting on glass stamp (face up); (b) Optical image of microLEDs with exposed contacts after removal of Ni layer and seed; (c) Contact probing of microLEDs on stamp confirming successful operation [1].

Although the microLEDs were uncracked, it was found that the P & N contacts on most of the devices had delaminated once the Ni layer was removed, see **Figure 4.7**. In fact, the contacts on these devices seem to start delaminating the moment they are singulated, by etching the uGaN between the devices before LLO, see **Figure 4.8**. Further investigation into the process showed that this delamination of the contacts was due to the structure of the prefabricated microLEDs itself and not due to the mass transfer. The microLEDs used for these experiments were commercially purchased and based on a standard LED process. Standard LEDs are never released from their growth sapphire substrate and do not experience the high stresses involved during a typical mass transfer process. They are directly diced from the epi wafer and packaged in epoxy. The standard LED process is hence not well suited for the current process due to the contact delamination. In the future, to perform mass transfer, custom microLEDs must be designed and fabricated with engineered stress buffer layers to make the contacts more robust, see **Chapter 5**. The current process was however continued with the contactless microLEDs to show successful assembly of the devices on FlexTrate™.

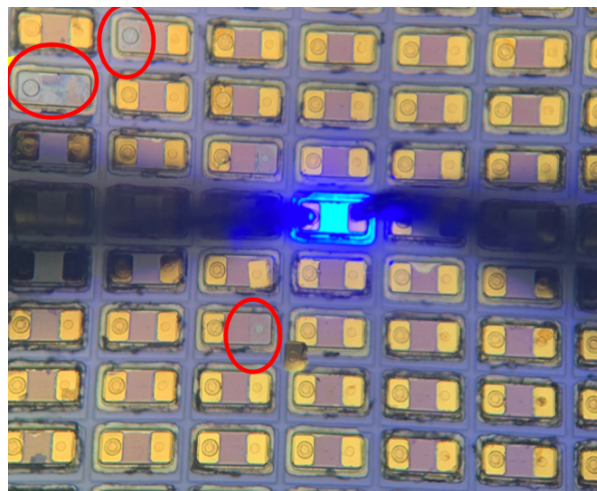


Figure 4.7. Contact delamination after the wet etching of Ni stress buffer. Regions where the contacts are delaminating is indicated by the red circles.

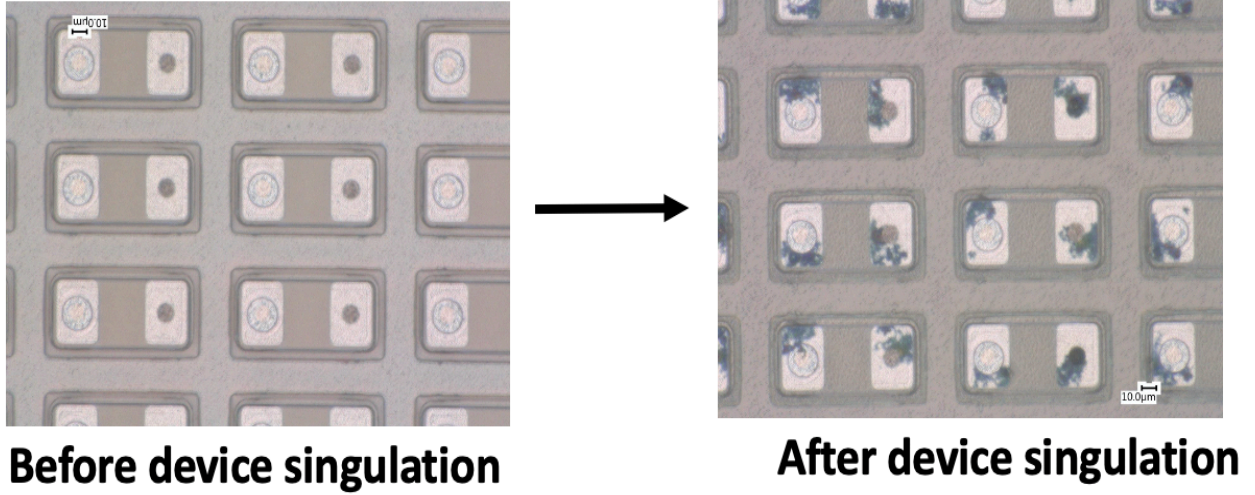


Figure 4.8. microLED contacts looking through the polished sapphire side before device singulation (left), after singulation (right). The dark discolorations on the contacts are regions where the contact layer is slowly delaminating.

4.1.6. Electrical characterization of μ LEDs on glass stamp

I-V measurements of the microLEDs on the glass stamp where the contacts were still intact was taken and compared with virgin devices on sapphire [1]. The results of this measurement are summarized in **Figure 4.9**. We observe that there is less than 5% degradation in the forward current at the operating forward voltage of 4V for the released devices which indicates that there is no significant process induced damage due to LLO or laser debonding.

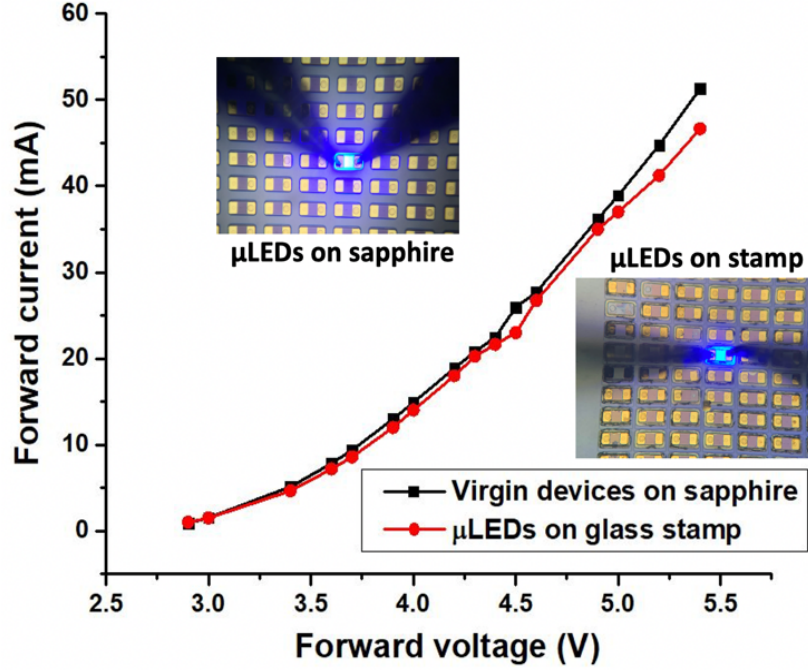


Figure 4.9. Comparison of I-V measurements of the microLEDs on glass stamp vs. virgin devices on sapphire [1].

4.1.7. Heterogeneous assembly on FlexTrate™

KGD glass stamps along with other heterogeneous components like Si dielets (1mm²) are tacked onto a common TRT laminated on a 100mm glass wafer (handler 1), as part of the FlexTrate™ process [1], see **Figure 4.10**. The samples are then sent for laser debonding. After debonding of the glass stamp to completely transfer the microLEDs to the tape [1] (see **Figure 4.11**), Poly Di-Methyl Siloxane (PDMS, Silastic MDX4-4210) is compression molded directly on top of the microLEDs & Si dielets using a second Si wafer (handler 2). The handler 2 is laminated with its own TRT having a higher release temperature. After curing of the PDMS, the handler 1 is then thermally debonded, exposing a relatively planar surface with microLEDs (~200PPI res.) and Si dielets embedded in PDMS ready for metallization [1], see SEMs

in **Figure 4.12**. After metallization and testing of the devices, the handler 2 can be thermally debonded to release the fully flexible PDMS package with heterogeneously integrated microLEDs and Si dielets [1]. Photos of the released FlexTrate™ sample, without interconnect metallization now, is given in **Figure 4.13**. The package is highly flexible and can be bent even to a bending radius of $< 5\text{mm}$ without damaging the microLEDs or Si dielets.

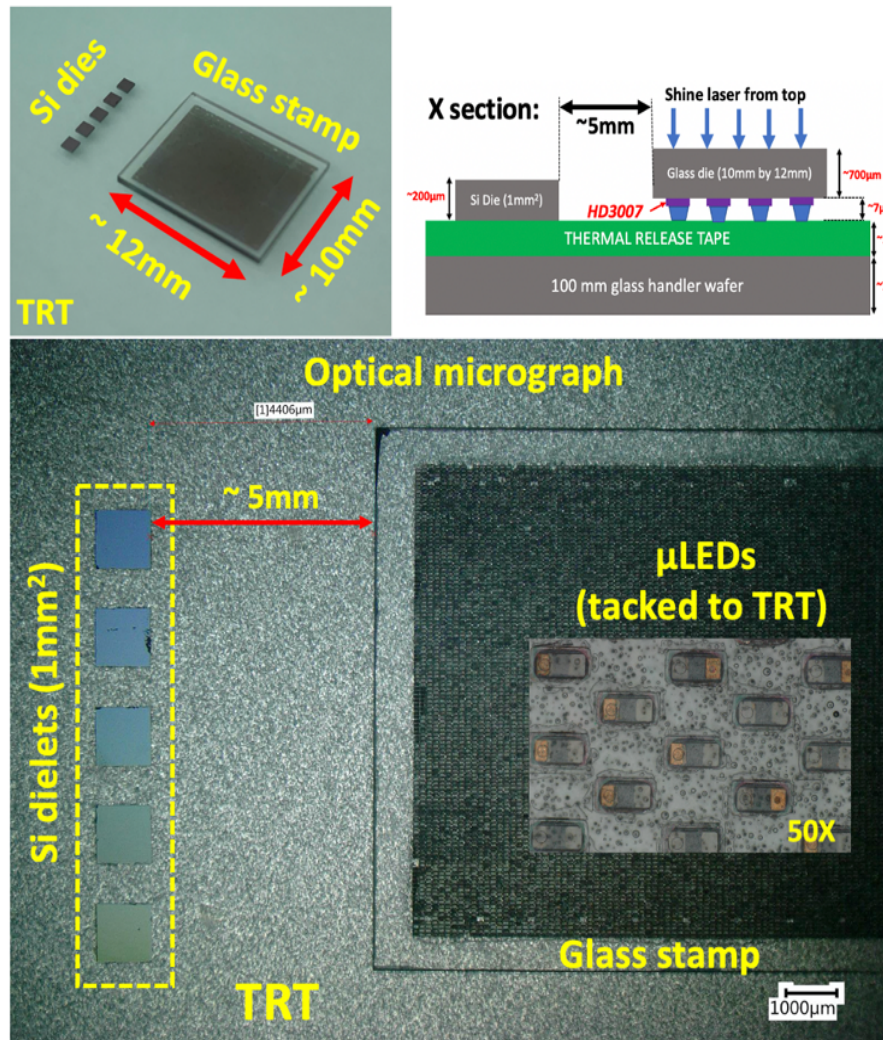


Figure 4.10. Image of KGD glass stamp and Si dielets (1mm^2) tacked onto common TRT laminated on glass wafer. These samples are sent for laser debonding [1].

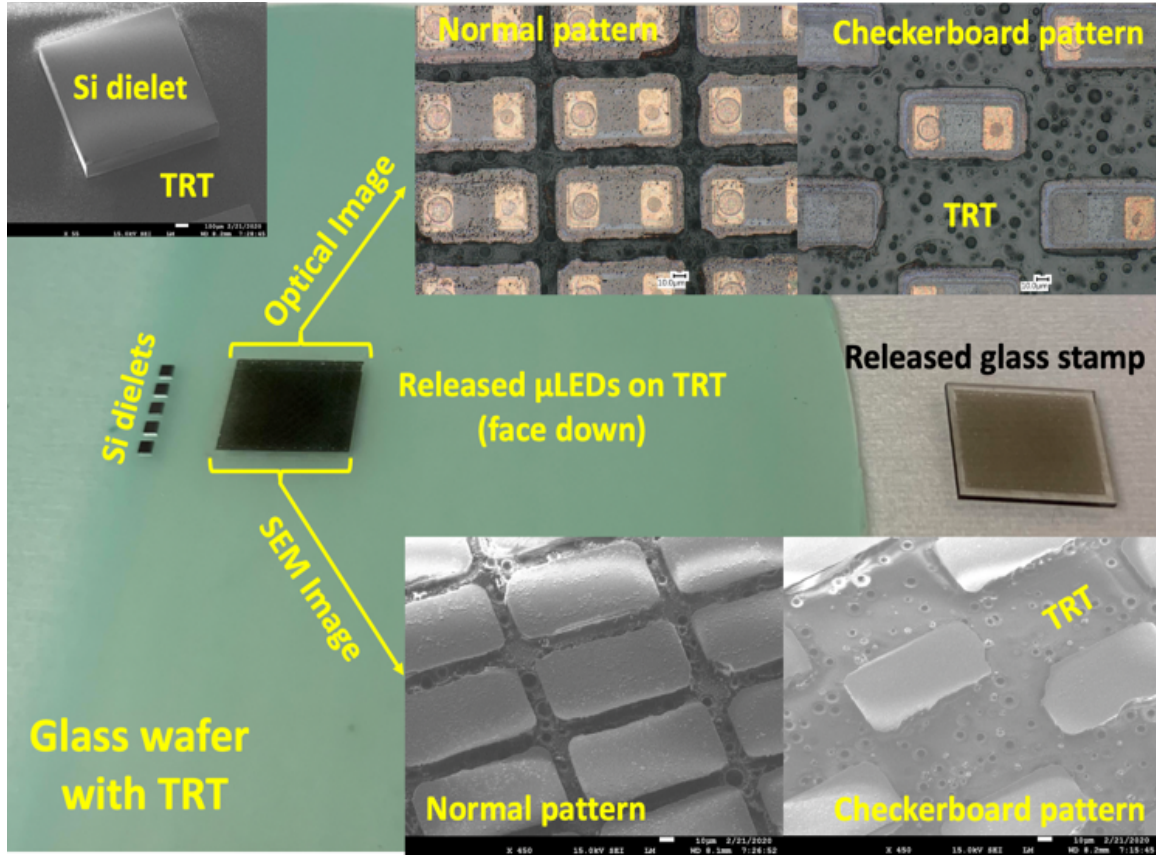


Figure 4.11. After laser debonding of glass stamp, the microLED matrix array is completely transferred to the TRT on a 100mm glass wafer [1].

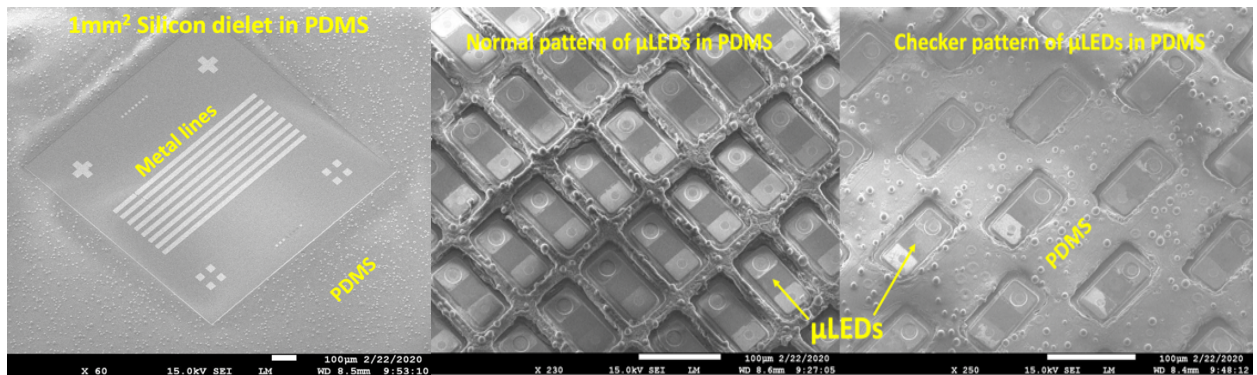


Figure 4.12. SEM images of microLEDs and Si dielets embedded in PDMS ready for metallization. The globular topography of the PDMS is an artifact of the TRT [1].

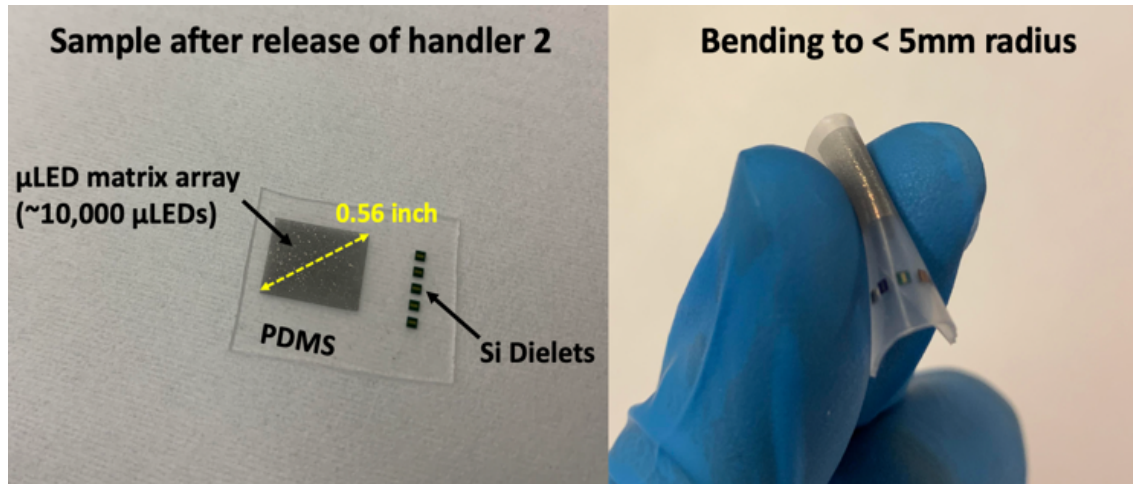


Figure 4.13. Photos of the released FlexTrate™ sample with microLEDs and Si dielets embedded in PDMS [1].

4.2. Dielet approach for fabricating microLED display

In the previous section, the mass transfer process was successfully demonstrated to assemble $50 \times 100 \mu\text{m}^2$ LEDs on PDMS substrate at $\sim 300\text{PPI}$ resolution. Although the microLEDs were assembled without any cracking, the contacts had delaminated thus preventing us from performing metallizations and demonstrating a functional display. The reasons for this contact delamination were also discussed in the previous section. In this section, to demonstrate a fully functional microLED display on FlexTrate™, a dielet approach was used instead. A 100mm standard thickness ($500\text{-}700\mu\text{m}$) sapphire wafer with prefabricated microLEDs ($50 \times 100 \mu\text{m}^2$) was thinned down to less than $200\mu\text{m}$ thickness using a lapping and CMP process. The thinned wafer was then diced into 1mm^2 sapphire dielets. Each dielet has 135 microLEDs ready for integration.

4.2.1. Design of microLED display on FlexTrate™:

A schematic of the full display design is given in **Figure 4.14**. The design uses a 10 by 10 array of sapphire dielets to form the full display area. Each dielet has 135 microLEDs out of which 40 are driven by the display drivers (one out of every 2 along the horizontal and vertical directions). The reason for driving only 40 microLEDs per dielet was to simplify the complex 2-level metallization scheme on FlexTrate™ by easing the interconnect pitch. There is a total of 13,500 microLEDs on the entire display area out of which 4000 are connected in a passive matrix configuration and driven by the current (MAX6971) and voltage (MIC5891) driver ICs paced at the top and bottom peripheries of the display respectively. The resolution of this 48 X 80 display is ~150PPI. The actual resolution of integrated microLEDs is ~300PPI. The row of five current driver ICs (MAX6971) placed at the top are connected to the vertical lines of the matrix and drive a current of 3mA per microLED. This drive current of 3mA is set by a row of 15k ohm current set resistors that are placed at the top. The row of six voltage driver ICs (MIC5891) placed at the bottom are connected to the horizontal lines of the passive matrix & provide the source voltage for driving the microLEDs. The control signals that are needed by the current and voltage driver ICs can be provided through the set of large rectangular probe pads located on the left and right periphery of the display design. There are two levels of metallization that is to be used in this design at a pitch of 40μm. The horizontal lines constitute metal 1 while the vertical hires are made using metal 2 in the passive matrix.

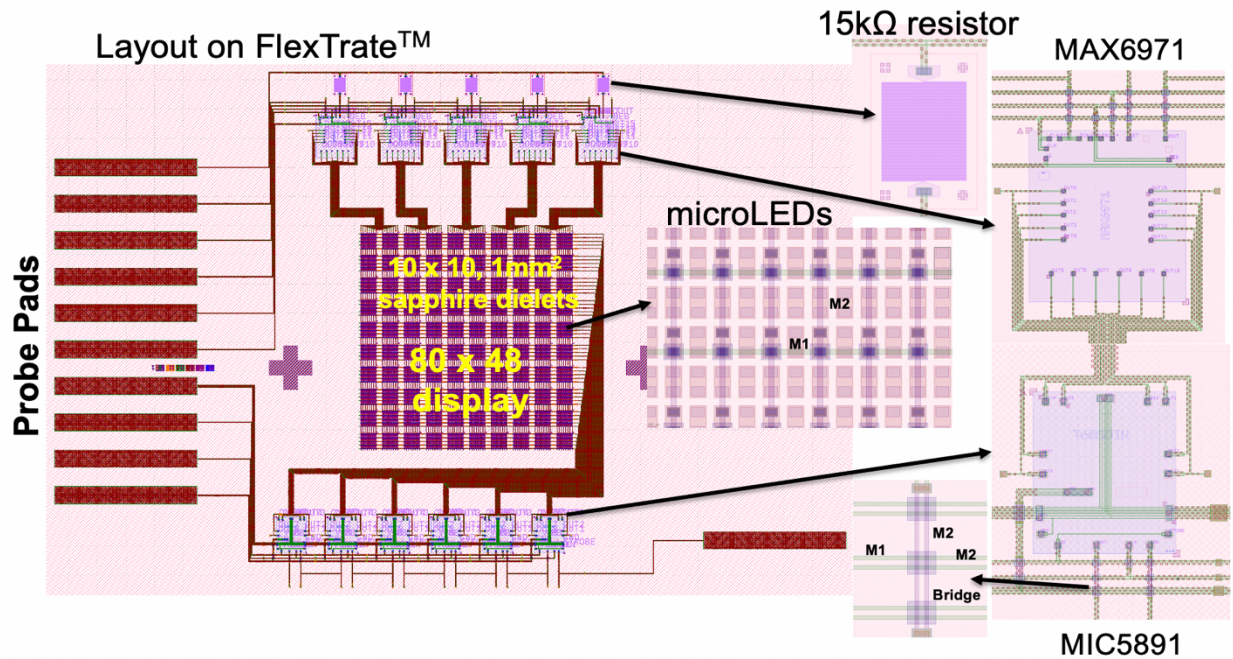
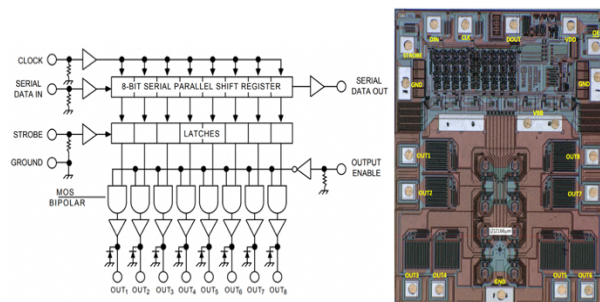


Figure 4.14. Schematic of full FlexTrate™ microLED display design.

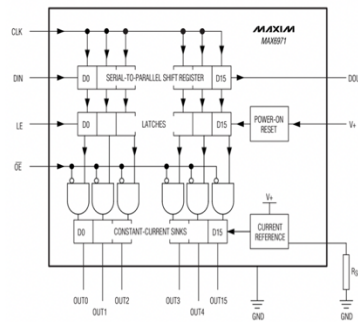
The current & voltage driver ICs that were used in this design were de-packaged from commercially available PDIP packages to obtain the bare dies. The detail of these driver dies is shown in **Figure 4.15**. The MIC5891 source voltage driver has a shift register that is connected in parallel with a set of latches to provide the source voltage to the output pins. It is capable of high-power driving and can supply up to 500mA current at 50V. The MAX6971 current sink IC has a shift register connected in parallel to a set of latches that latch a current mirror to the output pin to sink a preset value of current. The current is set using a current set resistor. As these bare dies were obtained through die-extraction from a PDIP package, the components were tested before assembly on FlexTrate™ to guarantee functionality. This testing was done by wire bonding the bare dies to a chip carrier and testing the functionality using an Arduino setup as shown in **Figure 4.16**.



ABSOLUTE MAXIMUM RATINGS

Voltage with respect to GND.	
V+	-0.3V to +6V
OUT ₊	-0.3V to +40V
DIN, CLK, LE, OE, SET	-0.3V to (V+ + 0.3V)
DOUT Current	±10mA
OUT ₊ Sink Current60mA
Total GND Current960mA

Output transistors capable of sourcing up to 500mA



ABSOLUTE MAXIMUM RATINGS

Voltage with respect to GND.	
V+	-0.3V to +6V
OUT ₊	-0.3V to +40V
DIN, CLK, LE, OE, SET	-0.3V to (V+ + 0.3V)
DOUT Current	±10mA
OUT ₊ Sink Current60mA
Total GND Current960mA

15kΩ resistor sets drive current to 3mA

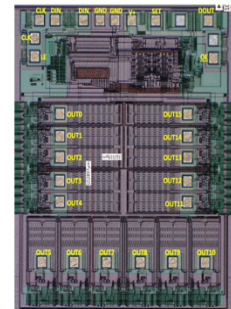


Figure 4.15. Details of display driver ICs MIC5981 (left) & MAX6971(right).

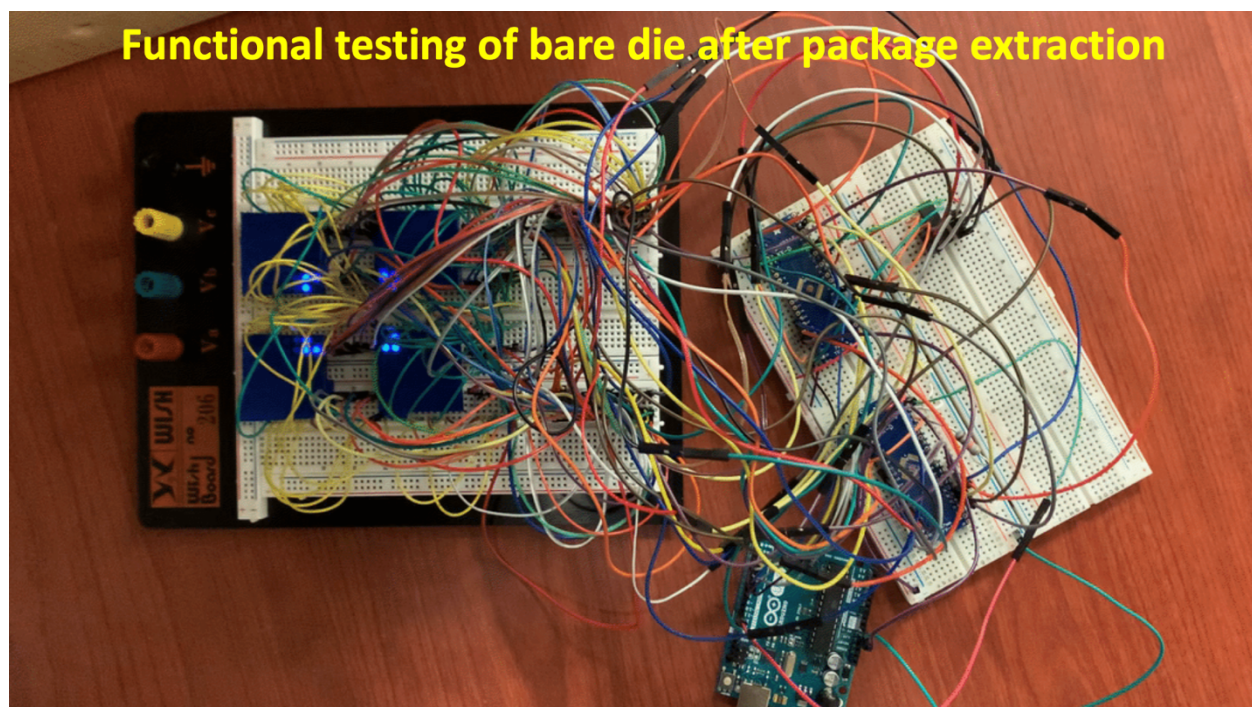


Figure 4.16. Functionality testing of bare die display driver ICs after depackaging.

4.2.2. Fabricated FlexTrate™ microLED display:

An optical micrograph of the fabricated FlexTrate™ microLED display is shown in **Figure 4.17 (left)**. The inset shows the powering of the display using a manual probe station. **Figure 4.17 (right)** shows the fully released FlexTrate™ microLED display after being conformed to a 10mm bending surface. We can notice that the display is highly flexible and transparent. Zoomed in images of the various integrated ICs is shown in **Figure 4.18**. Two levels of metallization are used to connect the various pads of the driver ICs to the corresponding output lines and control terminals. The 15k ohm resistor dies were fabricated in-house by patterning 100nm Au thin films into serpentine structures on a Si wafer using liftoff and then dicing the wafer.

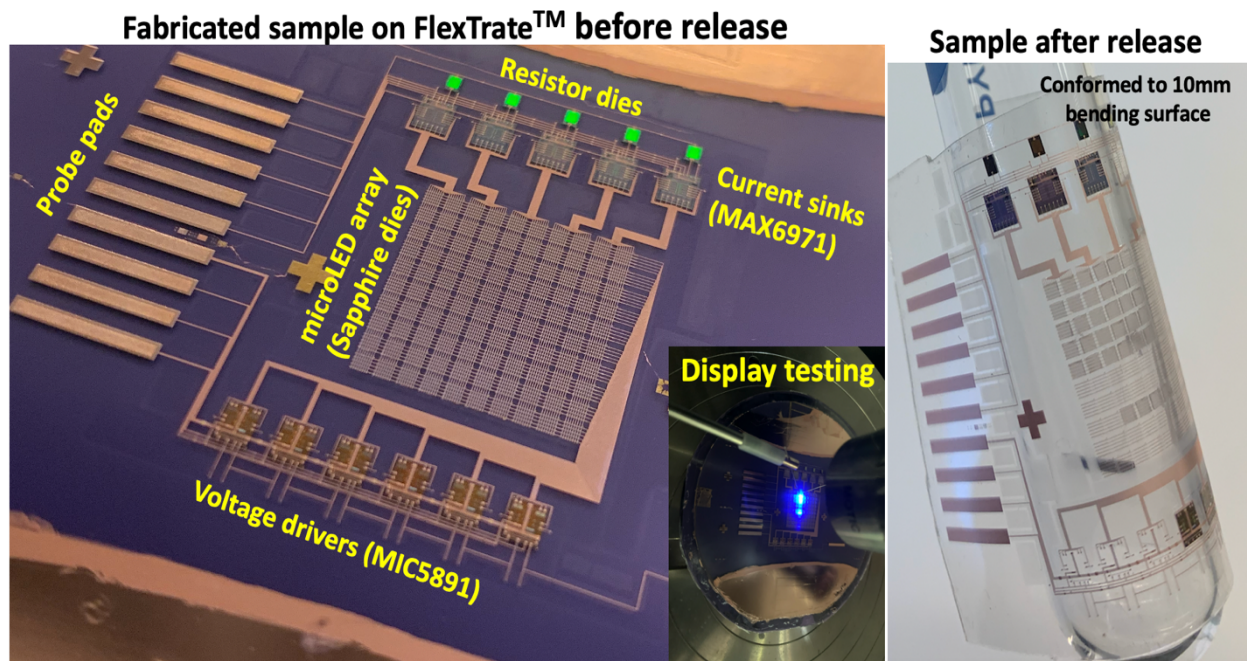


Figure 4.17. Optical micrograph of fabricated FlexTrate™ microLED display (left), Powering of fabricated display using a manual probe station (inset), sample after release from handler 2 (right).

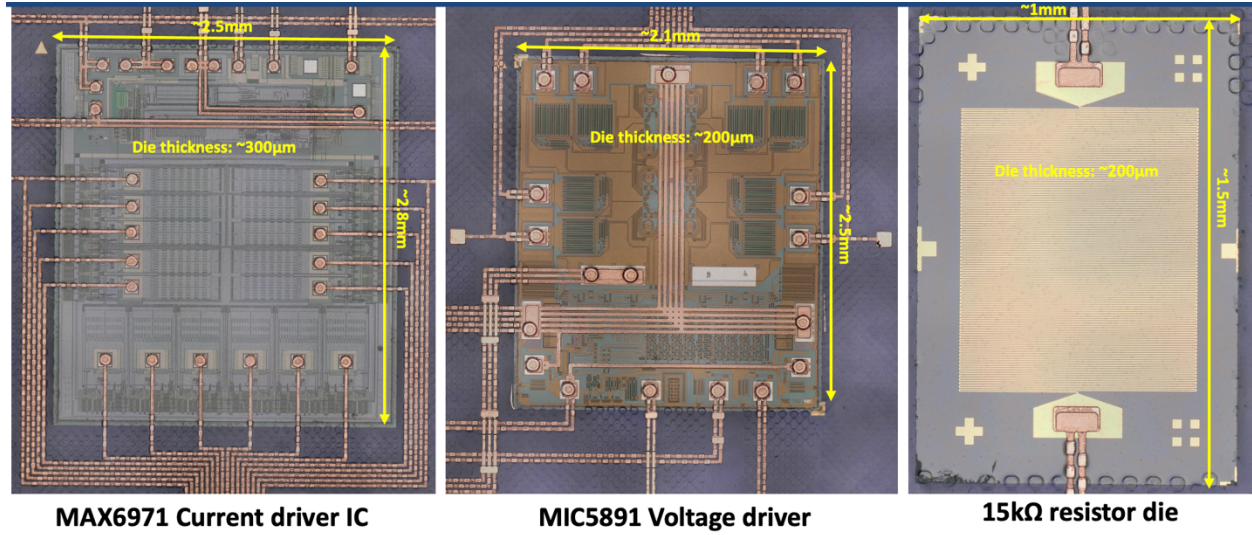


Figure 4.18. Optical images of various heterogeneously integrated ICs on the fabricated display.

Figure 4.19 shows the zoomed-in image of an individual sapphire dielet with 135 microLEDs. We can see that only 40 microLEDs are connected to the passive matrix. If we further zoom in on the metallization, we see how the two levels of metal wiring have been realized. The horizontal metal line is realized using metal layer 1 while the vertical metal line using metal layer 2. Both these metal wires use electroplated copper to a thickness of $5\mu\text{m}$ and are vertically corrugated, see [2]. Both metal wires lie on the same FlexTrate™ plane except in those areas where they intersect. At the intersection regions, a $5\mu\text{m}$ SU-8 bridge (patterned SU82005) is used to prevent the two lines from shorting as shown in **Figure 4.19**. This method of patterning the separation dielectric (SU-8) to only those regions where the wires intersect significantly improves the mechanical flexibility of the sample and makes the interconnects more reliable. If the dielectric was deposited throughout the sample area, the stiffness of the SU-8 (Young's modulus $\sim 2\text{GPa}$) compared to PDMS

(Young's modulus $\sim 400\text{KPa}$) will increase the mechanical stresses on the interconnects and limit overall sample flexibility.

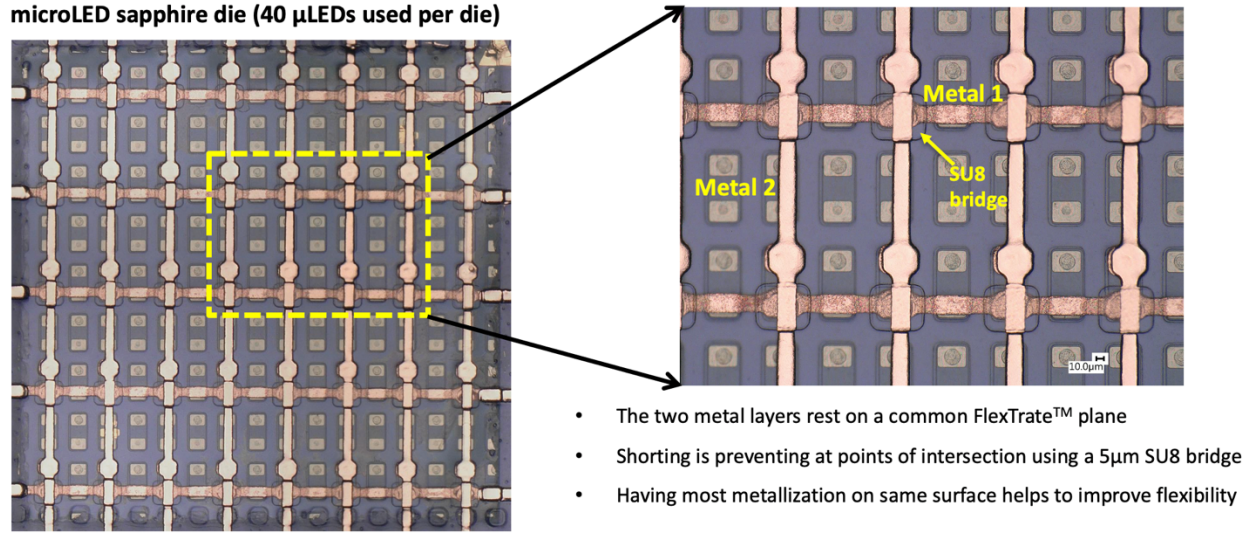


Figure 4.19. Optical image of an individual sapphire dielet integrated on the FlexTrate™ display with a zoomed in view of the two metallization levels.

4.2.3. Testing of Fabricated FlexTrate™ microLED display:

The fabricated microLED display was driven using the MAX6971 and MIC5891 display drivers where the control signals and data were provided using an Arduino setup through a manual probe station. A row scan operation of the passive matrix display is shown by the series of optical images in **Figure 4.20**. The microLEDs were driven by a current of 3mA per device as set by the 15k ohm resistor. The display brightness was measured using an optical luminance meter and comes out to around 10^5 Cd/m^2 (around 1000X of an OLED display). A comparison between the demonstrated flexible microLED display and other such displays in literature is given in **Table 4.1**. We find that our demonstrated display stands out in minimum microLED

pitch, minimum wiring pitch, flexibility, and display PPI. To the best of our knowledge, this demonstration is also the only one that heterogeneously integrates bare-die display driver ICs to show full functionality. There however needs to be improvement when it comes to the size of microLEDs integrated as well as the resolution. The integrated microLED size must reduce to less than $50 \times 50 \mu\text{m}^2$ and display resolution extended beyond 100 x 100.

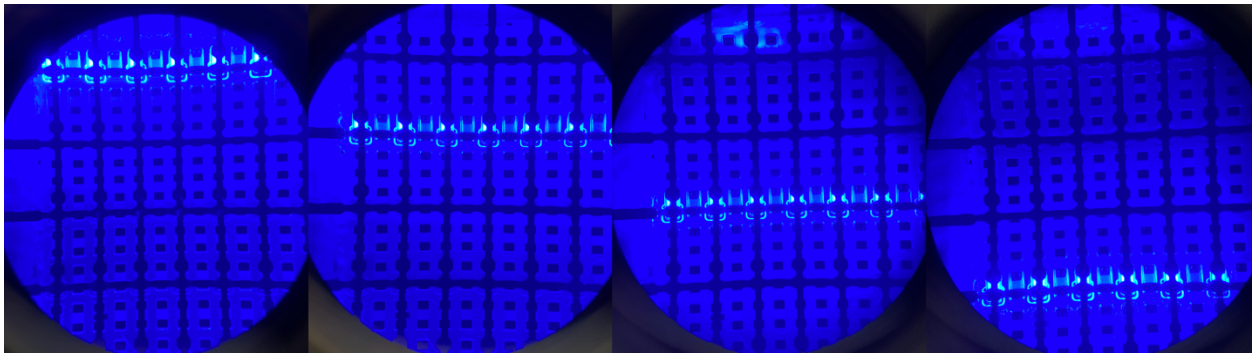


Figure 4.20. Row scan operation of fabricated passive matrix display.

Reference	μLED size (μm)	Min. μLED pitch (μm)	Min. wire Pitch (μm)	Display Resolution	Pixel Per Inch (PPI)	Drivers integrated ?	Substrate	Flexibility (mm rad.)
[1]	100 x 100	300	50	5 x 5	100	No	PET	20
[2]	50 x 50	> 300	> 300	16 x 16	N.R.	No	PET	7
[3]	8 x 15	100	40	100 x 100	254	No	PEN	N.R.
This work	100 x 50	75	40	48 x 80	150-300	Yes	PDMS	5

N.R. : Not Reported

[1] Tae-il Kim et al., *small* 2012, 8, No. 11 1643-1649

[2] Sang-il Park et al., *Science* Vol 325, Aug 21, 2009

[3] C. A. Bower et al., Vol 5., No. 2, 2017. *Photonics Research*

Table 4.1. Comparison between the demonstrated flexible microLED display and other such displays in literature.

4.2.4. Calculation of Wall Plug Efficiency (WPE) of the fabricated display:

Firstly, to calculate the maximum power consumed by the fabricated display by assuming that every microLED in a row lights up during the scan operation of the Passive Matrix (PM) display. A rough schematic of the fabricated PM display on FlexTrate™ using the dielet approach is given in **Figure 4.21**. In this figure, the first scan line is switched ON and hence all the microLEDs in the first row are lit (all current sinks ON for maximum power) while the devices in all other rows are OFF.

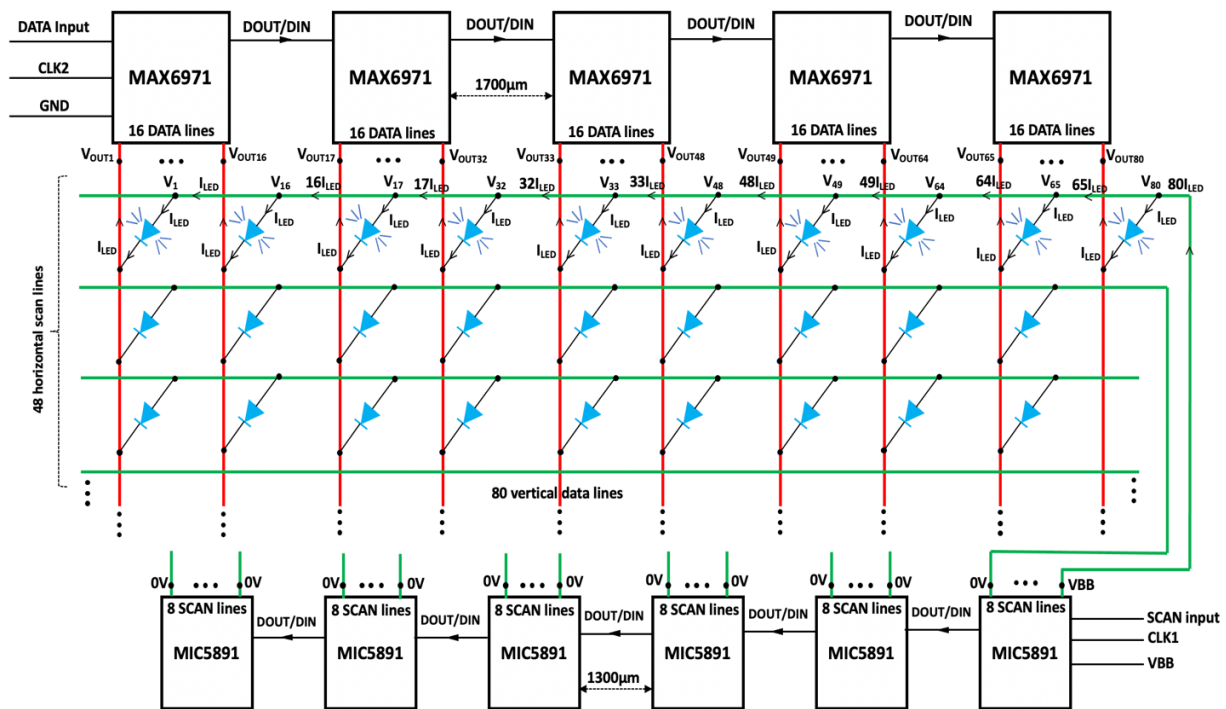


Figure 4.21. Electrical schematic of the fabricated 48 X 80 PM microLED display on FlexTrateTM using the dielet approach. The currents and voltages in different branches and nodes along the first scan line (ON) are also identified. All microLEDs on the first scan line are assumed to be lit.

Detailed schematics of the MAX6971 current driver IC, MIC5891 voltage source IC and the top left-most sapphire dielets are given in **Figure 4.22**.

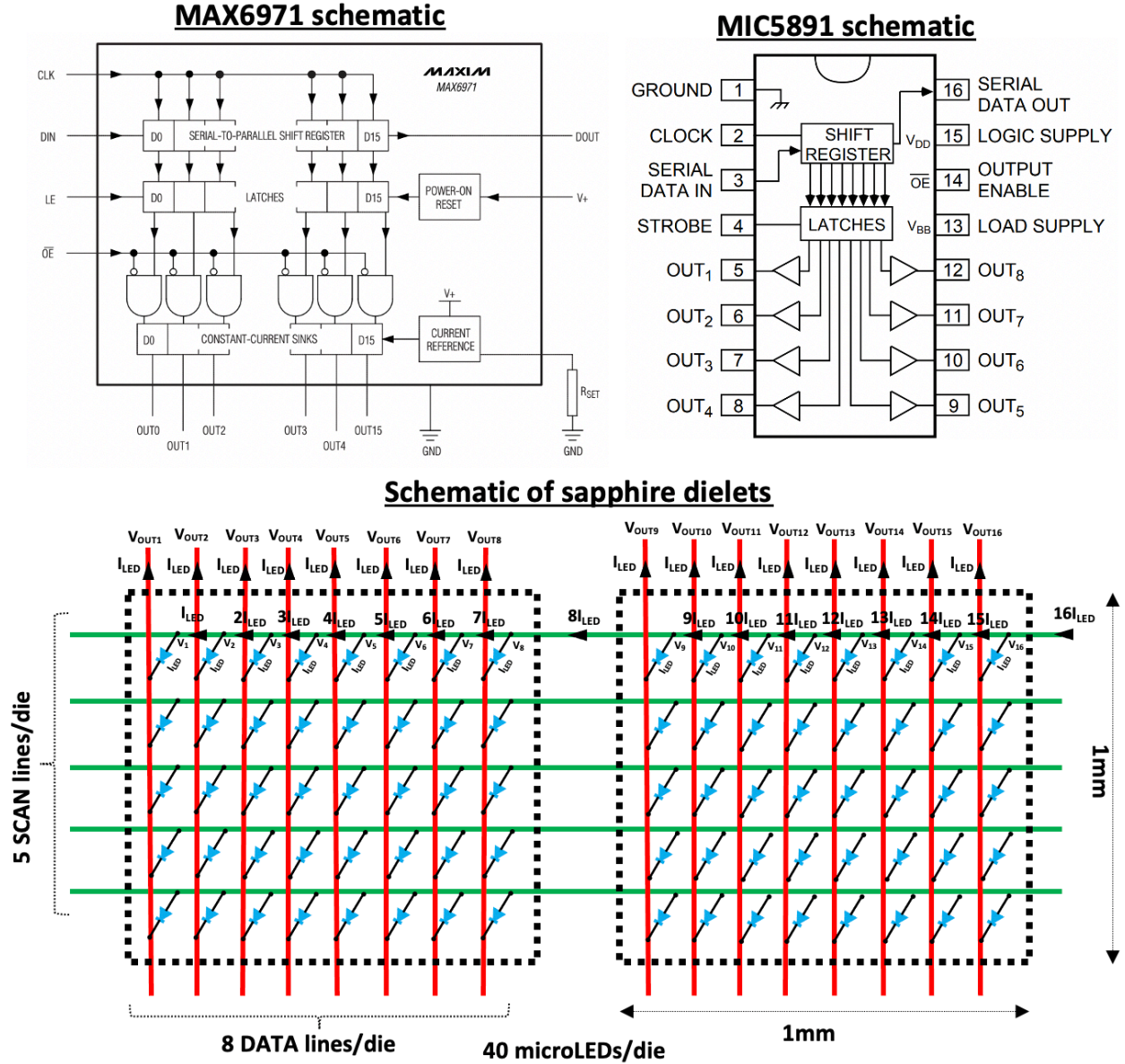


Figure 4.22. Schematic of MAX6971 current driver IC, MIC5891 voltage source IC, & top left-most sapphire dielets.

Let P_{LED} be the average power consumed by each individual LED, $P_{SCAN,dyn}$ is the dynamic charge-discharge power consumed by each scan line during its selection and

subsequent de-selection, $P_{DATA,dyn}$ is the dynamic charge-discharge power consumed by each data line, $P_{MAX6971}$ is the total power consumed by MAX6971 dielets (Current sink) due to internal logic and output current sinks, $P_{MIC5891}$ is the total power consumed by the MIC5891 dielets (Voltage source) due to internal logic, & P_{Loss} is the I^2R heating losses in the metal lines during operation.

The display has 48 scan lines and 80 data lines (48 x 80 display) driven by five MAX6971 and six MIC5891 ICs respectively at the display peripheries. The total average power consumed by the display is hence:

$$P_{TOTAL} = 3840 P_{LED} + 48 P_{SCAN,dyn} + 80 P_{DATA,dyn} + P_{MAX6971} + P_{MIC5891} + P_{Loss} \quad (4, 1)$$

Assuming an operational frame rate of 120Hz for the display, the frame period is hence 8.33ms. During a full frame period, the duration of time that a microLED is switched ON is 0.1735ms, as the duty cycle of operation is given by 1/ (No. of scan lines). For a microLED that is switched ON, its average power consumed is hence given by:

$$P_{LED} = \left(\frac{1}{48}\right) V_{LED} I_{LED} ; I_{LED} = 3mA \text{ \& } V_{LED}(I_{LED}) = 3.5V \quad (4, 2)$$

Hence the calculated average power consumed per LED is hence $P_{LED}=0.22mW$. Power consumed by all 3840 microLEDs is **844.8mW**.

The capacitance per unit length of the given scan and data lines are negligibly small due to the small width ($\sim 20\mu m$) and thickness ($\sim 5\mu m$) of the metal lines, also the switching frequency is only 120Hz for the scan line and 5.76KHz for the data line. Hence the dynamic switching power for the scan ($P_{SCAN,dyn}$) and data ($P_{DATA,dyn}$) lines

given by CV^2f is negligible compared to the other power components in equation (4,1) and can be neglected.

Now to compute the frequency of **CLK1** and **CLK2** (see **Figure 4.21**); frequency of **CLK1** for the MIC5891 is $48 \times 120\text{Hz} = 5.76\text{KHz}$ and frequency of **CLK2** for the MAX6971 is $80 \times 48 \times 120\text{Hz} = 460.8 \text{ KHz}$. Under these operational frequencies of the ICs, to determine their average power consumed P_{MIC5891} and P_{MAX6971} .

Firstly, to compute the total power consumed by the six MIC5891 ICs, we note that one of the scan lines is always ON, hence the total logic power consumed by ICs is:

$$P_{\text{MIC5891}} = 6 V_{DD} I_{DD} \quad (4,3)$$

The logic supply (V_{DD}) to the MIC5891 IC is 5V from the Arduino and the measured logic current (I_{DD}) drawn by each IC during its scan operation is 2mA. The total power consumed by the MIC5891 ICs for the scan operation is hence **60mW**.

Now to compute the total power dissipated in the MAX6971 current driver ICs. The dissipated power has two components: a logic component due to the power consumed by the internal switching of the IC's logic as well an output component due to the sinking of the microLED drive current at the output pins of each IC. Assuming that the logic supply voltage for each MAX6971 IC is V_+ (=5V from the Arduino) and the corresponding logic supply current is I_+ (=5mA per IC, measured), the total logic power drawn by all the MAX6971 ICs during their current drive operation is $5V_+I_+=125\text{mW}$. To compute the output component of the power consumed for all the MAX6971 ICs during their microLED drive operation (all devices in a scan line

turned ON), we can refer to the equivalent circuit diagram along a full scan line (that is ON) during the current drive operation as shown in **Figure 4.23**.

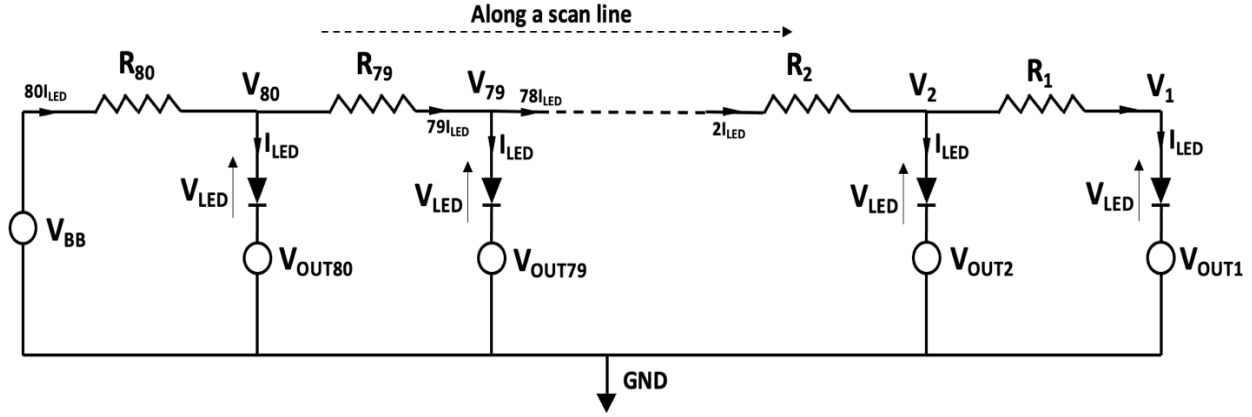


Figure 4.23. Equivalent circuit diagram of a single scan line during selection while all microLEDs are ON.

The total output component of the power $P_{out,MAX6971}$ of all the MAX6971 ICs during their current drive operation is given by:

$$P_{out,MAX6971} = \sum_{k=1}^{80} I_{LED} V_{OUTk} \quad (4,4)$$

From the equivalent circuit diagram shown in **Figure 4.23**, we find that:

$$V_{OUT80} = V_{80} - V_{LED} = V_{BB} - 80R_{80}I_{LED} - V_{LED}$$

$$V_{OUT79} = V_{79} - V_{LED} = V_{BB} - 80R_{80}I_{LED} - 79R_{79}I_{LED} - V_{LED} \dots\dots\dots$$

$$\text{Thus, } V_{OUTi} = V_{BB} - V_{LED} - I_{LED} \sum_{j=i}^{80} j R_j \quad (4,5)$$

Substituting equation (4,5) in equation (4,4) we get an expression for the total output component of the power $P_{out,MAX6971}$ of all the MAX6971 ICs during their current drive operation:

$$P_{out,MAX6971} = I_{LED} \sum_{K=1}^{80} (V_{BB} - V_{LED} - I_{LED} \sum_{j=k}^{80} j R_j) \quad (4,6)$$

The value of $V_{BB} = 8V$ is the load supply voltage provided by the external power supply to all the MAX6971 ICs. The value of the various line resistances along the scan line, R_{1-80} can be calculated assuming a Cu metallization width of $20\mu m$ and a thickness of $5\mu m$ with a resistivity of $1.9 \times 10^{-8} \text{ ohm-m}$:

$$R_{1-7} = R_{9-15} = R_{17-23} = R_{25-31} = R_{33-39} = R_{41-47} = R_{49-55} = R_{57-63} = R_{65-71} = R_{73-79} \\ = 0.02 \text{ ohms}$$

$$R_8 = R_{16} = R_{24} = R_{32} = R_{40} = R_{48} = R_{56} = R_{64} = R_{72} = 0.078 \text{ ohms}$$

$$R_{80} = 5.25 \text{ ohms}$$

The calculated $P_{out,MAX6971}$ is 735mW and hence the total power consumed by all the MAX6971 ICs during the current drive operation is **860mW**.

From the equivalent circuit diagram in **Figure 4.23**, we find that the average total I^2R heating losses in the metal lines during the display operation, P_{Loss} is given by the expression:

$$P_{Loss} = (I_{LED})^2 R_1 + (2I_{LED})^2 R_2 + (3I_{LED})^2 R_3 + \dots + (80I_{LED})^2 R_{80} \quad (4,7)$$

For the $I_{LED} = 3mA$, the calculated $P_{Loss} = 345mW$.

The total average power consumed by the full display according to equation (4,1) is thus **2.11W**.

The experimentally measured output optical power of the FlexTrate™ fabricated PM microLED display at a viewing distance of 20 centimeters when all the microLEDs during a row scan are turned ON is **210mW**. The calculated wall plug efficiency of the FlexTrate™ microLED display using the dielet approach is hence approximately **10%**.

4.2.5. Fabrication issues of current microLED display on FlexTrate™:

There were two major fabrication issues that were faced during the building of this prototype:

(1) Yield issues during copper electroplating: During the electroplating of the copper metal interconnects, nodular growth due to current crowding could cause shorting of adjacent wires as shown in **Figure 4.24**. If these adjacent wires carry control or power signals for the display, catastrophic failures can occur. To prevent this issue, better plating chemistries and optimized plating conditions are needed to be used in the future for a more uniform electroplating.

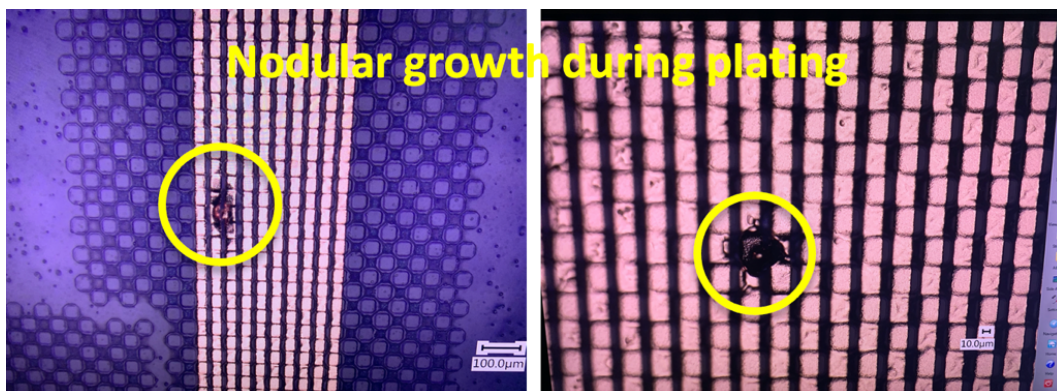


Figure 4.24. Nodular growth due to current crowding causing shorting of adjacent wires.

(2) Un-singulated microLEDs on sapphire dielets:

The microLEDs on the sapphire dielets of the fabricated prototype are un-singulated due to the contact delamination issue. The thin uGaN between the devices is however conductive, leading to the shorting of the nGaN regions of the microLEDs allowing us to only demonstrate the row scan operation of the display now. In the future, in-house fabricated microLEDs are to be used to prevent the contact delamination issue upon singulation and make full functionality demonstrations of the FlexTrate™ display using either the mass transfer or dielet approach, see **Chapter 5**.

REFERENCES

1. G. Ezhilarasu et al., "A Heterogeneously Integrated, High Resolution and Flexible Inorganic microLED Display using Fan-Out Wafer-Level Packaging," © 2020 *IEEE 70th ECTC*.
2. A. Hanna et al., "Extremely Flexible (1mm bending radius) Biocompatible Heterogeneous Fan-Out Wafer-Level Platform with the Lowest Reported Die-Shift ($<6\mu\text{m}$) and Reliable Flexible Cu-based Interconnects," © 2018 *IEEE 68th ECTC*.
3. G. Ezhilarasu et al., "High Yield Precision Transfer and Assembly of GaN microLEDs Using Laser Assisted Micro Transfer Printing," © 2019 *IEEE 69th ECTC, Las Vegas, NV*.

5. Future Work

5.1. FlexTrate™ microLED displays with custom microLEDs

As we discussed in previous chapters, the mass transfer process is incompatible with microLEDs fabricated using a conventional LED process. In particular, the contacts of such a microLED structure are not capable of withstanding the high mechanical stresses involved during device singulation (GaN dry etching), GaN Laser Lift-Off (LLO), adhesive bonding or Excimer laser debonding. Thus, at any of these process steps, the contacts could easily delaminate. In a conventional LED process [1], the contacts (P & N) are directly evaporated onto the pGaN and nGaN regions without any stress buffer layers to protect the contacts, see **Figure 5.1 (left)**. To make the contacts survive the mass transfer process, custom microLED structures must be designed considering the stresses produced at the various process steps. The mechanical stresses during these processing steps could be modeled using FEM and used to engineer stress buffer layers as part of the microLED structure. Preliminary work in this direction can be seen in the modified, mass - transfer 'safe' microLED structure shown in **Figure 5.1 (right)**. Here, once the P and N contacts have been evaporated, a stress buffer dielectric layer is patterned on top of the microLEDs in such a way that the dielectric overlaps a certain area of the contact metallization from its boundary. This overlapping dielectric essentially holds the contacts down, thus making them more robust to stress-induced delamination, see **Figure 5.2**. Preliminary

results show that even after complete singulation of this microLED, the contacts do not show any signs of delamination.

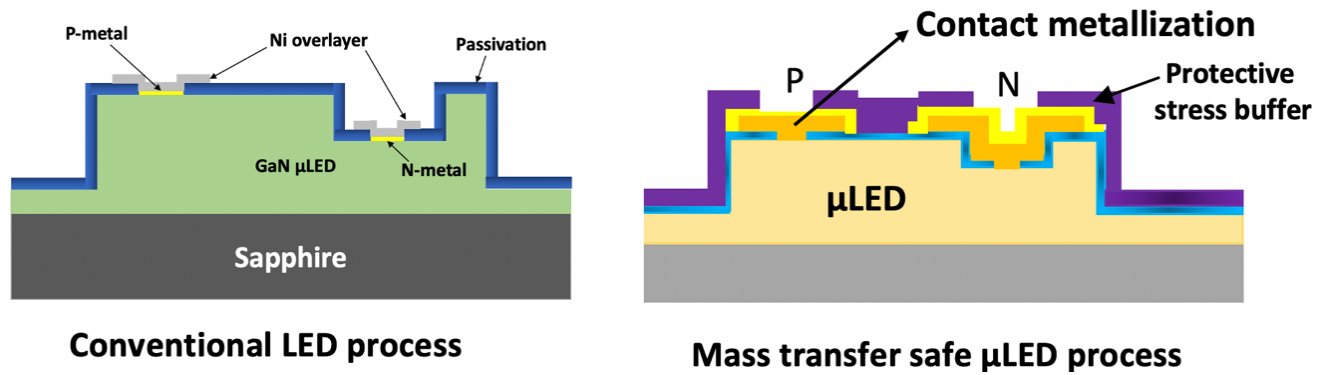


Figure 5.1. Conventional LED process Vs. Mass transfer safe microLED process.

Mass transfer safe μLEDs (fabricated at UCLA)

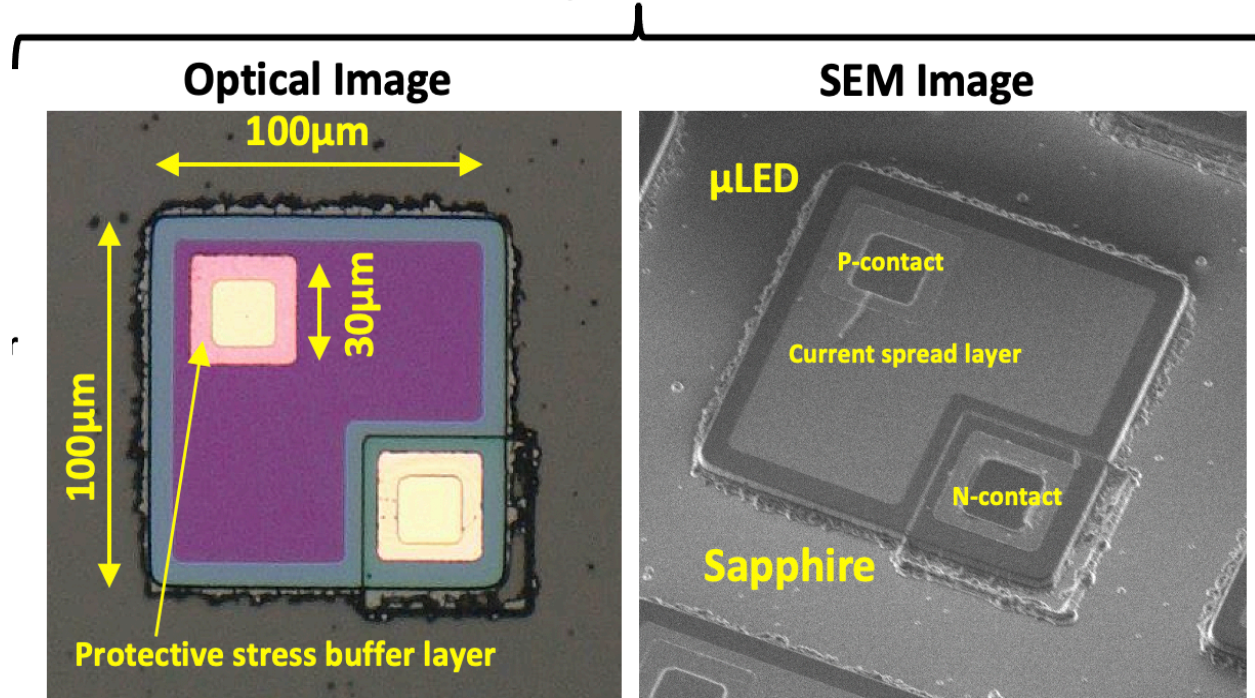
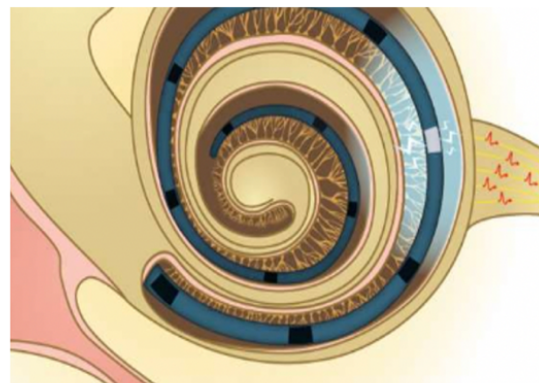
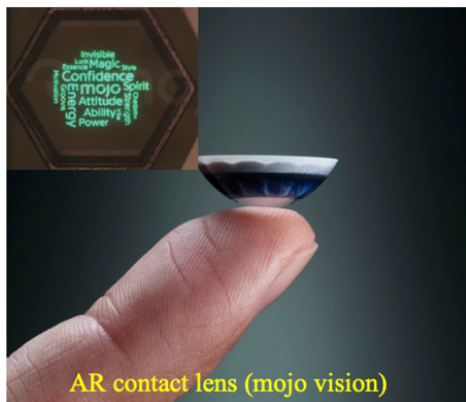


Figure 5.2. Mass transfer safe microLEDs fabricated at UCLA.

5.2. Wireless Power Transfer for FlexTrate™ microLED display

There are several application spaces where the form factor of the full microLED display is critical. For example, in the case of wearable Augmented Reality (AR), the entire display along with all the peripherals must fit within the area & volume of a standard contact lens [2], see **Figure 5.3 (left)**. In the case of implantable microLED displays for Optogenetics, the fact that the flexible display must be placed within the body of a living organism significantly limits the form factors [3]. The display needs to be flexible, ultra-thin, light weight and completely autonomous to enable insertion into any part of an animal's body for study without interfering with its normal behavior [4]. **Figure 5.3 (right)** illustrates a microLED display that is to be surgically inserted into the cochlea of a rat where the form factors of the display are severely restricted [5].



Flexible Optical cochlear implant
(Medical Xpress, 07/12/18)

Figure 5.3. Small form factor microLED displays used in AR (left) and Optogenetic cochlear implant (right).

FlexTrate™ [6] allows the heterogenous integration of all the display components including the display drivers and the microcontrollers. As these components are integrated in bare die form with ultra-fine pitch wires, extremely small form factors could potentially be obtained. For a real working product, we must also consider other aspects such as powering & communicating with the display device. If the communicating and powering is done using wires, it would make the overall display bulky due to the need for connectors which is highly impractical in the application spaces reported here. The use of an energy storage element such as a battery or super capacitor is also stymied by their poor energy densities and hence bulky form factors [7]. The most practical solution is hence to send power and data to the display wirelessly through an RF link [8]. To demonstrate that such an RF link can be successfully designed and implemented on FlexTrate™, we fabricated an NFC (Near Field Coupled) power system to demonstrate efficient wireless power transfer [9].

A near-field Wireless Power Transfer (WPT) system based on 2-coil resonant magnetic coupling at 13.56 MHz that supplies a regulated voltage to a single green (AlGaInP) microLED was demonstrated on FlexTrate™ [9]. Both the primary/external coil and secondary/implant coil were integrated on FlexTrate™. The circuit schematic of the integrated system is given in **Figure 5.4**. As we can see, the primary side is in series resonance while the secondary is in parallel resonance at a resonant frequency of 13.56 MHz. Up to eight commercially purchased heterogeneous dies were integrated at 40 μm interconnect pitch with a high Q (>30) implant coil on FlexTrate™ to realize the full system. **Figure 5.5** shows an optical image of the

fabricated implantable system and a proposed system concept for wireless subdural Optogenetics.

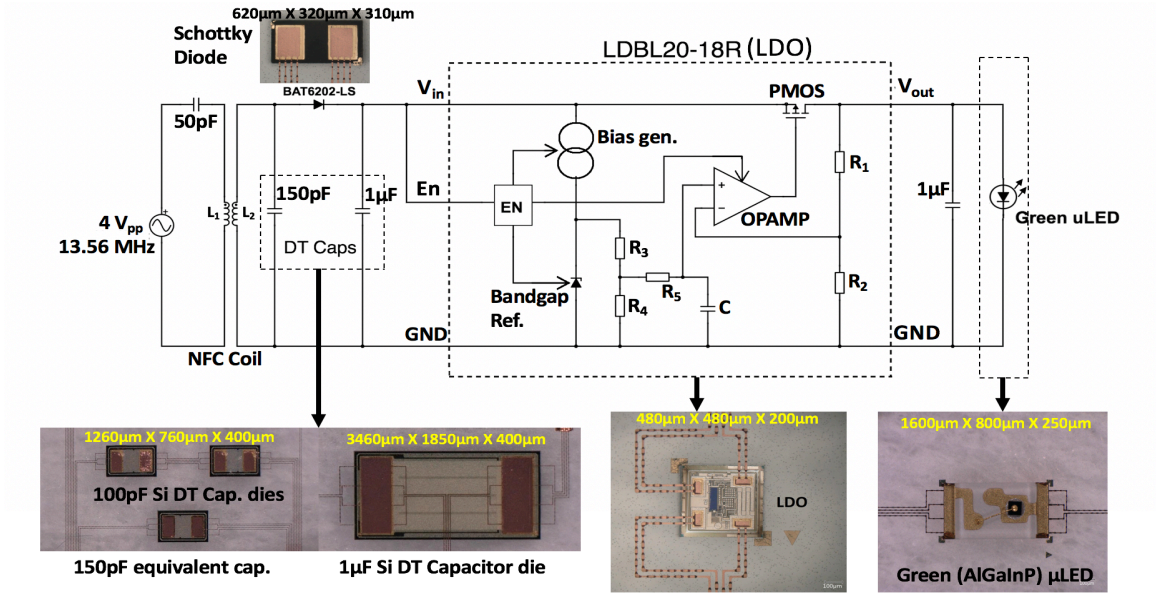


Figure 5.4. Circuit schematic of WPT system on FlexTrate™ [9].

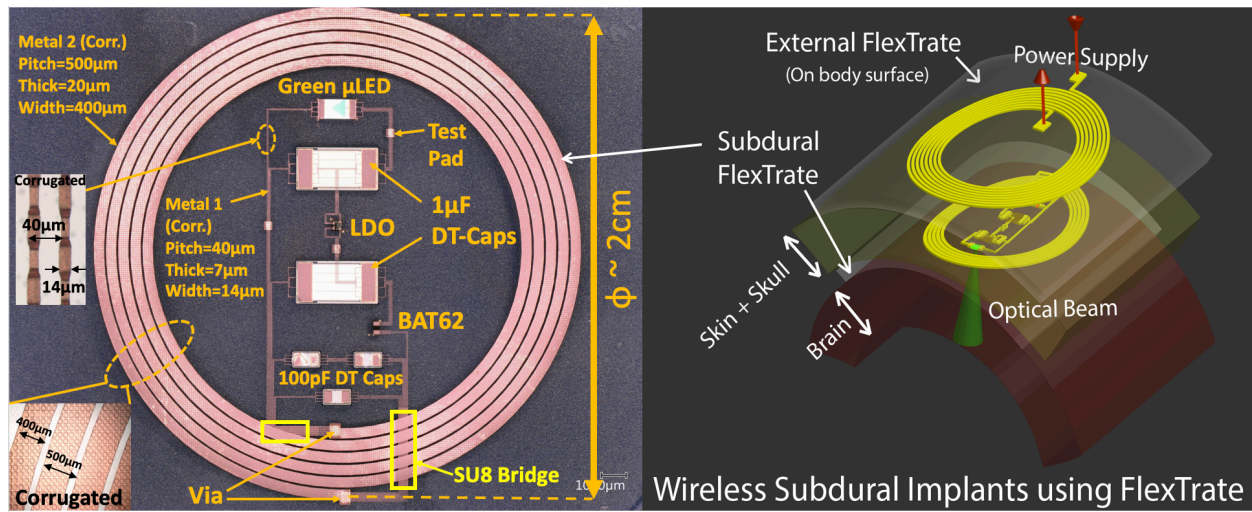


Figure 5.5. Optical image of integrated system (left) & schematic of a system concept (right) [9].

To characterize the performance of this system in different environments and coupling conditions, we experimentally measured the link Power Transfer Efficiency (PTE) using a Vector Network Analyzer (VNA) as shown in the setup schematic, **Figure 5.6**. The measurement results are summarized in **Figure 5.7**. The WPT link was shown to operate at $> 30\%$ Power Transfer Efficiency (PTE) in a Phosphate Buffered Saline (PBS) solution at transcutaneous (<0.6 cm) coupling distances [9]. The system is also shown to be operational even at an exaggerated bending of 5mm radius. The performance of the fully integrated system was also studied by comparing with a breadboard duplicate as shown in **Figure 5.8**. We find that the FlexTrate™ system performance closely matches that of the breadboard duplicate except for a $<5\%$ voltage droop at the output possibly due to the increased series resistance of the fine electroplated interconnects.

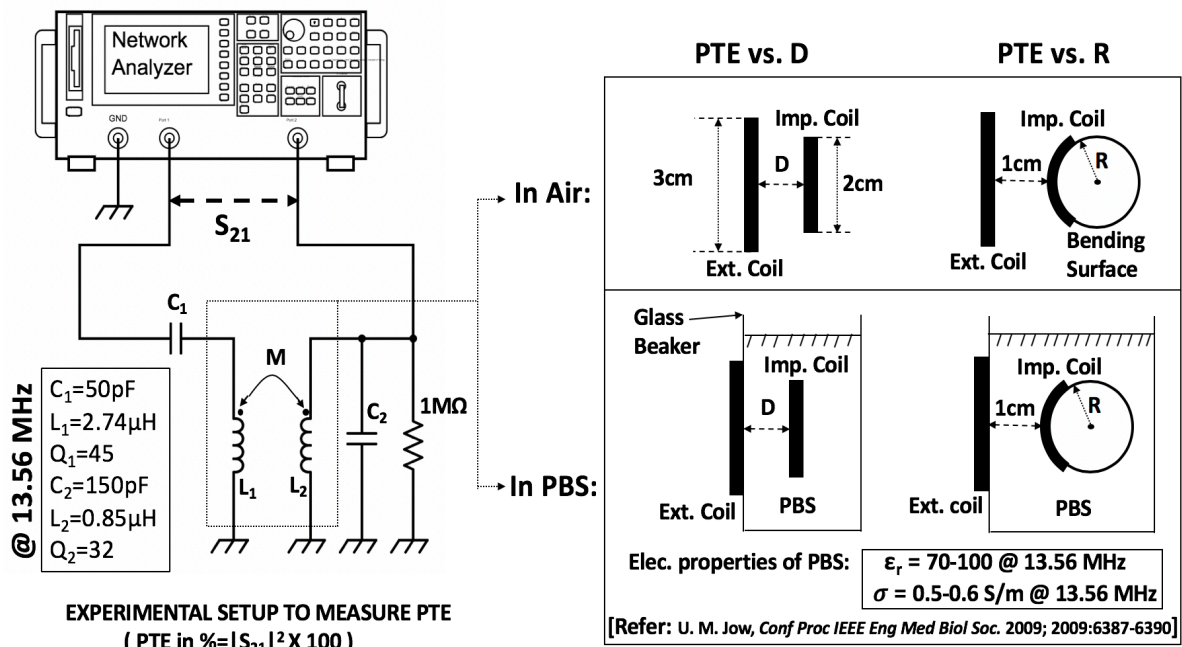


Figure 5.6. Experimental setup for WPT link characterization.

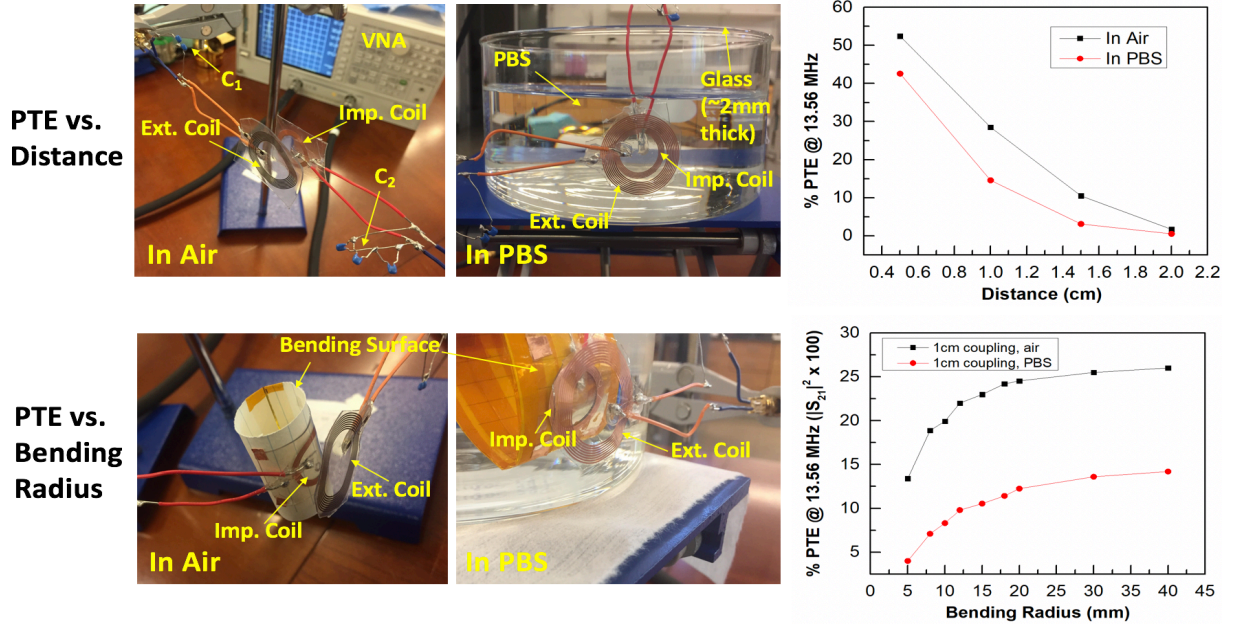


Figure 5.7. Characterization results of link PTE (%) for different conditions [9].

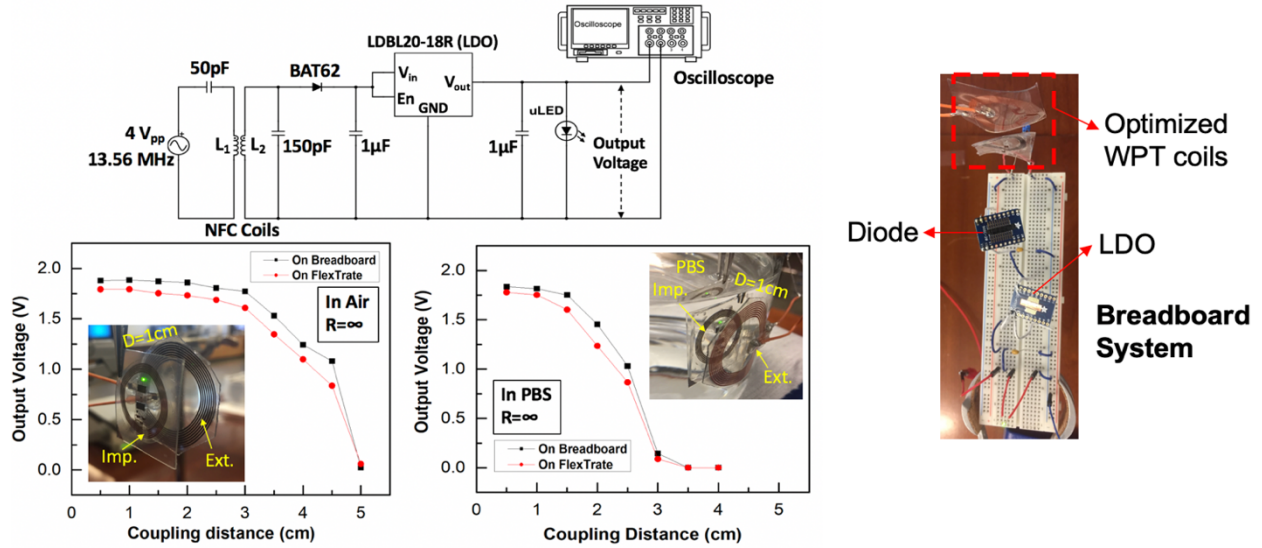


Figure 5.8. Full wireless power transfer system characterization results [9].

The successful operation of this wireless power transfer system under different conditions of bending is also shown qualitatively in **Figure 5.9**.

Coupling Distance= 1cm ; Frequency= 13.56MHz ; $V_{pp}= 4V$

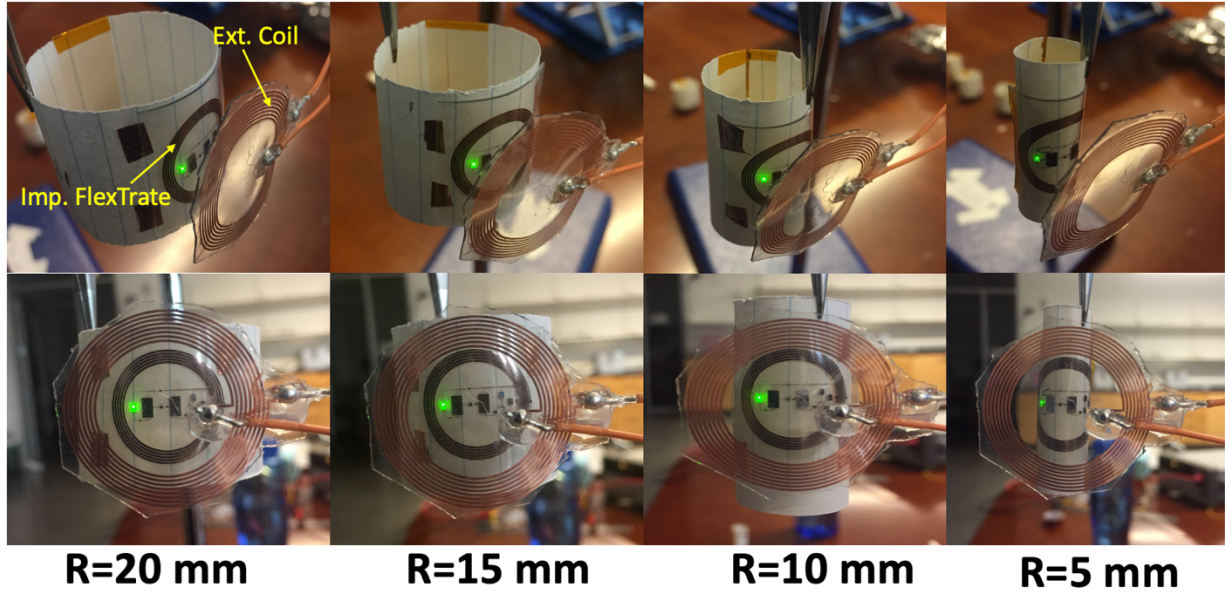


Figure 5.9. Operation of WPT system under different conditions of bending of the Implant coil [9].

In Optogenetics, a display must be run at pulsed mode in a passive matrix configuration [10]. The current design can readily power a 50 X 50 microLED display at 1mA current per device. The patterns to be displayed could be stored in an integrated microcontroller.

5.3. Demonstration of full color microLED displays on FlexTrate™

Until this point, we had shown how to fabricate a monochrome microLED display on FlexTrate™. For any commercial display application, the ability to demonstrate a full color display is critical [11]. There are essentially two approaches to fabricating a full color flexible microLED display: (1) Transfer printing of each color (RGB) microLEDs separately using three separate mass transfer steps [12] & (2) Having one

color of microLED, usually UV, as an optical pump to a color conversion medium such as Phosphors or Quantum Dots (QDs) to generate the other colors [13].

Approach (1) is impractical due to several reasons: Mass transfer processes are expensive and compounding them can significantly impact yields, green & red microLEDs are highly power inefficient compared to UV/ blue microLEDs [14], red microLEDs cannot be scaled down due to large surface recombination velocities [15], and complexity in driving schemes due to different turn-on voltages of each microLED color [12]. Approach (2) using phosphors is impractical due to the large particle size of phosphors (10's of micron) which causes emission non-uniformity issues as microLEDs are also scaled down to 10's of micron sizes [13]. Approach (2) using QDs is hence the most practical for this display technology due to their small size, uniformity, and color saturation quality [13].

Colloidal QDs have several advantages when used with microLED displays:

- Based on CdSe or InP and have narrow emission linewidths (FWHM~20-30nm)
- High PL quantum yield (PLQY > 90%), high color saturation
- Inexpensive solution processability: Inkjet or Aerosol Jet printing used for dispensing

A process flow for the integration of colloidal QDs with an optical UV microLED 'optical pump plane' for the demonstration of a full color, flexible display on FlexTrateTM is shown in **Figure 5.10**.

This process flow leverages the earlier work of fabricating monochrome microLED displays on FlexTrate™; UV microLEDs are used here to fabricate an 'optical pump plane' that excites the QD color conversion layer to generate the RGB colors.

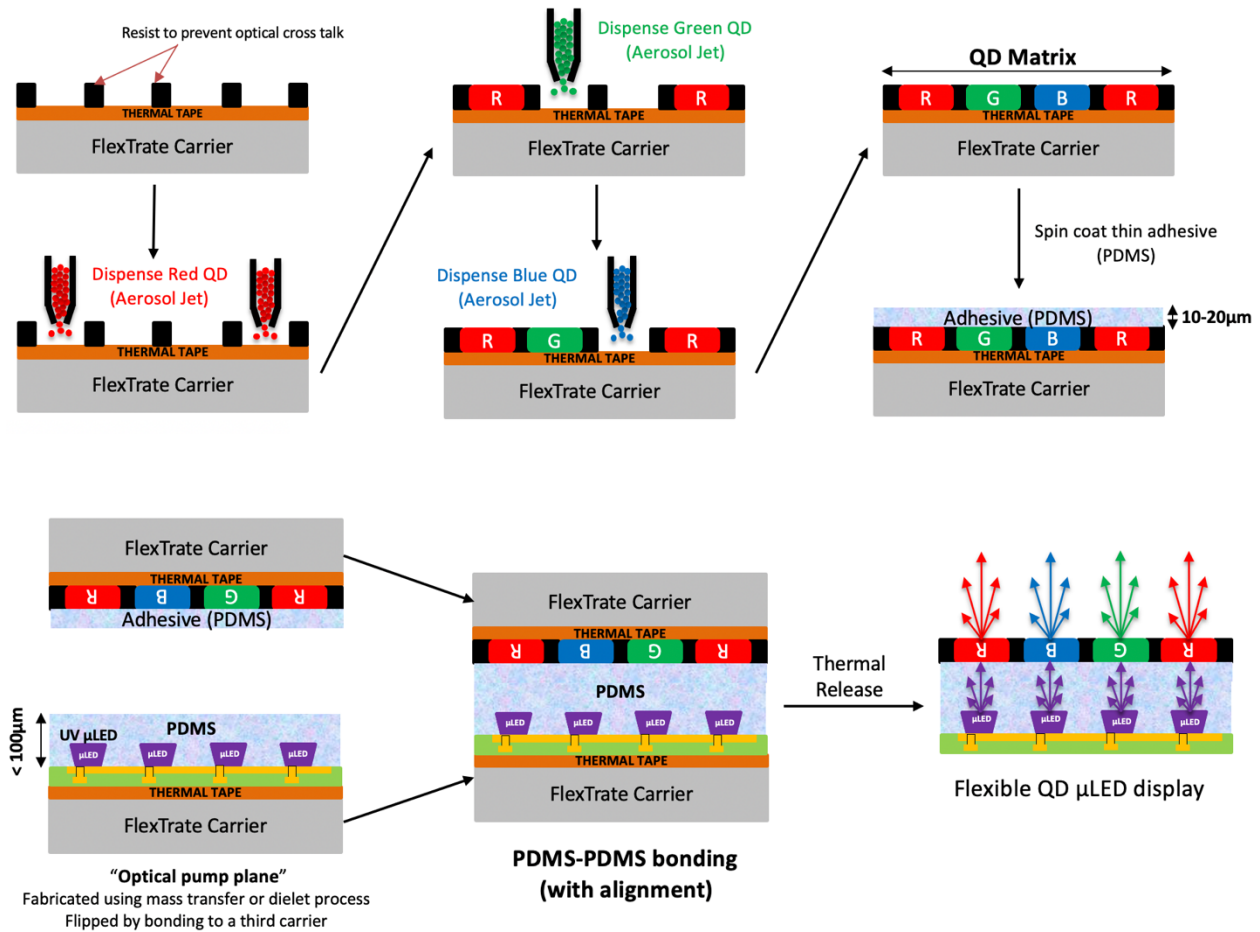


Figure 5.10. Process flow for the integration of colloidal QDs with an optical UV microLED 'optical pump plane' for the demonstration of a full color, flexible display on FlexTrate™.

Figure 5.11 shows some preliminary work done in using UV microLEDs and colloidal QD color conversion layers to generate green and red light. There is a significant leak of the UV backlight (microLED) causing the bluish halo observed in the emitted light.

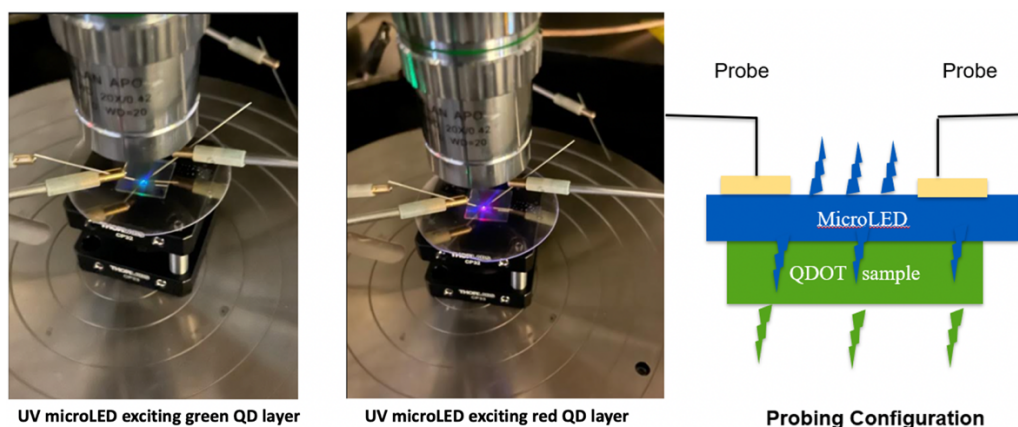
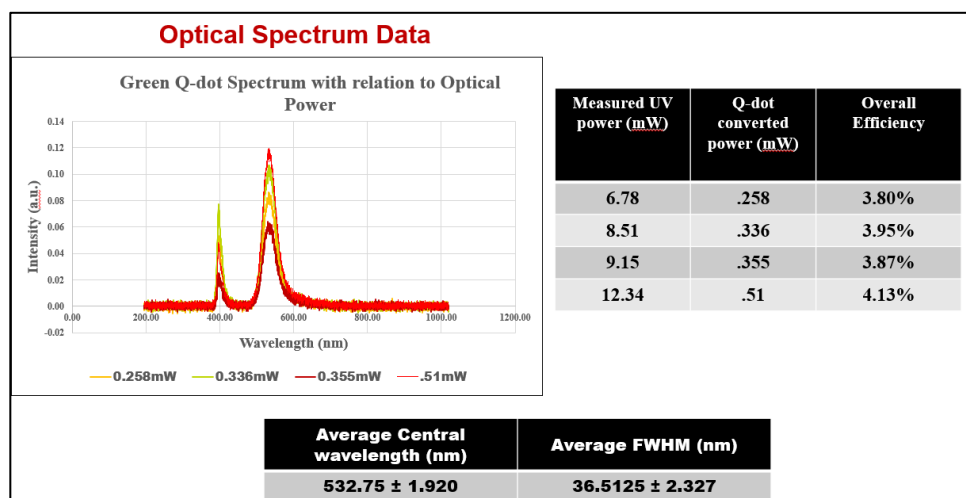


Figure 5.11. UV microLEDs exciting green and red QD color conversion layers respectively.

Figure 5.12 shows the spectral data of color conversion from the UV microLED backlight using green and red QD color conversion layers. The conversion efficiency is only around 2-4% possibly due to limited thickness ($\sim 5\text{-}10\mu\text{m}$) of the QD layers used, causing significant leak of the UV backlight. The light conversion efficiency can be increased significantly by using $> 10\mu\text{m}$ QD layers coupled with a reflector (DBR) to further provide optical recycling of unconverted UV backlight. Research in this direction is ongoing.



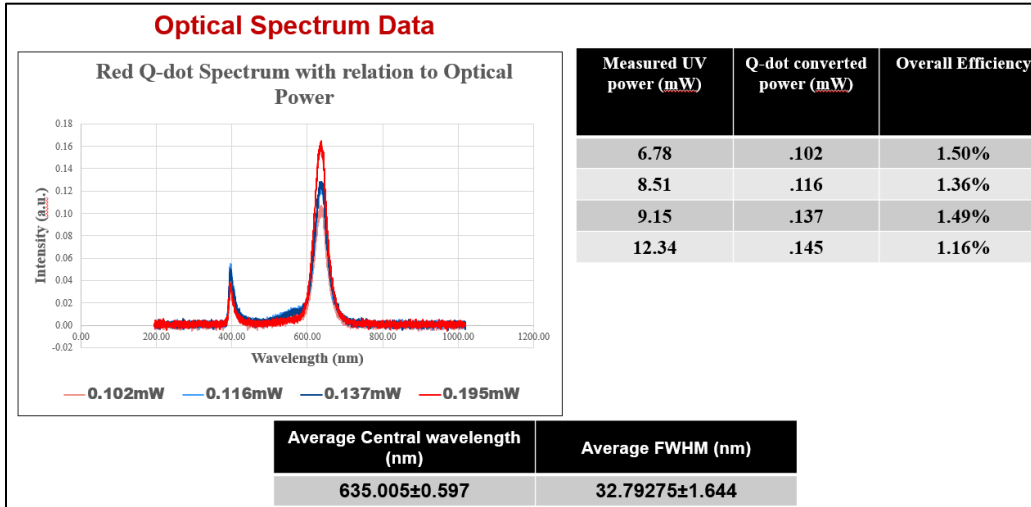


Figure 5.12. Spectral data of color conversion from UV microLED backlight using green and red QD color conversion layers.

REFERENCES

1. Xu Lin Nguyen et al., “The fabrication of GaN-based light emitting diodes (LEDs),” *Adv. Nat. Sci.: Nanosci. Nanotechnol.* 1(2010) 025015 (5pp).
2. Manu Peethambar, “AR evolution towards smart contact lens: A hit or a miss ?,” *University of Maryland*.
3. Seung H. L. et al., “Optogenetic control of body movements via flexible vertical light-emitting diodes on brain surface,” *Nano Energy* 44(2018) 447-455.
4. Gunchul Shin et al., “Flexible Near-Field Wireless Optoelectronics as Subdermal Implants for Broad Applications in Optogenetics,” *Neuron* 93, 509-521, February 2017.
5. C. Gobler et al., “GaN-based micro-LED arrays on flexible substrates for optical cochlear implants,” *J. Phys. D: Appl. Phys.* 47(2014) 205401 (6pp).
6. Takafumi Fukushima et al., “Flexible Hybrid Electronics Technology Using Die-First FOWLP for High-Performance and Scalable Heterogeneous System Integration,” *IEEE Transactions on Components, Packaging, and Manufacturing Technology*, Vol. 8, No. 10, October 2018.
7. Yifan Zhao, Juchen Guo, “Development of flexible Li-ion batteries for flexible electronics,” *InfoMat.* 2020; 2:866-878.
8. J. Pandey et al., “A Fully Integrated RF-Powered Contact Lens With a Single Element Display,” *IEEE Transactions on Biomedical Circuits and Systems*, Vol. 4, Issue: 6, Dec 2010.
9. G. Ezhilarasu et al., “A Flexible, Heterogeneously Integrated Wireless Powered System for Bio-Implantable Applications using Fan-Out Wafer-Level Packaging,” © IEEE 2018 *International Electron Device Meeting (IEDM18-683)*, San Francisco, USA.

10. V. Poher et al., “Micro-LED arrays: a tool for two-dimensional neuron stimulation,” *J. Phys. D: Appl. Phys.* 41(2008) 094014(9pp).
11. F. Templier et al., “GaN-based emissive microdisplays: A very promising technology for compact, ultra-high brightness display systems,” *Journal of the SID* 24/11, 2016.
12. Z. Chen et al., “MicroLED technologies and applications: characteristics, fabrication, progress, and challenges,” *J. Phys. D: Appl. Phys.* 54(2021) 123001(34pp).
13. Zhaojun Liu et al., “Micro-light-emitting diodes with quantum dots in display technology,” *Light: Science & Applications* (2020) 9:83.
14. Virey E. H. et al., “Overlooked Challenges for microLED Displays,” *SID Symposium Digest of Technical Papers 2019*, 50 pp129-32.
15. Bulashevich K. A. and Karpov S. Y., “Impact of surface recombination on efficiency of III-nitride light-emitting diodes,” *Phys. Status Solidi RRL* 10 480-4.

6. Summary of Contributions

A summary of the contributions made in this dissertation is given below:

- Developed and experimentally demonstrated a novel microLED mass transfer and assembly process using adhesive bonding. Process was used to embed 50 X 100 μm^2 LEDs on an elastomeric substrate at $\sim 300\text{PPI}$ resolution.
- Developed a novel approach to high yield LLO of GaN thin films using an engineered metallic stress buffer layer. The use of stress buffer layer in improving GaN LLO yield was experimentally verified in a DPSS LLO process.
- Formulated an empirical model to study ablation stresses during GaN LLO. A simplified analytic model along with FEM analysis in ANSYS[®] was used to confirm the efficacy of the Ni stress buffer layer.
- Demonstrated a prototype flexible microLED display using FlexTrate[™] FOWLP process. A dielet approach was used to heterogeneously integrate commercial GaN microLEDs at $\sim 150\text{PPI}$ with off the shelf display driver ICs on a PDMS substrate. Flexibility of $\sim 5\text{mm}$ bending radius was successfully demonstrated.